Geochemistry, Geophysics, Geosystems

RESEARCH ARTICLE
10.1029/2019GC008464

Ice, Fire, or Fizzle: The Climate Footprint of Earth's Supercontinental Cycles

A. M. Jellinek[1], A. Lenardic[2], and R. T. Pierrehumbert[3]

[1]Department of Earth, Ocean, and Atmospheric Sciences, University of British Columbia, Vancouver, British Columbia, Canada, [2]Department of Earth Science, Rice University, Houston, TX, USA, [3]Department of Atmospheric Physics, Clarendon Laboratory, Oxford University, Oxford, UK

Key Points:
- Supercontinent assembly modulates volcanic sources and weathering sinks for CO_2 through effects on mantle convective thermal mixing
- Punctuated mixing during Pangea/Rodinia epochs can induce climate cooling-warming consistent with Mesozoic and Cryogenian-Ediacaran proxies
- Thorough thermal mixing during Precambrian Nuna assembly and breakup can maintain an ice-free climate consistent with geological data

Correspondence to:
A. M. Jellinek,
mjellinek@eoas.ubc.ca

Citation:
Jellinek, A. M., Lenardic, A., & Pierrehumbert, R. T. (2020). Ice, fire, or fizzle: The climate footprint of Earth's supercontinental cycles. *Geochemistry, Geophysics, Geosystems*, *21*, e2019GC008464. https://doi.org/10.1029/2019GC008464

Received 23 MAY 2019
Accepted 26 NOV 2019

Abstract Supercontinent assembly and breakup can influence the rate and global extent to which insulated and relatively warm subcontinental mantle is mixed globally, potentially introducing lateral oceanic-continental mantle temperature variations that regulate volcanic and weathering controls on Earth's long-term carbon cycle for a few hundred million years. We propose that the relatively warm and unchanging climate of the Nuna supercontinental epoch (1.8–1.3 Ga) is characteristic of thorough mantle thermal mixing. By contrast, the extreme cooling-warming climate variability of the Neoproterozoic Rodinia episode (1–0.63 Ga) and the more modest but similar climate change during the Mesozoic Pangea cycle (0.3–0.05 Ga) are characteristic features of the effects of subcontinental mantle thermal isolation with differing longevity. A tectonically modulated carbon cycle model coupled to a one-dimensional energy balance climate model predicts the qualitative form of Mesozoic climate evolution expressed in tropical sea-surface temperature and ice sheet proxy data. Applied to the Neoproterozoic, this supercontinental control can drive Earth into, as well as out of, a continuous or intermittently panglacial climate, consistent with aspects of proxy data for the Cryogenian-Ediacaran period. The timing and magnitude of this cooling-warming climate variability depends, however, on the detailed character of mantle thermal mixing, which is incompletely constrained. We show also that the predominant modes of chemical weathering and a tectonically paced abiotic methane production at mid-ocean ridges can modulate the intensity of this climate change. For the Nuna epoch, the model predicts a relatively warm and ice-free climate related to mantle dynamics potentially consistent with the intense anorogenic magmatism of this period.

1. Introduction

The intermittent assembly of supercontinents punctuate an otherwise continuous redistribution of continental landmasses that has been an expression of Earth's mantle convective regime since at least 2 Ga (e.g., Bleeker, 2003; Hallam, 1987; Jacoby, 1981; Li et al., 2008, 2013; Meert, 2012; Pesonen et al., 2012; Rogers & Santosh, 2004; Rolf et al., 2014; Wegener, 1924; Zhang et al., 2012). These transient 300- to 500-million-year long events, which are expressed in plate reconstructions (e.g., Evans, 2009; Li et al., 2008, 2013; Merdith et al., 2019; Rogers & Santosh, 2004; Zhang et al., 2012) and emerge in three-dimensional geodynamic models (e.g., Höink et al., 2012; Li & Zhong, 2009) are inherent features of the punctuated character of mantle convective stirring and thermal mixing that define the highly time-dependent heat transfer properties of plate tectonics (Lenardic et al., 2016). Aspects of the myriad expressions of key processes such as orogenesis at continental arcs, sea-level change, the opening of oceans, arc-continent collisions, and the clustering of mantle plumes and large igneous provinces (LIPs) in space and time on the volcanic sources and particularly the surface and seafloor weathering sinks for CO_2 that govern Earth's climate are explored explicitly and implicitly in many modeling as well as observational studies (e.g., Ahnert, 1970; Brady & Gíslason, 1997; Brune et al., 2017; Coogan & Gillis, 2013; Cox et al., 2016; DiBiase & Whipple, 2011; Donnadieu et al., 2004; Ferrier & Kirchner, 2008; Ferrier et al., 2010, 2016; Gaillardet et al., 1999; Gillis & Coogan, 2011; Gernon et al., 2016; Goddéris et al., 2003, 2008, 2017; Goudie & Viles, 2012; Kump, 2018; Kump et al., 2000; Lee & Lackey, 2015; Macdonald et al., 2019; Maher & Chamberlain, 2014; McKenzie et al., 2016; Montgomery & Brandon, 2002; Ouimet et al., 2009; Plank & Manning, 2019; Roe et al., 2008; Swanson-Hysell & Macdonald, 2017; Whipple & Tucker, 1999; Whipple & Meade, 2006).

During the assemblies of supercontinents Nuna (~1.8–1.3 Ga) (Zhang et al., 2012), Rodinia (~1.1–0.6 Ga) (Li et al., 2008, 2013), and Pangea (~0.335–0.173 Ga), continental fragments were drawn together through

continent-continent collisions to form transient but relatively long-lived and large landmasses. The formations of all three supercontinents reduced the global chemical weathering sink for atmospheric CO_2 by concentrating the majority of topography production and erosion within the very dry interiors of these landmasses, at large distances from moisture sources (Cox et al., 2010; Donnadieu et al., 2006; Fiorella & Poulsen, 2013; Goddéris et al., 2008; Otto-Bliesner, 1995; Veevers & Powell, 1994). During the breakups of Pangea and Rodinia, plate reconstructions and geological data suggest that disaggregating supercontinental fragments overran neighboring island arcs forming an initial perimeter (Lee et al., 2013; Macdonald et al., 2019; Merdith et al., 2019; Spencer et al., 2019). A resulting relatively rapid tectonic transition into continental arc modes is also correlated with large increases in mid-ocean ridge and arc magmatism (Brandl et al., 2013; Kelemen & Holbrook, 1995; Van Avendonk et al., 2017) and continental arc magmatism (Lee et al., 2013; McKenzie et al., 2016) and also marked by extensive orogenesis and chemical weathering occurring close to oceans (e.g., Donnadieu et al., 2004; Goddéris et al., 2017; Hartmann et al., 2017).

As we discuss in the next section, a shifting behavior of volcanic CO_2 sources as well as the predominant weathering sinks over supercontinental assembly and breakup is expressed in proxy data for Pangea and Rodinia. Intense Cretaceous global warming and volcanic CO_2 outgassing following the breakup of supercontinent Pangea were, for example, preceded by a protracted period of unusual global cooling characterized by polar ice caps extending well into the midlatitudes (e.g., Blättler et al., 2012; Blättler & Higgins, 2014; Feulner, 2017; McKenzie et al., 2016; Royer et al., 2004; Veizer et al., 2000). A more intense cooling-warming climate variability is mirrored in form albeit with far greater intensity in the Neoproterozoic and is associated with the formation, breakup, and fragmentation of the longer-lived supercontinent Rodinia (Hartmann et al., 2017; Hoffman et al., 2017; McKenzie et al., 2014). The protracted Sturtian (717–659 Ma) and relatively short Marinoan (645–635 Ma) global glaciations mark the cold Cryogenian period that was terminated as Earth entered the Ediacaran period (Hoffman & Li, 2009; Hoffman et al., 2017). This period is initially marked by an advance of polar ice to potentially midlatitudes (60°–<40° S, Trindade & Macouin, 2007) during the relatively short-lived ≤340-kyr-long Gaskiers event at 580 Ma (Hoffman & Li, 2009; Ivanov et al., 2013; Pu et al., 2016; Trindade & Macouin, 2007), possibly less than 10 million years before the abrupt rise of complex animals (see Hoffman et al., 2017; Knoll, 2011; Pu et al., 2016, and references therein) and Earth's transition to the nonglacial Cambrian period at 541 Ma.

Such temporal correlations between extreme variability in Earth's tectonic and climatic regimes suggest that this class of ~100-million-year cooling-warming variability is an inherent feature of the way in which supercontinental cycles modulate the volcanic sources and weathering sinks for CO_2 that define Earth's long-term carbon cycle (e.g., Lee et al., 2013; McKenzie et al., 2016). Indeed, because the temporal patterns differ primarily only in the magnitude of the climate change, it is tempting to hypothesize that they were each driven by a common set of underlying processes, which simply acted over a longer period during the Rodinia epoch. However, a no less engaging feature of Earth's record of long-term climate variability is that the formation and breakup of the most long-lived supercontinent Nuna are correlated with a climate variability that is exceptional for a monotony expressed partly a protracted absence of significant polar ice sheets (Kaufman & Xiao, 2003; Meert, 2012; Planavsky et al., 2015).

In this paper we draw on the results of extensive theoretical, numerical, and laboratory studies of the mechanical and insulating effects of continents on mantle convection (Coltice et al., 2009; Grigné et al., 2007; Jellinek & Lenardic, 2009; Korenaga, 2007; Lenardic et al., 2005, 2011; O'Neill et al., 2009; Phillips & Coltice, 2010; Rolf et al., 2012) to investigate a hypothesis that the temporal cold-warm climate pattern characteristic of the Pangean and Rodinian climates and the absence of any significant climate change related to the Nuna epoch are primarily consequences of differing effects of the formation and breakup of supercontinents on the structure and heat transfer properties of Earth's mantle convective regime. A more general motivation for this paper is the question of the extent to which Earth's record of long-term climate variability can rigorously constrain key features of Earth's current plate tectonic mode of mantle convection.

In particular, on the basis of published theoretical, numerical, and experimental studies (Lenardic et al., 2011, and references therein), we will argue that the cooling-warming climate pattern expressed in through proxy data for the Rodinia and Pangea epochs reflects a “Mantle thermal isolation-to-remixing” mode of supercontinental climate control that is characterized by dramatic temporal shifts in global volcanic CO_2 outgassing rates as well as in the predominant modes of chemical weathering (cf. Figures 1 and 2). Operating in this regime, Pangea and Rodinia were bounded to a potentially large extent by curtains of subducting

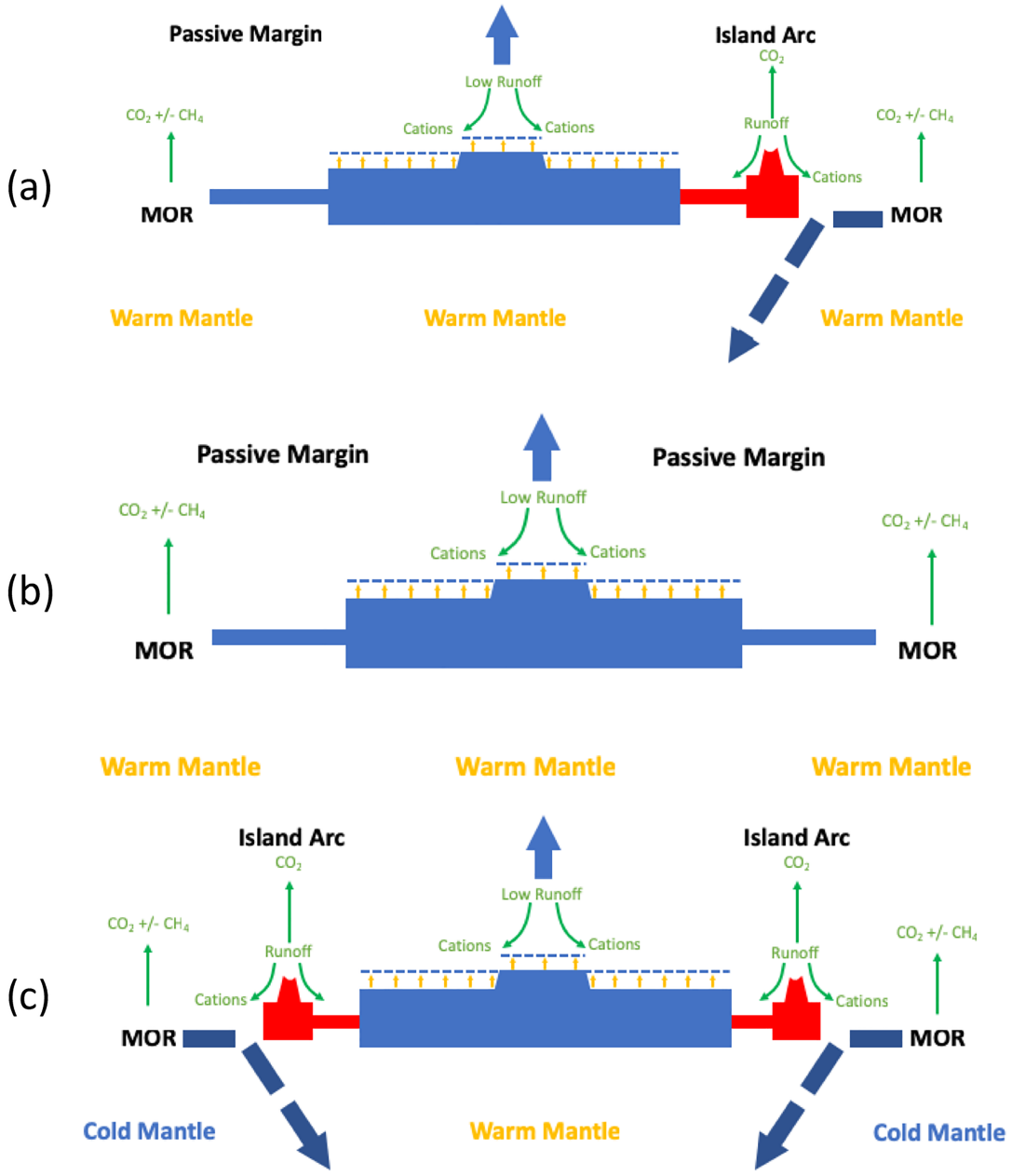

Figure 1. Schematic illustration of the effects of supercontinent assembly on volcanic sources and temperature-dependent surface and seafloor weathering sinks for CO_2. Continental fragments are drawn together to form a supercontinent that eventually becomes centered near the equator. If the resulting supercontinent is, say, (a) only partly bounded by a subducting slab at an island arc or (b) surrounded predominantly by passive margins, mantle convective thermal mixing will remain extensive, and lateral mantle temperature variations are minimized. The global rate of volcanic CO_2 outgassing at mid-ocean ridges (MORs) and at arcs is unchanged, as is the rate of CH_4 production at MORs. However, continent-continent collisions will drive the growth of intracontinental plateaux with a height and aspect ratio that increases during this collision in proportion to time $t^{1/3}$ (Appendix B), causing the majority of mechanical erosion to become increasingly concentrated within the dry supercontinent interior. The combined effects of an expected reduced precipitation rate and a greater distance between the sources of divalent cations such as Ca^{2+}, Mg^{2+}, and Fe^{2+} (alkalinity) by chemical weathering processes and the oceans will cause the strength of the terrestrial surface weathering sink for CO_2 to decline while the seafloor weathering sink strength remains approximately constant. An unchanged volcanic source for CO_2 and a reduced overall weathering sink leaves relatively more CO_2 in the atmosphere, leading to a warmer world. If the resulting supercontinent is bounded by a continuous curtain of strong subducting slabs (c), inhibited thermal exchange and mixing of insulated subcontinental mantle into the oceanic mantle domain will lead to lateral oceanic-continental mantle temperature variations. Reduced melt production and volcanic CO_2 outgassing at mid-ocean ridges (MORs) and at arcs related to the declining temperature and increased viscosity of the oceanic mantle can lead to a colder world, depending particularly on the predominant mechanism of seafloor weathering and on the longevity of this thermal isolation regime (see text).

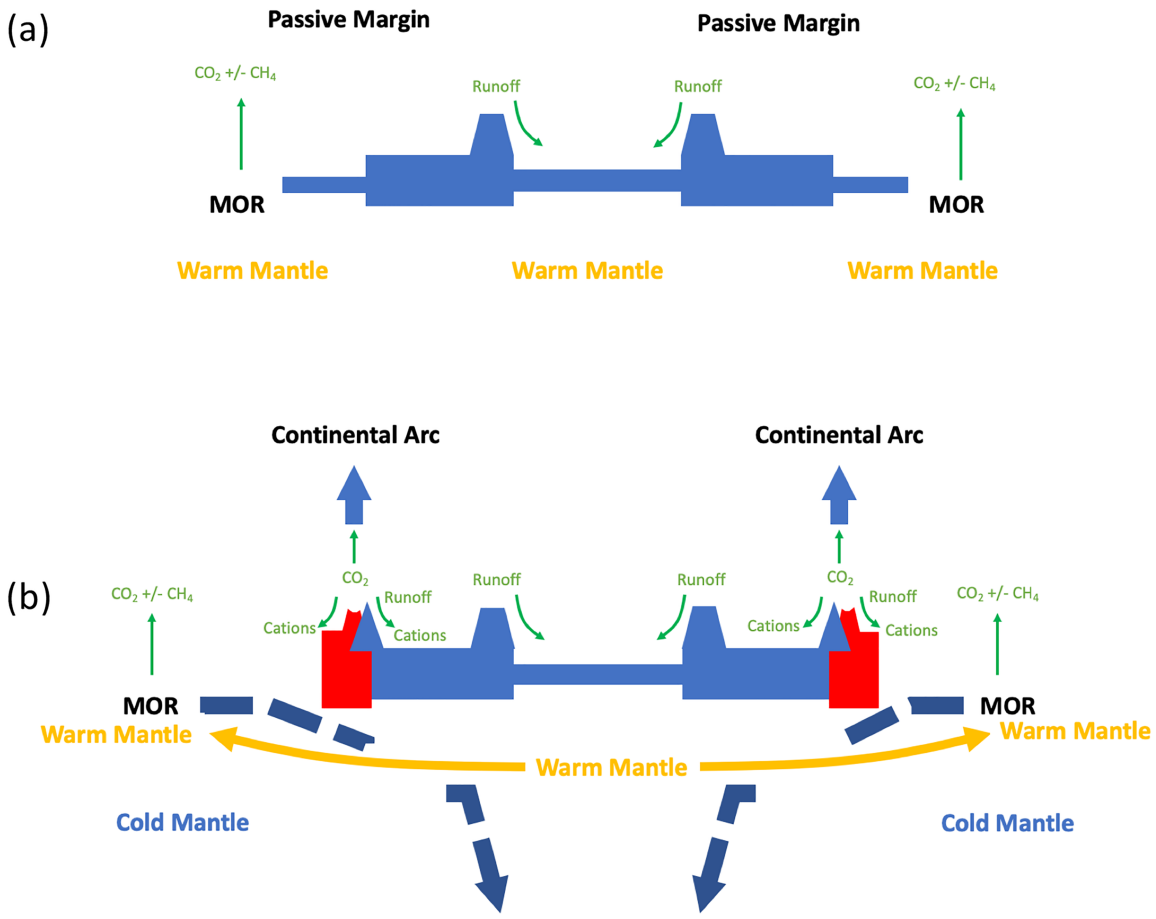

Figure 2. Schematic illustration of the effects of supercontinent breakup on volcanic sources and weathering sinks for CO_2. For a fragmenting supercontinent centered within the tropics, the dynamics of arc-continent collision will drive orogenesis at continental margins. Depending on the global mean surface temperature and humidity, resulting topographic uplift that increases over the collisional time $t^{1/3}$ will stimulate orographic precipitation as well as erosion that depends also on the aspect ratio of mountain ranges, which also grows as $t^{1/3}$ (see Appendix B and section 6.1). For a given surface temperature, precipitation rates onto topography closer to nascent oceans will enhance the delivery of divalent cations, carbonate precipitation in the ocean, and the strength of the weathering sink for CO_2, in turn. If the mantle is thermally well mixed prior to supercontinent fragmentation (top), there is no change to the global arc and MOR outgassing rates and no change to the seafloor weathering sink (see text). This enhanced surface weathering sink, however, drives Earth into a cooler climate. By contrast, supercontinental breakup following a period of ocean-continental mantle thermal isolation related to an impermeable encircling curtain of subducting slabs (bottom) affects both volcanic sources and weathering sinks for CO_2. The rise and spread of warm subcontinental mantle into the oceanic mantle domain and into the melting regions at mid-ocean ridges enhances melt production and CO_2 outgassing significantly at arcs and at MORs. Continental fragments overrun bounding subduction zones to open an ocean driving these arcs into compressive continental modes. Resulting uplift and rainfall, governed by the rates of subduction and crustal accretion, leads to an enhanced and tectonically modulated weathering sink for CO_2 (see text). Concurrently, the seafloor weathering sink for CO_2 potentially evolves from being controlled by fault and fracture permeability at predominantly slow spreading ridges to becoming controlled by the MOR crustal production rate at generally relatively fast spreading ridges. Where thermal isolation leads to significant lateral mantle temperature variations, the increase in volcanic CO_2 during breakup gradually exceeds the increase in the surface weathering sink, leading to a relatively warm climate.

slabs, the presence of which reduced the advective exchange of relatively insulated, warm subcontinental and colder, more strongly cooled suboceanic mantle material. Depending on the spatial extent to which suboceanic and subcontinental mantle was isolated thermally, and on the longevity of this arrangement, this mantle mixing mode modulated to differing extents the strengths of the major volcanic CO_2 sources as well as the surface and seafloor chemical weathering sinks for atmospheric CO_2. An alternative end-member mode of supercontinental control is “Perfect thermal mixing” where the mantle is convectively well stirred and approximately isothermal during formation as well as breakup (Figure 1). In the absence of extensive proxy data beyond a well-established dearth of significant concurrent ice sheets (Hoffman, 2009), on the basis of published numerical simulations (Coltice et al., 2009; Korenaga, 2007; Phillips & Coltice, 2010), we hypothesize that character and planform of subduction zones related to the supercontinent Nuna

maintained extensive mantle thermal mixing. As we will discuss, such a condition may have ensured the resilience of the clement and largely ice-free climate of this period.

Our focus on the climate effects of mantle dynamic thermal transients related to supercontinent assembly and breakup on key underlying processes governing volcanic sources as well as the predominant weathering sinks for CO_2 is unusual. Indeed, although studies of mantle-climate interactions have a long history, there are essentially two common modeling strategies. In typical "long-time averaged" coupled models, outgassing rates and Earth's surface weathering response are tied to a mantle thermal history model (see Jellinek & Jackson, 2015; Lenardic et al., 2016, and references therein). Models of this class typically evolve the dynamics of volcanic CO_2 outgassing and the production and weathering of topography with a plate spreading or accretion rate. In these models, plate spreading rates generally evolve smoothly in temporal and spatial character in response to the very slow mantle cooling that occurs as Earth's inventory of radiogenic heat producing elements declines over billion year time scales.

The most common modeling approach to investigating aspects of Mesozoic and Neoproterozoic climate variability is to use coupled geochemical, biogeochemical, and climatological models of varying complexity to explore the climate response characteristics of model near-surface Earth systems for specified volcanic forcings. Models of this type vary enormously in their design and goals but typically interrogate processes and feedbacks governing critical controls on surface and seafloor weathering, primary productivity, and organic burial and sea-level change acting over weathering time scales of order 1 million years (e.g., Abbot et al., 2012; Bergman et al., 2004; Berner, 1998, 2004; Bjerrum & Canfield, 2011; Beerling & Royer, 2011; Bjerrum et al., 2006; Dessert et al., 2001, 2003; Donnadieu et al., 2004; Edmond & Huh, 2003; Feulner, 2017; Gaillardet et al., 1999; Goddéris et al., 2003, 2012; France-Lanord & Derry, 1997; Hayes & Waldbauer, 2006; Higgins & Schrag, 2003; Jagoutz et al., 2016; Johnston et al., 2012; Kump, 2018; Kump et al., 2000; Le Hir et al., 2009; Lenton et al., 2018; Mills et al., 2014, 2014; Roberson et al., 2011; Ridgwell & Zeebe, 2005; Rothman, 2015; Rothman et al., 2003; Rothman & Forney, 2007; Royer et al., 2007, 2004; Schrag et al., 2002; Tennenbaum et al., 2013). This approach is particularly powerful for building understanding of various critical triggers for discrete events including anomalous rapid global warming and ocean anoxia, oxygen rise, transient partial and global glaciation, and essential changes in Earth's biosphere (e.g., Anbar & Knoll, 2002; Beerling & Royer, 2011; Cox et al., 2016; Donnadieu et al., 2004; Hartmann et al., 2017; Hoffman et al., 2017; Jenkyns, 2010; Jones & Jenkyns, 2001; Kump, 2018; Kump et al., 2005; Macdonald & Wordsworth, 2017; Macdonald et al., 2019; Mills et al., 2011; Tziperman et al., 2011).

Elegant and carefully calibrated long-term carbon cycle models have been constructed to identify and understand the major biogeochemical controls over the Mesozoic and Neoproterozoic climates (e.g., Berner, 2004; Bjerrum & Canfield, 2011; Lenton et al., 2018). However, for the Cryogenian period, a challenge remains to find self-consistent conditions for both entry into and exit from global glaciations, as well as an intermittency of this panglacial climate state that is marked by the occurrence of discrete Sturtian and Marinoan events with an intervening nonglacial interlude of order 10 million years in length (Hoffman et al., 2017). Rich climate models have emerged with evident success in terms of identifying plausible underlying dynamics that give rise to the initiation and maintenance of panglacial climates (see Hoffman et al., 2017, and references therein). However, by their design, such models do not explain the order 100-million-year longevity of the Cryogenian period itself. Furthermore, why a Cryogenian panglacial climate was intermittent remains unclear. Moreover, taken together, the relative brevity of the Marinoan glaciation compared to the Sturtian event and the advance of the short-lived Ediacaran Gaskiers ice sheet to low latitudes are enigmatic.

To build understanding of the essential features of a supercontinental modulation of Earth's climate in terms of effects on the character and heat transfer properties of mantle convection, we emphasize distinct consequences of mechanical connections across the Earth system for CO_2 sources and sinks. In marked contrast to existing analyses of Neoproterozoic and Mesozoic climate change (Bjerrum & Canfield, 2011; Lenton et al., 2018), we hypothesize that the predominant regimes as well as average intensities of volcanism and weathering can shift significantly during Rodinia and Pangea assemblies and breakups. We will show that some predictable controls on the dynamics of volcanic sources and weathering sinks for CO_2 can explain the cooling-warming climates defining the "Rodinian" and "Pangean" epochs, as well as the absence of climate variability during the Nuna period. This class of tectonically modulated climate change, along with considerations of related effects including the temporal clustering of LIP volcanism following the breakup of Pangea, is ultimately consistent with Mesozoic global ocean anoxia events, permits intermittent global glaciations

during the Neoproterozoic, and provides a potential explanation for a geologically rapid transition from the Marinoan global glaciation defining the end of the Cryogenian into the Ediacaran period.

This paper is organized in the following way. We review briefly proxy data constraining the climate change associated with the Pangean epoch as well as the characters of the volcanic sources and weathering sinks for CO_2 during the Rodinian epoch in section 2. We defer a necessarily more speculative discussion of tectonic climate controls during the Nuna epoch until section 7. In section 3 we review how the process of supercontinental assembly and breakup might perturb the thermal mixing properties of Earth's mantle convective regime through the establishing (or not) of transient peripheral "curtains" of subducting slab. In section 4 we discuss qualitative consequences of Earth's evolving mantle convective thermal mixing regime through supercontinent assembly and breakup for arc, mid-ocean ridge, and ocean island (OIB)/large igneous province (LIP) volcanic sources of CO_2. We also introduce effects of this thermal mixing on the predominant mechanics and regimes of surface and seafloor weathering sinks for CO_2 acting in various limits. Significantly, we discuss key factors that enter into this problem that are within as well as beyond the scope of this paper with a deliberate aim of showing limitations of our modeling study to point to opportunities for future work. From this discussion we develop in section 5 quantitative parameterizations of tectonically controlled changes in global volcanic CO_2 outgassing and introduce a novel abiotic CH_4 source that is potentially an important additional climate forcing in the Neoproterozoic that can enable an intermittent panglacial climate. We construct parameterizations for surface and seafloor weathering sinks for atmospheric CO_2 in section 6 and explore consequences for the long-term CO_2 cycle with an approximate analytical scaling relationship developed for a simplified, constant albedo Earth model. In section 7 we couple our weathering parameterizations to a one-dimensional Budyko-style energy balance model with an ice-albedo feedback to understand climate consequences of an expected sharply changing character and intensity of volcanic sources and weathering sinks for CO_2 during the Rodinia and Pangea epochs. We explore the extent to which predictions are consistent with proxy data reviewed in section 2 as well as additional geological constraints including the latitudinal extent of polar ice sheets in the Mesozoic and the occurrence and intermittency of global glaciation events in the Neoproterozoic, in turn. To the very limited extent geological data permit, we use climate calculations to discuss the apparently polar ice-free climate that persisted during the Nuna episode. We conclude in section 8 with an overall message that bearing in mind the significant assumptions and limitations of our modeling study, strong Moesozoic and Cryogenian-Ediacaran cooling-warming climate variability, including intermittent Neoproterozoic global glaciations, can be consequences of the transient assembly and fragmentation of supercontinents on the character of Earth's mantle convective thermal mixing. A provocative implication of our work is that the extreme 100-million-year cooling-warming climate variabilities of the Neoproterozoic and possible the Mesozoic periods are challenging and potentially impossible to reconcile with a mantle that remains thoroughly mixed thermally through the Rodinia and Pangea supercontinental episodes.

2. Pangean and Rodinian Proxy Data: Rapid Transitions in Sources and Sinks for Atmospheric CO_2

Long-term climate variability is ultimately governed by a balance between the rate at which mantle-controlled volcanic sources deliver CO_2 to the atmosphere and the rate at which this CO_2 is drawn down through surface and seafloor chemical weathering processes. The cooling-warming variability evident in reconstructed tropical sea-surface temperatures during the Pangean epoch (Figure 4) and implicit in the transition into and out of Cryogenian global glaciation during the Rodinia episode consequently imply that both the sources and sinks for CO_2 evolved over $\leq$10-million-year time scales to produce this temporal pattern in response to Earth's changing tectonic mode. It is, for example, well established that the fragmentation of Pangea is correlated with increased rates of volcanism across the Earth system. On average, links between mid-ocean ridge crustal production and sea-level rise loosely constrain a factor of $\sim$1.9 increase in Createaceous volcanic outgassing (see discussions in Berner, 1998 and Lenton et al., 2018). In addition, as we discuss in greater detail in section 4, enhanced mid-ocean ridge (MOR) crustal production following Pangean breakup (Brandl et al., 2013; Kelemen & Holbrook, 1995; Van Avendonk et al., 2017; Whittaker et al., 2008) was complemented by magmatism and CO_2 outgassing along an extensive system of collisional continental arcs (Beerling & Royer, 2011; Lee & Lackey, 2015; Lee et al., 2013), as well as temporally clustered LIP volcanism are distinctive features of the Mesozoic (Figure 4). Volcanism and CO_2 outgassing from stratovolcanoes related to mantle

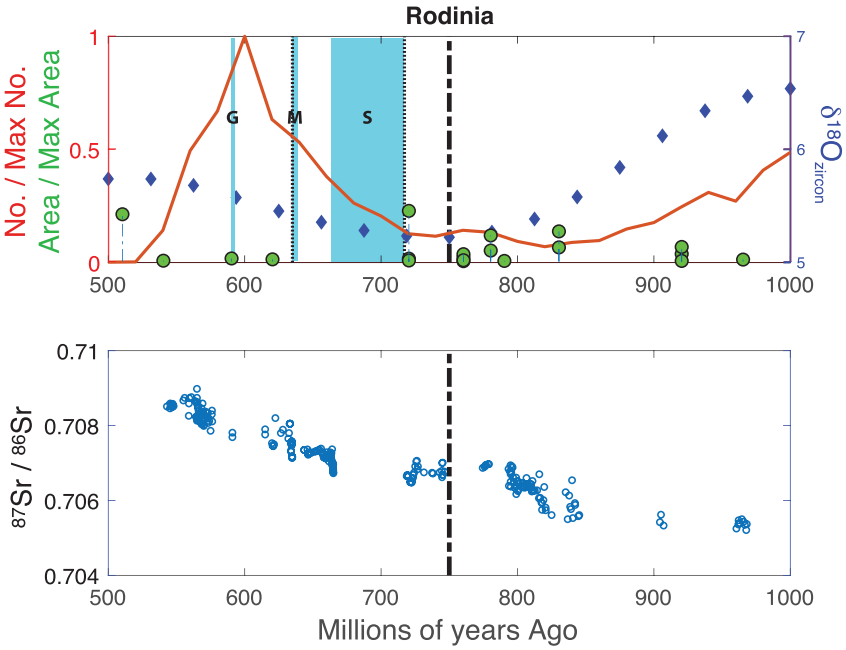

Figure 3. Proxy data indicating some of the evolving controls on climate correlated with the assembly and breakup of Rodinia. Rodinia breakup occurs by 740 Ma (vertical heavy black dashed line) and is marked by the Sturtian (S) (717–662 Ma) and much shorter Marinoan (M) (640–635 Ma) global glaciations (blue shaded regions) that mark the Cryogenian period (720–635 Ma, Shields-Zhou et al., 2016) (vertical black dotted lines). The comparatively much shorter extensive but nonglobal Ediacaran Gaskiers (G) glaciation at 580 Ma is also shown. Also included are the normalized frequency distribution of regionally binned detrital zircon ages (heavy red line) (McKenzie et al., 2016) and the frequency of large igneous province (LIP) events with areas normalized to the maximum area over the period shown (solid green circles; time series data from http://www.largeigneousprovinces.org/record). The two notably large LIPs are the Franklin-Thule (720 Ma) and Kalkarindji (510 Ma) events. The minimum in the $\delta^{18}O$ data on detrital zircons (blue diamonds) at around 770 Ma correlates with a minimum in both the number of detrital zircon ages and a notable plateaus in seawater $^{87}Sr/^{86}Sr$ (Halverson et al., 2007) that may indicate minima in weathering and crustal production rates (see text). Following breakup, the rise in seawater $^{87}Sr/^{86}Sr$ and $\delta^{18}O$ values for detrital zircons, as well as an increase in the number of detrital zircon ages, signals potentially more intense magmatism as well as mechanical erosion and chemical weathering.

melting was further amplified by perhaps a factor of 2–3 by additional crustal contributions of accreted carbonate rocks (Lee et al., 2013).

More generally, varied proxy data consistent with evolving rates and characters of volcanism, as well as weathering, suggest that the sources and sinks for atmospheric CO_2 varied in strength over 1- to 10-million-year time scales during both supecontinental cycles (Figures 4 and 3). Furthermore, the behaviors of these climate controls were similar in form, although distinct in detail. During breakup of Rodinia (Li et al., 2013), mass-independent $\Delta^{17}O$ anomalies require low atmospheric O_2 and ultimately very high post-Marinoan pCO_2 (Bao et al., 2008; Cao & Bao, 2013; Crockford et al., 2016). Following a decline in the rate of continental arc silicic magmatism with Rodinia formation, global averages of regionally binned age distributions in detrital zircons suggest an overall increase beginning near the start of the Sturtian glaciation and progressing through the Marinoan event and into the relatively warm Ediacaran period (Cawood et al., 2012; Condie & Aster, 2010; Condie et al., 2009; McKenzie et al., 2016). To the extent that an increase in the frequency of given zircon crystallization ages reflects partly an age bias related to the spatial extent to which continental granitic rocks are exposed tectonically and eroded mechanically (e.g., Dickinson et al., 2009; Moecher & Samson, 2006; Rainbird et al., 2011; Summerfield & Hulton, 1994; Squire et al., 2006), these data are also consistent with a transition to a predominant globally averaged mechanical and chemical weathering regime involving orogenesis (Cawood et al., 2012). The Sturtian global glaciation is also correlated with the deposition of sedimentary iron deposits (banded iron formation) during intensified periods of deep ocean ferruginous anoxia, potentially related to enhanced exposure and weathering of LIPs (e.g., Cox et al., 2013; Donnadieu et al., 2004; Hoffman et al., 2017). The reality of such a picture is, however,

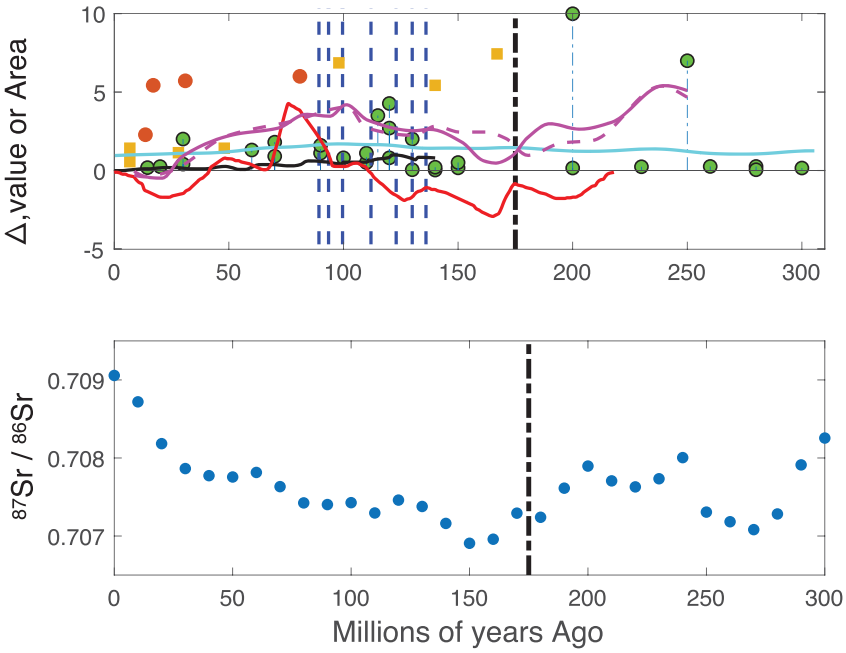

Figure 4. Proxy data indicating some of the evolving controls on climate correlated with the assembly and breakup of Pangea. Pangea breakup and opening of the Atlantic Ocean at 175 Ma (vertical heavy black dashed line) occur near a minimum in the tropical sea-surface temperature (SST) record inferred from $\delta^{18}O$ data (heavy red and magenta lines). Tropical sea-surface temperature changes (° C) compared to present day (indicated by Δ on the *y* axis) inferred from raw $\delta^{18}O$ data on calcite and aragonite shells (red line) are from Veizer et al. (2000). These data are pH-corrected and compared with additional climate proxies (solid magenta lines) as well as GEOCARB calculations in Royer et al. (2004) (dashed magenta line). A temperature minimum following the start of the opening of the Atlantic precedes a gradual transition into the Cretaceous warm period characterized by global ocean anoxic events (OAE 1a–d, OAE 2, and OAE 3, Jenkyns, 2010) (vertical dashed blue lines). The Creataceous warm period evident in the SST reconstructions is correlated with an approximate factor of 1.9 increase in average volcanic outgassing rates (cyan line), which is inferred from high-resolution paleosea-level reconstructions and reproduced using the COPSE biogeochmical model (cf. Lenton et al., 2018, and references therein). This increase in outgassing is correlated with a temporal clustering of LIPs of various areal extents [Mkm^2] (filled green circles; time series data from http://www.largeigneousprovinces.org/record) and a factor of 2 increase in the average rate of plate spreading normalized to present day (black line) (Becker et al., 2009). For reference, the largest area LIPs are the Siberian Traps (250 Ma), the Central Atlantic Magmatic Province (200 Ma), and the Ontong Java (120 Ma). Post-breakup seawater $^{87}Sr/^{86}Sr$ (c.f. Lee et al., 2013) increases starting around 150 Ma (see text). Also shown are the CO_2 from carbonate in basalt crust as a result of low-temperature, off-axis hydrothermal circulation at slow spreading MAR (open red circles) and intermediate-to-fast spreading Pacific sites (open orange squares) (Gillis & Coogan, 2011, table 1). These data do not include calcareous sediment and are normalized to the average value reported from the EPR at 6.8 Ma (see text).

also affected by the distribution and potentially complex delivery dynamics of organic carbon from terrestrial sedimentary systems (Torres et al., 2017) as well as an increased solubility of hydrothermal Fe during large eustatic sea-level falls (Kump & Seyfried, 2005).

Recent analyses of $\delta^{18}O$ data on zircons (Hartmann et al., 2017) provide support for a changing surface weathering sink during the Rodinia epoch that largely tracks continental arc magmatism. A monotonic increase in continental surface weathering from the low rates that define the pre- and syn-Sturtian worlds suggested previously (e.g., Derry et al., 1992) evolves to very high rates during the Ediacaran period (Figure 3), a feature that is also consistent with coupled GCM-pCO_2 models in which weathering is strongly enhanced during Rodinia fragmentation (Donnadieu et al., 2004; Le Hir et al., 2009). The increase in seawater $^{87}Sr/^{86}Sr$ between 665 and 719 Ma provides additional support for this hypothesis if this signal is modulated mostly by the flux of old (high Rb/Sr) continental material, although these data certainly permit other interpretations. Among other effects, $^{87}Sr/^{86}Sr$ variability is sensitive to bottom water temperature and local sources and sinks of high Rb/Sr material including contributions from MOR hydrothermal systems (Coogan & Dosso, 2015; Coogan & Gillis, 2018). Coogan and Dosso (2015) argue, for example, that the relatively steep rise in $^{87}Sr/^{86}Sr$ during the Cenozoic (Figure 3) reflects a reduced seawater-basalt exchange

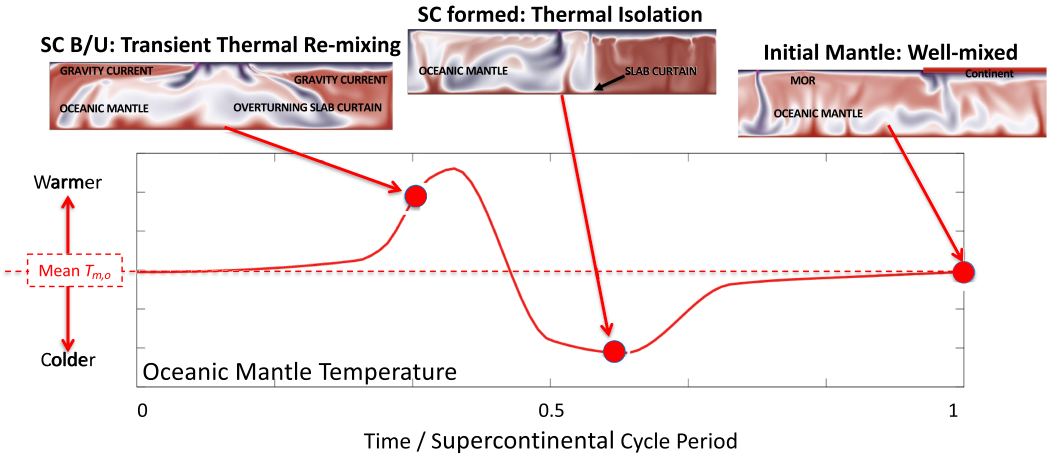

Figure 5. Two-dimensional numerical simulations of supercontinental formation in a perfect thermal isolation-to-remixing mantle convective regime. The establishing of an impermeable curtain of subducting slab at supercontinent (SC) formation (beginning at time = 1) inhibits the advection and mixing of relatively slowly cooled subcontinental mantle into the oceanic mantle domain, causing a decline in ocean mantle potential temperature $T_{m,0}$, in turn. The magnitude of this oceanic mantle cooling increases with each overturn and reaches a maximum that increases with the longevity of the subducting slab barrier to lateral mantle flow (around time = 0.45). Gravitationally unstable lateral differences in hydrostatic pressure produced as a result of this subducting slab curtain eventually drive the overturning of this unstable mantle system. A resulting transient period of mantle thermal remixing causes the oceanic mantle potential temperature to overshoot the initial value before the system recovers a new steady-state thermal regime.

related to cooler bottom water temperatures. Nevertheless, connections among the trends in these data and an increase in both weathering rates and continental magmatism during a breakup involving a transition to extensive continental arc-style subduction remain a plausible picture.

The character of the Pangean weathering sink for atmospheric CO_2 was also time varying (e.g., Blättler et al., 2011, 2012; Jenkyns, 2018). For example, in addition to an intensified uptake of seawater CO_2 into basalt crust in the Pacific hosting low-temperature MOR hydrothermal systems (Coogan & Gillis, 2013, 2018; Gillis & Coogan, 2011), Pangea breakup is correlated with intermittent "ocean anoxic events" (OAE Ia–d and II) (Figure 4). These approximately global features can be explained, in part, through increases in CO_2 outgassing and continental surface weathering fluxes expressed through their effects on seawater Sr, Os, and Ca isotopic variability, as well as surface temperature. Coupled $^{87}Sr/^{86}Sr$-$\delta^{13}C$ isotopic variability support a picture in which a corresponding increase in the fluvial delivery of nutrients to the oceans increased primary productivity to drive deep ocean anoxia through an enhanced respiration of organic matter, in turn (see Jenkyns, 2010, and references therein). In addition, higher average surface temperatures will reduce O_2 solubility in the surface ocean and reduce vertical mixing of this O_2 into the deep ocean, enhancing the likelihood for anoxia (Williams & Follows, 2011). The seawater Sr data in Figure 4 are, however, also consistent with an increased delivery of radiogenic material to the ocean following breakup but possibly more striking is the emergence of a clearly increasing trend in the data by 150 Ma, within about 25 millions of years of the start of breakup.

3. The Mantle Response to the Assembly and Breakup of Supercontinents

Earth's present mantle interior potential temperature reflects a balance between internal heat generation and a rate of surface cooling (Christensen, 1984; Davies, 1980; Tozer, 1972) that is modulated by the distribution and total surface area of insulating continents (Cooper et al., 2006; Jaupart & Mareschal, 2010; Lenardic et al., 2005; Pekeris, 1935). Over time scales much greater than the order 10^2-million-year mantle convective overturn time, a well-defined mean interior temperature is possible as a result of thorough thermal mixing by spatially complex and time-dependent oceanic plate-scale overturning motions related to the pattern and wavelength of subduction. This "perfect thermal mixing" requires an efficient exchange of warm mantle beneath insulating continents and the relatively more strongly cooled suboceanic mantle and is a special case.

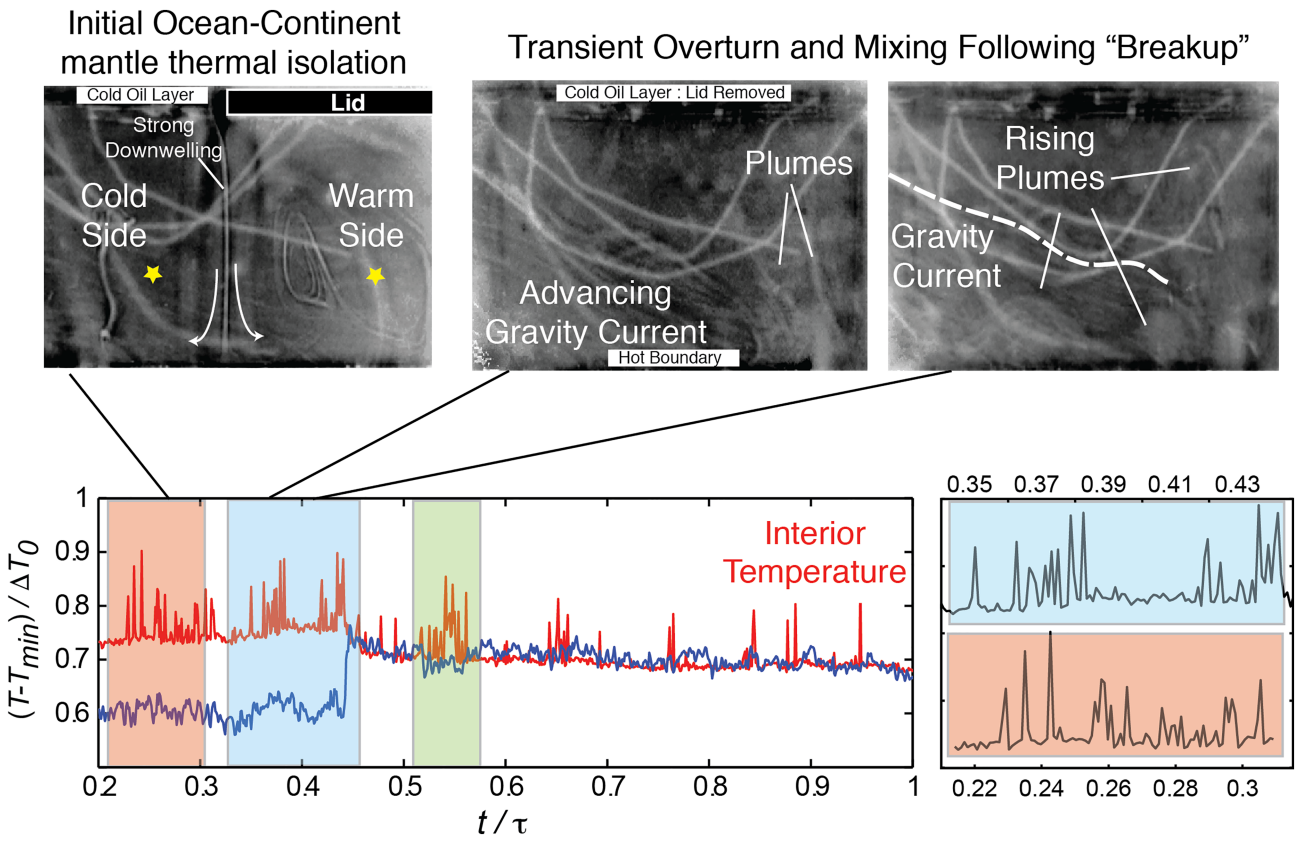

Figure 6. Laboratory experiment illustrating a generic effect of introducing and removing analog partial continental insulation at the top of a laboratory-scale convecting mantle system in which a layer of corn syrup is heated from below with a resistance heater cooled from above using a cold low viscosity oil bath (cf. Jellinek & Lenardic, 2009; Lenardic et al., 2011). The time series of photographs and accompanying time series of temperature over a vertical thermal diffusion time across the convecting layer τ show an evolution from initial steady-state thermal isolation (t/τ<0.43) through a transient regime following continental removal ($0.43 < t/\tau < 0.47$) that leads to remixing, which is qualitatively similar to the pattern in the simulations in Figure 5. Average oceanic (blue time series of temperature)-continental (red time series of temperature) mantle temperature variations are initially about 20% of the vertical temperature difference across the system. The thermal isolation of the subcontinental mantle is maintained by a strong downwelling of cold corn syrup, which drives a large-scale circulation in both domains. Intermittent rising hot thermals on the subcontinental side govern the majority of the heat transfer within this domain. Careful removal of the analog continent ($t/\tau \approx 0.43$) leads to a rapid collapse of this planform: Warm analog subcontinental rises across the cold side as the cold oceanic mantle spreads across the hot lower boundary as a gravity current (see text). Spread of this cold material bulldozes the hot thermal boundary layer ($0.39 < t/\tau < 0.42$), reducing the frequency of plumes. This process and the introduction of very cold and highly viscous material causes new plumes to become larger as well as clustered in time (cf. Figure 5 and Lenardic et al., 2011; Robin et al., 2007; Thayalan et al., 2006).

Plate reconstructions and geological data suggest that subduction zones probably encircled Rodinia and to a lesser extent Pangea by the time these supercontinents were each formed (e.g., East et al., 2019; Evans, 2009; Lee et al., 2013; Le Pichon et al., 2019; Li et al., 2013; Müller et al., 2016). Depending on the continuity, geometry, and age of subducting slabs, such a planform can have varied consequences for the character and extent of mantle thermal mixing. For a given low viscosity asthenosphere channel thickness (Höink et al., 2012), because the speed of subduction scales as the square of a plate thickness (Davies & Richards, 1992) and bending resistance scales as the cube of plate thickness (Conrad & Hager, 2001; Buffett & Rowley, 2006), asymmetries in subduction regime and in the ages and thicknesses of bounding subducting slabs can guide mantle convective flows spatially and drive them to higher speeds and to wavelengths that are much larger than the supercontinent is wide, enforcing thorough mixing.

However, the partial or complete encircling of a single large continental land mass by effectively a curtain of downgoing cold, stiff, and rheologically complex slabs can also reduce or prevent entirely the advective exchange and stirring together of subcontinental and cold suboceanic mantle material. Using results from simulations and laboratory experiments discussed above (Lenardic et al., 2011) (Figures 5 and 6), together with proxy data for Pangean magmatism (Figure 4) as a guide, in Figures 1 and 2 we illustrate schematically consequences of "thermal isolation" as well as "remixing" compared with perfect mantle thermal mixing

with formation and breakup for mantle thermal structure. Also shown are effects on the major controls on CO_2 sources and sinks, which we discuss in the next section.

During supercontinent formation in a "thermal isolation-to-remixing" regime, the lateral advection of insulated and warm subcontinental mantle is impeded, and potentially large continent-ocean upper mantle temperature variations emerge and grow over time. Critically, these lateral temperature variations are unrelated to spatial variations in the rate of radiogenic heat production in the mantle and are driven entirely as a result of the character of the convective stirring and cooling imparted at the base of oceanic lithosphere into the oceanic mantle domain and the relatively weak or negligible cooling delivered into the continental mantle domain as a result of continental insulation. Laboratory experiments and numerical simulations suggest that in the extreme case of perfect thermal isolation, lateral temperature variations of potentially 10–15% of the total vertical temperature drop across the mantle occur near the top of the mantle after about four mantle overturn times (Lenardic et al., 2011). More generally, however, the magnitude of any lateral temperature variations related to effects of the formation of supercontinents will lie between these endmember thermal mixing situations and will depend on the geometry, structure, continuity, permeability, and spatially varying longevity of a subducting curtain.

In contrast to the thorough mixing case, any thermal isolation solution is transient by definition (Lenardic et al., 2011). Lateral temperature variations (Figures 5 and 6) lead to proportionally large differences in hydrostatic pressure between the oceanic and continental mantle domains that increase over time and that are unstable to gravitational overturning. Relatively buoyant subcontinental mantle will inevitably deform, penetrate, and overturn bounding subduction slabs, and ascend and spread above relatively cold oceanic mantle to form a hot layer that persists until mantle convective stirring produces a new well-mixed thermal state (Figures 2 and 5). This intrusion and spread of relatively warm mantle along the base of the lithosphere into mid-ocean ridges will cause extensive crust production consistent with proxy data for Pangea, as well as increased MOR CO_2 outgassing and a transition in the mechanics and strength of the seafloor weathering sink for atmospheric CO_2. Although these qualitative effects on the surface Earth system are robust features of this remixing mantle thermal regime, their timing depends on the buoyancy-driven advance of the front of this warm, low viscosity gravity current over a distance D_{mor} to an adjacent mid-ocean ridge against the viscous resistance of thermally heterogeneous but relatively cold and viscous, on average, oceanic mantle. For a fixed volume Vol of gravitationally unstable subcontinental mantle material with an excess temperature ΔT_m and a cold oceanic mantle with a kinematic viscosity ν_o, a balance of buoyancy and viscous forces (e.g., Griffiths & Campbell, 1991) gives a lag time

$$t_{lag} \sim \frac{D_{mor}^5}{Vol^2} \frac{\nu_m}{g\alpha\Delta T_m}. \quad (1)$$

This lag time is particularly sensitive to the volume of the laterally flowing mantle material, and thus the longevity of any thermal isolation regime, and the distance to the mid-ocean ridge melting region. Consequently, beyond an order of magnitude calculation, this lag is model dependent or simply requires calibration from proxy data and plate motion models. Nevertheless, for volumes $Vol = 10^{17} - 10^{18}[\mathrm{m}^3]$, $D_{mor} \sim 10^6[\mathrm{m}]$, $\nu_o = 10^{22} - 10^{23}$ [Pa s], and $\Delta T_m = 100 - 200$ [° C], the climate expression of breakup will emerge order 10–100 million years after breakup. We discuss this lag in greater detail in section 7.

4. Supercontinental Cycles, Mantle Thermal Mixing, and Earth's Long-Term Climate Variability: A Conceptual Model

The schematic evolution through a supercontinental cycle operating in a mantle thermal isolation-to-remixing regime in Figures 1 and 2 illustrates how such an event can exert a basic control on Earth's long-term carbon cycle and climate. In addition to modulating the global rates of volcanic CO_2 outgassing at arcs through effects on mantle melting rates, these mantle dynamics exert tectonic controls on the mechanics and location of chemical weathering sinks for atmospheric CO_2 on land and within low-temperature mid-ocean ridge hydrothermal systems. We discuss some specific effects qualitatively here and parameterize them quantitatively in section 5.

4.1. Mantle Controls on Climate During Supercontinent Assembly

Supercontinents form plausibly as a consequence of subduction at island arcs drawing together continental fragments to close an ocean. This picture of growth through continent-continent collision predicts that

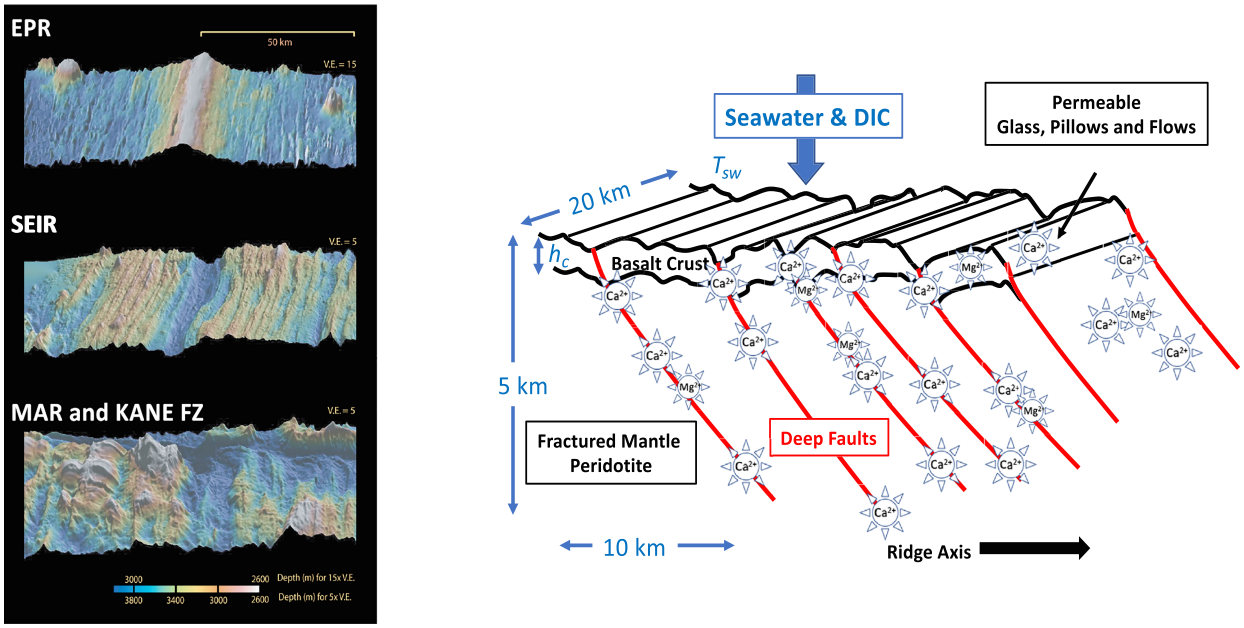

Figure 7. Schematic illustration of the spreading rate-crustal production rate controls on the seafloor weathering. (Left) Examples of relatively smooth topography of a fast ridge (East Pacific Rise, EPR), rough and highly fractured and faulted topography of a slow ridge (Southeast Indian Ridge, SEIR), and complex and highly fractured and faulted topography of a slow ridge-fracture zone (Mid-Atlantic Ridge, MAR and the Kane Fracture Zone, Kane FZ) (images modified from Buck et al., 2005). (Right) Cartoon showing the net production of alkalinity by low-temperature water flows through permeable basalt pillows and lava flows forming a crust with thickness h_c and by water flow that penetrates mantle peridotite via the deep fractures and faults that distinguish slow from fast spreading ridges. This alkalinity flux can drive carbonate precipitation within the hydrothermal system, depending on the appropriate thermodynamic conditions (e.g., Rudge et al., 2010) or elsewhere in the ocean basins.

orogenesis will be concentrated within supercontinental interiors during formation (Figure 1) (e.g., Veevers & Powell, 1994). Assuming that the geometry of resulting wedge-shaped mountain ranges and plateaux are governed predominantly by the average strength of the crust undergoing deformation (e.g., Dahlen, 1984; Roe & Brandon, 2011), both their height and aspect ratio will increase in proportion to time over a collisional episode $t^{1/3}$ (Appendix B). An implication of this prediction is that to the extent that orographic precipitation increases with topographic height and windward flank length for given atmospheric conditions (Roe & Baker, 2006), the majority of continental surface weathering will also increasingly become concentrated within the interiors of these landmasses. However, although the distribution of rainfall and surface runoff generally depends on the character and geometry of uplift (Appendix B and Roe & Baker, 2006), the intensity of this rainfall and surface runoff is governed mostly by the proximity to coastal moisture sources (Donnadieu et al., 2004). Supercontinent formation, on average, is thus expected to reduce rainfall and erosion, and the strength of the surface weathering sink for atmospheric CO_2, in turn (Cox et al., 2010; Donnadieu et al., 2006; Fiorella & Poulsen, 2013; Goddéris et al., 2008, 2012; Otto-Bliesner, 1995). Apatite-fission-track and apatite-(U-Th)/He data from the Gamburtsev subglacial mountains in interior East Antarctica, for example, indicate rates of topographic loss from 250 to 500 Ma comparable to the low relief Canadian shield (Cox et al., 2010). An additional prediction to which we return briefly in discussion in section 7 is that a reduced rate of surface weathering will also decrease the supply of limiting nutrients (P, N, Fe) from the continents to the oceans leading to less biological productivity.

If extensive mantle thermal mixing is preserved during supercontinent formation (cf. Lenardic et al., 2011, and references therein), there will be little change to outgassing rates beyond effects related to changing arc or mid-ocean ridge (MOR) lengths (Lee et al., 2013; Zahirovic et al., 2015). In response to a weakening surface weathering sink, more CO_2 will be retained in the atmosphere resulting in a warmer world, and the continental supply of nutrients to the oceans will be less, a prediction we discuss in section 7.3. By contrast, if subduction around the margins of a nascent supercontinent leads instead to lateral temperature differences between the suboceanic and subcontinental upper mantles as a result of some level of mantle thermal isolation (cf. Lenardic et al., 2011, and references therein), two additional effects enter to influence volcanic

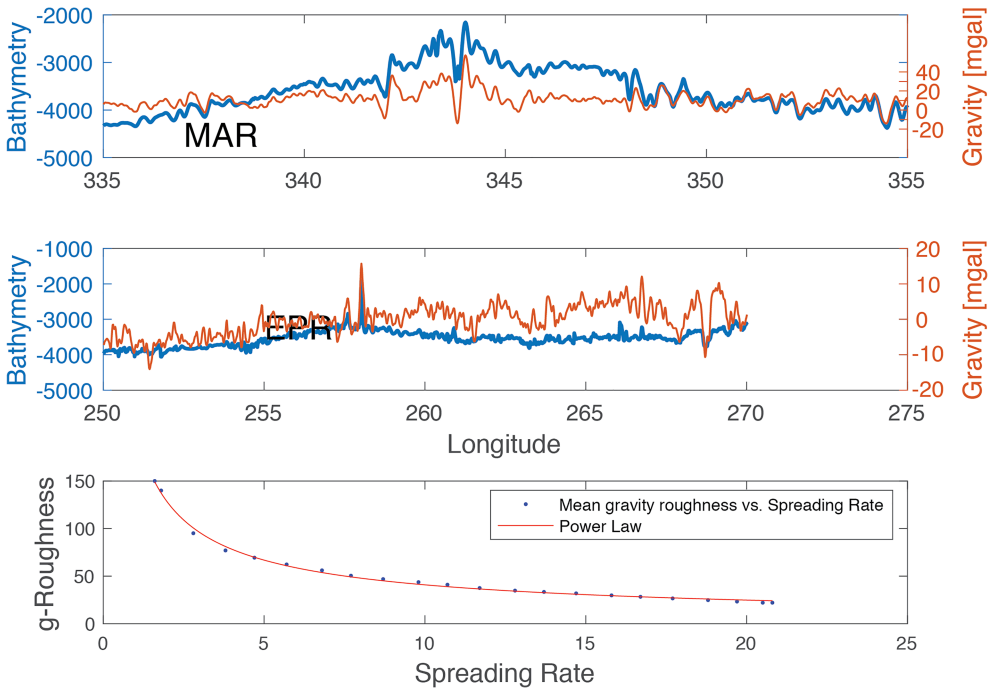

Figure 8. Examples of topographic and gravitational roughness for the East Pacific Rise and the Mid-Atlantic Ridge, as well as a power law fit to the mean gravitational roughness as a function of spreading rate reported in Small and Sandwell (1989) and Small (1998) (see text).

sources and weathering sinks for atmospheric CO_2 in distinct ways. First, global plate spreading and subduction rates will decline as the average suboceanic mantle viscosity increases exponentially with declining temperature, driving correspondingly less basalt magmatism and CO_2 outgassing at mid-ocean ridges and arcs. A second effect is that enhanced subcontinental warming will produce significant continental uplift and sea-level fall that can enhance mechanical erosion in the interior (Braun et al., 2014; Roe et al., 2008) and orographic precipitation (Roe, 2005), as well as the delivery of alkalinity to distant oceans in groundwater systems (Maher & Chamberlain, 2014). Depending on the magnitude of mantle thermal isolation, which sets the strengths of these effects on outgassing and weathering rates, Earth's climate during supercontinent formation may be significantly different to the perfect mixing endmember. If the surface weathering sink declines in a similar way as expected for perfect thermal mixing, the expected reduction in outgassing rates will, by contrast, lead to a relatively cold world.

CO_2 is drawn down from the atmosphere also by seafloor weathering processes (Figure 7). For a given pH and water temperature, the strength of this sink depends on the alkalinity produced as a result of the circulation in reactive low-temperature MOR hydrothermal systems and the subsequent precipitation of carbonate either within these systems or elsewhere in the ocean basins. A major control on the character of this circulation is the structure and depth extent of rock permeability. Assuming that long-time averaged fracture- and fault-controlled permeability increases in proportion to topographic and gravitational roughness (Small & Sandwell, 1989, 1994), in a way consistent with models (e.g., Buck et al., 2005), we hypothesize that seafloor hydrothermal flow and the vertical extent and intensity of resulting water-rock chemical reactions can increase inversely as approximately a power law function of spreading rate (Figure 8). Consequently, we suggest that the seafloor weathering sink will be maximized when seafloor spreading and crustal production rates are minimized in response to oceanic mantle cooling when a supercontinent forms. We propose that this potentially enhanced flow rate of seawater through more reactive mantle rocks composed of pyroxene-feldspar-olivine mineral assemblages may outweigh the temperature dependence of the kinetics of the weathering reactions in low-temperature systems (Brady & Gíslason, 1997; Coogan & Dosso, 2015; Coogan & Gillis, 2018; Krissansen-Totton & Catling, 2017) such that the magnitude of the seafloor weathering sink may become larger during supercontinent formation in an isolation regime, as outgassing and surface weathering rates decline. Inclusion of this intensifying of the seafloor weathering sink leads to a prediction for a colder world when a supercontinent is assembled compared to one governed by, for

example, surface weathering alone. An important caveat is that this picture assumes that normal faults are permeable on average, that this permeability remains open, and that processes governing a reaction-driven production and destruction of permeability (e.g., Peuble et al., 2018; Rudge et al., 2010) are in approximately steady-state over order 10^5- to 10^6-year time scales (and that a steady-state exists).

Our proposed tectonic control on permeability and, thus, on the extent of the interaction of hydrothermal flows with mantle rocks is in contrast to the typical view of how seafloor weathering operates (e.g., Spivack & Staudigel, 1994). Thus, some additional comments are warranted. Conventionally, reactive hydrothermal flows are thought to be controlled volcanically and concentrated within the permeable lava pillows and flows forming basaltic crust at MORs (e.g., Alt & Teagle, 1999; Brady & Gíslason, 1997). Seafloor weathering is, on this basis, usually parameterized to be maximized where crustal production rates are high (Brady & Gíslason, 1997; Sleep & Zahnle, 2001). A tectonic control on permeability predicts, by contrast, that seafloor weathering will be enhanced at slow spreading ridges, where crustal production rates are low. Furthermore, the strength and character of this seafloor weathering sink for atmospheric CO_2 will evolve with spreading rate in a way that is the reverse of the conventional view. However, our picture is potentially in line with the Gillis and Coogan (2011) findings that the link between CO_2 uptake and crustal production is at best tenuous and that the Cenozoic uptake of CO_2 is on average 2–5 times greater in the Atlantic than Pacific basin. This interpretation is at odds with the Gillis and Coogan (2011) conclusion that the predominant control is seawater temperature for a given $[Ca^{2+}]$, although these authors do not consider effects related to the potential for differing hydrothermal flow regimes. Nevertheless, we test this tectonic as well as the conventional volcanic parameterizations for the seafloor weathering sink in climate calculations in section 7. We show that the choice of seafloor weathering model can exert a strong control over climates predicted at peak supercontinent formation. For the Rodinia epoch, in particular, we show that whereas inclusion of this tectonically modulated seafloor weathering sink can lead to panglacial (snowball) climates in the Cryogenian, such snowball solutions are potentially impossible with the conventional volcanic control. As a final comment here, it is important to make clear that the two mechanisms are not mutually exclusive. The two conceptual pictures are endmembers and enter depending on global average MOR spreading and crustal production rates, which set the relative contributions of each mechanism through the depth extent of fault/fracture permeability and the vertical thicknesses of pillow/lava flow sequences (7). Our expectation is for the tectonic control to govern the drawdown of atmospheric CO_2 during formation in a thermal isolation-remixing regime where MOR spreading rates are minimized globally. Volcanic control will exert a strong control otherwise.

4.2. Climate Controls During Supercontinental Breakup and Mantle Thermal Remixing

If the mantle remains thermally well mixed during both formation and breakup, the major effect of opening oceans and strengthening the surface weathering sink, in turn, is to reduce atmospheric CO_2 and cause a colder climate, on average (Donnadieu et al., 2004; Goddéris et al., 2008). A corresponding enhanced delivery of limiting nutrients to the oceans will lead also to more biologically productive oceans and a potential proclivity for ocean anoxic events, which we discuss in section 7.

By contrast, in a mantle transitioning from a thermal isolation to a remixing regime, two geodynamic processes will act together to modulate a relatively more complex climate response (Figure 2). First, relatively warm subcontinental mantle will intrude and spread toward mid-ocean ridges between the lithosphere base and underlying cold, dense oceanic mantle as a relatively low viscosity gravity current (Figure 5). As the oceanic upper mantle temperature gradually rises, spreading and subduction rates will increase with the declining suboceanic mantle viscosity along with the rates of mantle melting (Figure 8). This order 10- to 100-million-year transition to a world of predominantly fast spreading ridges potentially causes a marked transition in the regimes of seafloor and terrestrial surface weathering. In particular, thickening crust at MORs, a decline in fracture permeability and a resulting reduction in the extent of interactions between seawater and mantle rocks with increasing spreading rate will cause this sink to weaken compared to surface weathering. This predicted evolution is consistent with the enhanced uptake of CO_2 in the Pacific immediately following Pangea breakup, when tropical SST temperatures are minimized and when we expect spreading rates to be low (Figure 4).

Depending on the magnitude of lateral mantle temperature variations acquired during supercontinent assembly, supercontinental breakup can involve spreading continental fragments that overrun adjacent subduction zones and drive them into compressional continental arc modes (Lee et al., 2013;

Spencer et al., 2019) (Figure 2). In addition to their sliding down dynamic topographic gradients, the viscous coupling of continental fragments to warm mantle material spreading into mid-ocean ridges causes them to be drawn toward adjacent subduction zones to drive accretion. When such arc-continent collisions are concentrated particularly within the tropics (Donnadieu et al., 2004; Hoffman et al., 2017; Goddéris et al., 2008, 2012), uplift, which may be enhanced isosatically by inferred increased silicic magmatism during the breakups of Pangea and Rodinia (Lee & Lackey, 2015; McKenzie et al., 2016), will increase gradually over the evolution time of breakup $t^{1/3}$ (Appendix B). Assuming that orographic precipitation effects on erosion increase with the height and aspect ratio of the orogeny and with a reduced distance to upwind moisture sources, this process will stimulate mechanical erosion and strengthen the chemical weathering sink for CO_2 (e.g., Dahlen, 1990; Dixon et al., 2012; Hilley & Strecker, 2004; Roe et al., 2008; Whipple, 2004; Whipple & Meade, 2004, 2006). Potential important consequences of this uplift include the marked exposure of highly weatherable ophiolite rocks in continent-forearc sutures (Macdonald et al., 2019), although there is current vigorous discussion of the reality of this compositional control (Zhang & Planavsky, 2019).

In summary, during breakup and mantle thermal remixing, Earth's climate is inherently transient, and the climate response can be complex. Generally, MOR melting, crustal production, and outgassing increase depending on the the rate at which the gravity current of warm mantle advances into the MOR melting region (the depth range over which melting can occur) and the distance over which this flow occurs. We consequently predict a time lag between the start of breakup and any increase in MOR outgassing rates that is plausibly of order 10 million years. As this intrusion of warm mantle cools, these rates decay back toward pre-supercontinent values. At the same time, surface weathering shifts in space as well as in intensity, while the main mechanical controls over the strength of the seafloor weathering sink evolve. Compared to a pre-supercontinental world, a qualitative expectation where mantle thermal isolation occurs is that this period will be marked by a geologically rapid transition from relatively cold to warm worlds, followed by a gradual recovery. Like the projected cooling at the peak of supercontinent formation, the longevity and intensity of any warming during this period will depend strongly on the magnitude of the mantle thermal isolation, which, in particular, governs the change in volcanic outgassing rates as well as the significance and strength of the tectonically modulated seafloor weathering sink. Where the mantle remains thermally well mixed and climate is affected only by an evolving strength of the surface weathering sink during formation, the opposite climate pattern is possible during breakup.

5. Mantle Thermal Isolation-to-Remixing and Global Volcanic Sources for CO_2 and CH_4: Parameterizations

5.1. Evolving Volcanic CO_2 Sources at Arcs, MORs, and Ocean Islands

Assuming approximately constant arc and MOR lengths, the change in the global CO_2 outgassing rate with supercontinent formation will be governed not only by the extent of any thermal isolation but also by the longevity of this regime compared to a mantle overturn time. The longer the thermal effect of continental insulation can remain restricted to mantle below a supercontinent, the larger will be the resulting ocean-continental mantle temperature and viscosity variations (Figure 9) (cf. Lenardic et al., 2011, and references therein), which controls the rate of vertical advection of mantle rocks across their solidus. For a given ascent speed, the vertically averaged flux of mantle melt depends on the depth range over which the mantle temperature T_m exceeds the solidus temperature T_{sol} (i.e., the melting region height). At each vertical position in the melting region z, where the average temperature $\bar{T}(z)$ is greater than the solidus temperature T_{sol}, the excess temperature available to drive melting is $\Delta T_m(z) = (\bar{T}(z) - T_{sol})$. This temperature difference implies, in turn, a melt fraction $\phi(z) = C_p \Delta T_m(z)/L$ and a melt production rate per area $\Gamma(z) = \phi(z)\bar{V}_m$. Here, C_p and L are the specific and latent heats, and $\bar{V}_m$ is the average mantle upwelling velocity. The total melt production per area over the height of the melting region h_{melt} gives the flux into MOR and arc magmatic systems:

$$Q_m = \int_0^{h_{melt}} \Gamma(z) dz. \tag{2}$$

If the temperature of ascending oceanic mantle is reduced during supercontinental formation, the height of the melting region will decline, and the flux of melt delivered to the crust and to the surface is less, in turn. However, mantle upwelling at MORs and at arcs is largely a passive response to subduction, the speed of which V_s is proportional to an appropriate mantle viscosity that increases by about an order of magnitude

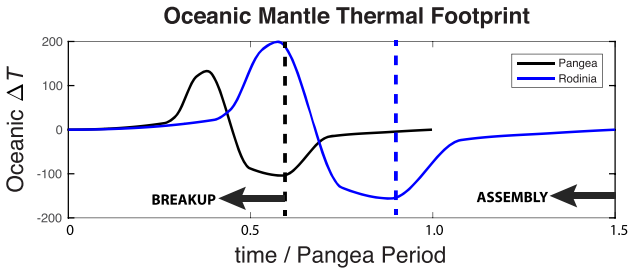

Figure 9. Hypothesized "temporally symmetric" evolutions of the oceanic mantle temperature during the Pangean and Rodinian epochs. Whereas the Pangean evolution is ground truthed using observations and geodynamic models (see text), the Rodininian evolution is proposed on the basis of a temporally similar cooling-warming climate variability . Assuming temporal symmetry in the responses of the mantle thermal regime to supercontinental assembly and breakup, the longer-lived Rodinia supercontinental epoch will produce a proportionally more extreme lateral mantle temperature variations (see text). Here the reference "Pangea Period" is 300 million years, and the vertical dashed lines indicate the start of supercontinental breakup and mantle thermal remixing.

per 100° of cooling. Neglecting potentially complex dependencies on plate size, subduction regime, and plate composition (Zahirovic et al., 2015), we take the global average mantle upwelling rate V_m at arcs and MORs to be approximately equal to the global average subduction rate. Relative to a scale for this overturn speed V_s^0 in an initial thermally well-mixed state (Figure 5), the change in subduction rate is approximately (e.g., Solomatov & Moresi, 2000)

$$\frac{V_s}{V_s^0} \propto \left(\frac{1}{\exp(-\zeta T_{m,o})} \right)^{2/3}. \tag{3}$$

Here, ζ is a rheological temperature scale appropriate for mantle rocks deforming, on average, in a diffusion creep regime (see Jellinek & Manga, 2004, and references therein).

The choice of an appropriate sub-oceanic mantle temperature $T_{m,o}$ requires discussion. In particular, our models show that lateral temperature variations will be confined largely to the upper mantle over time scales comparable to the Pangea and Rodinia supercontinental cycles. Furthermore, the spatial character of lateral temperature variations during breakup and mantle thermal remixing can be complex (Figure 5). The choice of an appropriate average temperature to apply to equation (3) is consequently not straightforward. Accordingly, rather than specifying $T_{m,o}$ on the basis of modeling results and introducing uncertainty through some assumption about the extent of isolation, which is then amplified through the exponential form of equation (3), we will follow Becker et al. (2009) and apply their observational and modeling constraints that limit the increase in the spreading rate at the breakup of Pangea to be about a factor of 2 larger than at present day. This bound on the maximal increase in spreading rate at Pangea breakup essentially implies an effective thermal mixing extent for the Pangean epoch. We recognize that that the magnitude of lateral oceanic-continental upper mantle temperature variations are sensitive to the distinctive style and heat transfer properties of mantle convective stirring motions, which are not uniquely predicted by analog experiments or numerical simulations (Lenardic et al., 2011). Seismic reflection and petrologic studies of overthickened crust related to the Atlantic Eastern Magmatic Province (Figure 4) and the major element chemistry of post-breakup lavas adjacent to rifted continental fragments (Brandl et al., 2013; Kelemen & Holbrook, 1995) are, however, consistent with lateral temperature variations of around 150 °C at the time of Pangea breakup. This result is in accord also with a recent global compilation suggesting that upper mantle temperatures, crustal production, and cooling rates were enhanced in the Atlantic and Indian ocean basins compared to the Pacific at 170 Ma (Van Avendonk et al., 2017), a picture which is also inferred on the basis of the unusually smooth Jurassic seafloor in the Atlantic (Whittaker et al., 2008). On the basis of these varied observational data, we take the maximum lateral upper mantle temperature variation during the Pangean epoch to be 150 ° C.

Beyond the post-breakup Cryogenian glaciations and the Ediacaran glacial retreat toward the poles, there are a dearth of proxy constraints for the detailed cooling-warming climate during the the Rodinia epoch. However, on the basis of a similar temporal shapes in the trends in proxy data for magmatism and surface weathering in Figures 3 and 4, we hypothesize similar mantle thermal mixing dynamics. Because we have no constraints on peak continental-oceanic mantle temperature variations, we make a further assumption that the extent of oceanic mantle cooling is in proportion to the longevity of this cycle compared to a Pangea baseline (Figure 9). Although we cannot rule out more or less extensive thermal mixing over the longer duration of the Rodinia cycle, this assumed temporal symmetry with Pangea is, on average, plausible. In particular, we can apply results from numerical simulations summarized in Figure 5 and constraints from published results (see Lenardic et al., 2011, and references therein), which show that the depth-averaged magnitude of lateral temperature variations ultimately scale with the number of mantle overturns on the ocean mantle side of a model slab in the case of perfect thermal isolation. An obvious caveat with this treatment is that in imposing temporal symmetry we are also assuming that there is a qualitative similarity in the planform of subduction, which determines the lateral heat transfer properties of the mantle flow. The notable difference between the temporal patterns of LIP volcanism during the breakups of Pangea and

Rodinia (Figures 3 and 4) indicates that this picture should be viewed cautiously and at this stage as only a reasonable thought experiment. Bearing in mind these assumptions, we test our hypothesis nevertheless and discuss implications of relaxing this assumption in section 8.

At arcs, the mantle temperature excess ($T_{m,c} - T_{sol}$) is enhanced during supercontinental formation because warm mantle is ponded beneath the continent. This effect is, however, modulated by a reduced average subduction rate related to the effect of relatively strong upper oceanic mantle cooling on the average mantle viscous stresses retarding plate subduction (cf. equation (2)). Thus, we take the mass flux of CO_2 related to mantle melting to be

$$F_{arc} \propto V_s^{\beta}(T_{m,c} - T_{sol}), \tag{4}$$

where $T_{m,c}$ is the average subcontinental mantle temperature and T_{sol} is the mantle solidus. The exponent $\beta < 1$, and we discuss this value below.

In constructing equation (4) we make three assumptions. First, we take the average efficiency of slab decarbonation, which increases with mantle potential temperature (Dasgupta, 2013), to be approximately constant and comparable to present day since 1 Ga. Although reasonable as a global average assuming around ~50K mantle cooling since 1 Ga (Jaupart & Mareschal, 2010), locally this picture may underestimate CO_2 outgassing driven as a result of melting relatively warm sub-arc mantle over the duration of a supercontinental cycle. Second, we assume that the average compositions of continental rocks and accreted material that are involved in melting and magmatism are unchanged. Although probably appropriate for the Nuna and Rodinia cycles, this assumption leads plausibly to a factor of 2–3 underestimate for the flux of volcanic CO_2 from arcs during the breakup of Pangea (Lee & Lackey, 2015; Lee et al., 2013). Finally, we assume that the total lengths of active volcanic arcs remain unchanged. Rigorous observational constraints on changes in arc and/or mid-ocean ridge lengths during Rodinia and Pangea supercontinental cycles are challenging, although recent reconstructions from varied geological data and plate kinematic models suggest increases in the total length of rifts at the times of Rodinia and Pangea assembly (Merdith et al., 2019) and increases on the length of continental arc at the start of the breakup of Pangea relative to present day (e.g., Lee et al., 2013; Müller et al., 2016; Spencer et al., 2019).

At mid-ocean ridges, the effects of a reduced mantle potential temperature and a slower upwelling rate compound to reduce overall melting and volcanic CO_2 outgassing from ridges

$$F_{mor} \propto V_s(T_{m,o} - T_{sol}). \tag{5}$$

Depending on the extent of thermal isolation and the magnitude of the resulting temperature variations, the consequences for outgassing as well as for the strength of the seafloor weathering sink for CO_2 can be significant. For example, in the special case that mantle melting and crustal production ceases entirely at MORs, on the basis of the present-day CO_2 mass balance, the total global volcanic outgassing of CO_2 might be reduced by as much as 50% compared to present day.

Finally, long-time globally averaged volcanic outgassing from ocean islands and LIPs F_{oib} contributes probably 10–15% of the global volcanic input of CO_2 at present day (e.g., Marty & Tolstikhin, 1998). Although numerical simulations and laboratory experiments (Jellinek & Lenardic, 2009; Lenardic et al., 2011; Robin et al., 2007; Thayalan et al., 2006) show that the changing planform of mantle stirring during isolation and in an isolation-to-remixing regime can cause this volcanism to cluster in time after breakup, consistent with the Pangea proxy data in Figure 4, this behavior is inevitably sensitive to the geometric setup of any model and to the detailed planform of subducting slabs. Indeed, this sensitivity of the timing of LIP volcanism to the planform of subduction and MOR spreading is inferred from new plate motion models of Pangea breakup (East et al., 2019). A practical consequence is that it is not possible to reliably parameterize changes in this class of volcanism in terms of globally averaged values for V_s or $T_{m,o}$. It is, thus, also not possible to explore global effects of this volcanism on the strength of the weathering sink for CO_2, which we address below. In calculations below we use the structure of the LIP time series in Figures 3 and 4 to constrain changes in F_{oib}: Whereas a delayed arrival of mantle plumes following Pangea breakup leads to an enhanced F_{oib} beginning around 130 Ma, there is no change in F_{oib} related to the assembly and the breakup of Rodinia.

5.2. Abiotic CH_4 Forcing From MORs in a Low-Oxygen Rodinian World

When a supercontinent is fully formed in an isolation regime, an important additional prediction is that oceanic crustal production at mid-ocean ridges will be minimized and can cease entirely. An important consequence is that Earth's oceans will be to a greater extent in contact with mantle peridotite than the basalt flows and pillows forming oceanic crust. A characteristic feature of present-day deep ocean hydrothermal vent plumes hosted in such ultramafic rocks within the mid-Atlantic ridge is a very large flux of abiotic CH_4 (Bougault et al., 1993; Charlou et al., 1998; German & Von Damm, 2006; German et al., 2010; Kelley et al., 2005; Konn et al., 2009; Rona et al., 1992). From these observations, as well as modeling (Bradley & Summons, 2010) and experimental studies of olivine serpentinization (Berndt et al., 1996; Horita & Berndt, 1999), the hydrothermal circulation of seawater with dissolved CO_2 leads to a volumetrically significant conversion of Fe(II) in olivine to Fe(III) in magnetite and to the production of H_2 and the release of CH_4 gas through "Fischer-Tropsch" reactions of the form:

$$(Fe, Mg)_2SiO_4 + nH_2O + CO_2 = Mg_3Si_2O_5(OH)_4 + Fe_3O_4 + CH_4. \quad (6)$$

If the resulting flux of CH_4 into the deep ocean drives a flux of CH_4 into the atmosphere, in turn, this process can provide an additional radiative forcing, depending on pO_2 and the ratio CH_4/CO_2 (Hörst et al., 2018). Furthermore, because the exposure of olivine-rich mantle rocks to hydrothermal seawater is maximized where the otherwise protective layer of basalt crust is thin or absent, CH_4 production will be enhanced when supercontinents are fully formed and minimized during their breakup.

The accumulation in the atmosphere of this abiotic CH_4 released into the deep ocean depends on sulfate and oxygen levels and the productivity of methanotrophs (Fakhraee et al., 2019; Olson et al., 2016). In the sulfate- and oxygen-rich, biologically productive present-day and Pangean oceans, through microbially mediated anaerobic oxidation of CH_4 that is coupled to efficient SO_4^{2-} reduction, little CH_4 is expected to escape to the atmosphere (Olson et al., 2016). Furthermore, what CH_4 enters these oxygen-rich atmospheres will be oxidized to form CO_2 within a few years to a decade. By contrast, more of this predicted abiotic methane flux into the deep ocean is likely to escape a low SO_4^{2-} and low O_2 Neoproterozoic ocean into the atmosphere (Fakhraee et al., 2019), although this expectation will depend on the predominant methanotrophic metabolisms, which remain uncertain (S. A. Crowe, personal communications, 2019). Constraining the magnitude of an abiotic CH_4 flux to the deep ocean and atmosphere even asymptotically is challenging and unavoidably speculative. In particular, this flux will depend not only on the average rate of abiotic methane production but also on complex factors including the magnitude and variability of marine sulfate levels, the particular metabolisms involved in anaerobic methane oxidation particularly at low SO_4^{2-} levels, the extent to which the ocean is oxygenated over its full depth, the areal extent of mid-ocean ridges compared to present day, and the heights to which CH_4 bubble-rich hydrothermal vent plumes penetrate stabilizing ocean density stratification, as well as their advection by ocean currents (Carazzo et al., 2013).

For the climate calculations in section 7, we do not try to predict the CH_4 flux to the atmosphere. We simply explore greenhouse forcing driven by 10- to 300-ppm CH_4 to the Neoproterozoic atmosphere (Olson et al., 2016; Pavlov et al., 2003). This maximal concentration is below values that could lead to haze formation and associated strong climate cooling through inverse greenhouse forcing (Haqq-Misra et al., 2008; Hörst et al., 2018; McKay et al., 1991). We will show in section 7 that this additional greenhouse forcing can enhance the likelihood for intermittency of a tectonically driven Neoproterozoic panglacial climate, depending on the predominant mechanisms of seafloor weathering.

6. Mantle Thermal Isolation-to-Remixing, Weathering Sinks, and a Mechanical Modulation of the Long-Term Inorganic Carbon Cycle

Over long geological time scales, the rate of change of the concentration or partial pressure of atmospheric carbon dioxide pCO_2 depends on the volcanic input of CO_2 discussed in the last section and the rate at which this greenhouse gas is drawn down as a result of chemical weathering processes on land and within low-temperature seafloor hydrothermal systems. Normalized to present-day conditions indicated by the subscript "$_0$" the rate of change of pCO_2 is

$$\frac{d}{dt}\left(\frac{pCO_2}{pCO_{2,0}}\right) = \frac{1}{\tau_{eq}}\left(\frac{\Sigma F_{volc}(t)}{\Sigma F_{volc,0}} - \frac{\Sigma W(t)}{\Sigma W_0}\right), \quad (7)$$

where $\tau_{eq} \sim 10^4$ [years] is the characteristic response time for the ocean-atmosphere system. This time scale is governed by processes governing the uptake of atmospheric CO_2 and carbonate compensation and is influenced by the total alkalinity of the ocean and the mechanics governing N, P, and Fe nutrient cycling (Williams & Follows, 2011). Assuming that seafloor and surface weathering processes act over time scales that are much greater than τ_{eq}, which is consistent with the variability evident in Figures 4 and 3, this carbon cycle can be approximately in balance (quasi steady state), and equation (7) simplifies to

$$\frac{\Sigma F_{volc}(t)}{\Sigma F_{volc,0}} = \frac{\Sigma W(t)}{\Sigma W_0}. \tag{8}$$

As an additional comment, in writing equations (7) and (8) we focus on the inorganic carbon cycle because it is in this contribution that mantle dynamic and plate tectonic controls on the sources and sinks for atmospheric CO_2 are most clearly expressed. Furthermore, the contribution of inorganic carbon burial to the carbon cycle is relatively large. On the basis of $\delta^{13}C$ values in the range 0–2‰ for Pleistocene carbonates, the rate of inorganic carbon burial is currently probably a factor of 5 larger than the rate of organic carbon ($\delta^{13}C_{org} = -25‰$) burial to balance the volcanic ($\delta^{13}C_{volc} = -5‰$) input (e.g., Hayes et al., 1999). Assuming the same $\delta^{13}C$ values for volcanic and organic carbon, the larger $\delta^{13}C$ values for Neoproterozoic cap carbonates suggest higher rates of organic burial, although this interpretation is made complex by potential significant additional diagenetic effects on the structure of the time series data that are potentially enhanced a low-oxygen Neoproterozoic ocean (Ahm et al., 2018, 2019; Schrag et al., 2013).

6.1. Surface Weathering

On land, the chemical weathering-driven removal of CO_2 from the atmosphere-ocean system typically involves the dissolution of silicate minerals through Urey reactions of the form:

$$H_2CO_3 + H_2O + (\text{pyroxene, olivine, feldspar, etc.}) = HCO3^- + (Ca^{2+}, Mg^{2+}, Fe^{2+}, \dots) + (\text{clays}), \tag{9}$$

where the resultant delivery of divalent cations on the right hand side of equation (9) (alkalinity) to the oceans leads ultimately to the precipitation and storage of carbonate minerals at the seafloor, which is ultimately subducted into the mantle.

In soils with a given concentration of reactable mineral faces, for a given surface and groundwater availability, the rate and extent to which Urey reactions proceed depends on Earth's surface temperature. In this kinetically limited picture (Kump et al., 2000; White & Brantley, 2019), the weathering rate

$$\dot{W} \propto \exp(-G_{eff,i}/RT); \quad i=_{\mathrm{g,b}}. \tag{10}$$

Here, for a zero-dimensional model the appropriate temperature T is the global mean surface temperature of the planet. The strength of the implied "weathering thermostat" (e.g., Li et al., 2016; Walker et al., 1981) is governed by the magnitude of the activation energy G, the laboratory values for which differ for granitic and basaltic rocks (subscripts "$_g$" and "$_b$").

More generally, the strength of this sink is modulated by the availability of surface water, which governs mechanical bedrock erosion, the delivery of fresh (unreacted) silicate mineral faces to growing soil profiles, and the extent of reactions within soil profiles (e.g., West, 2012; West et al., 2005). To explore the link between chemical weathering and physical erosion in a transport limited regime involving bedrock erosion, it is convenient to write

$$\dot{W} \propto \dot{E}(\dot{P}(T))^{\alpha}. \tag{11}$$

In this form, $\dot{P}(T)$ is a surface temperature-dependent precipitation rate (Pierrehumbert, 2010) and is a proxy for global mean surface runoff (see Perron, 2017, and references therein). The quasi steady state erosion rate $\dot{E}$ balances a long-time averaged tectonic uplift rate in convergent arc settings and depends on the bedrock being eroded (Whipple, 2004). The power law exponent α is usually obtained from data or models (see below). From global climate models, compared to present day, precipitation rates increase or decrease by approximately 3% per degree of warming or cooling (Pierrehumbert, 2010). This relationship will break down in the limits of global glaciation ($\dot{P}(T) \to 0$) as well as for extreme greenhouse forcing where the rate of latent heat release implied by the precipitation rate balances the incoming short-wavelength solar flux.

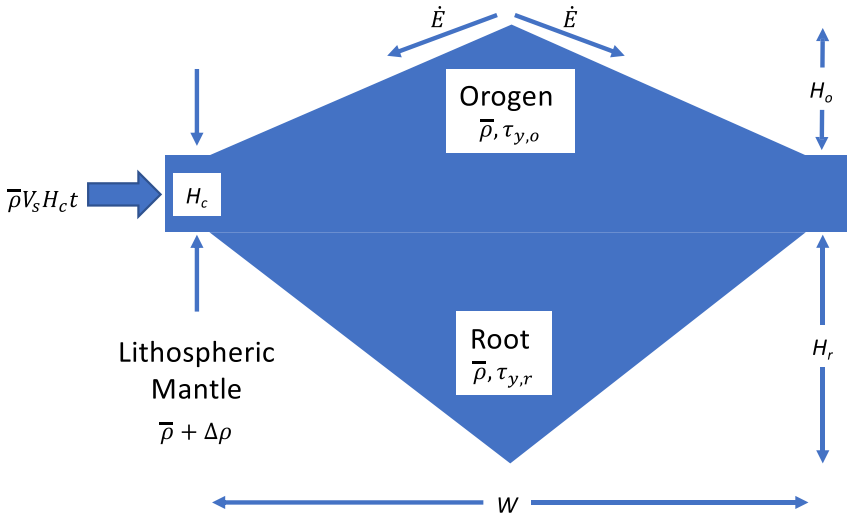

Figure 10. Cartoon showing the relationships among subduction rate, one-sided accretion, orogenesis, and erosion at continental arcs expected to be active during supercontinental breakup. This sketch is for a symmetric critically tapered wedge (see text). A similar picture holds for the production of plateaux related to continent-continent collision during supercontinent assembly. One difference is that accretion can be from both sides of the wedge. The notation shown applies to a scaling analysis for the growth of a wedge-shaped orogen developed in Appendix B.

A power law relationship between weathering and erosion at the landscape scale is consistent with field-based studies and global compilations for a range of climates and rock types (Ferrier et al., 2016; Riebe et al., 2004). At convergent continental arcs (Figure 10), a power law behavior is expected on theoretical grounds where accretion can drive a self-similar uplift of approximately wedge-shaped crustal orogens with a frictional (yielding) rheology (Dahlen, 1984, 1990; Hilley & Porder, 2008; Roe et al., 2006, 2008; Whipple & Meade, 2004). Consistent with this work, scaling arguments to which we refer in section 1 and Figures 1 and 2 and develop in Appendix B show that the height and aspect ratio of nascent mountain ranges will increase as time $t^{1/3}$.

Because the climate response to the breakups of Rodinia and Pangea record transients over 1- to 10-million-year time scales (Figures 4 and 3), an important question related to the reality of a meaningful global mean tectonic control on this response is at what stage in the evolution of a nascent compressional orogen will erosion and chemical weathering be in balance such that equation 11 holds globally. A bound on the appropriate time scale is the order 1-million-year chemical weathering response time inferred from the chemistry of large rivers (e.g., Gaillardet et al., 1999), which is consistent with theoretical considerations for the fluvial response time governed by a stream-power incision model (Whipple, 2001). Taking critical evolution times to be 10^5–10^6 years for reasonable crustal properties and tectonic conditions (Appendix B), such ranges will be order 1 km high and order 10^2 km wide. For given climate variables (air temperature and humidity), modest wind speeds of order 10 m/s and droplet condensation altitudes of 2–4 km, rainfall will occur over the majority of such extensive windward flank lengths leading to spatially extensive rainfall and surface runoff (i.e., a maximal "rainfall efficiency" defined as the rainfall rate onto an orogen flank normalized to a droplet condensation rate) (Roe & Baker, 2006) (Appendix B). Over time scales for the climate change in the proxy data for Rodinia and Pangea (Figures 4 and 3), equation (11) with a globally averaged temperature-dependent precipitation rate is, thus, reasonable.

Orogens at the margins of continents in the humid tropics will have higher average rates of rainfall on their windward flanks than interior ranges that are a long distance from moisture sources, leading to a prediction that the surface weathering sink will be relatively weak during supercontinent assembly and relatively strong during breakup for a given surface temperature (cf. Figures 1 and 2) (Donnadieu et al., 2004; Fiorella & Poulsen, 2013). We crudely explore climate consequences of expected reduced total precipitation rates during supercontinent assembly in section 7 by modifying the total temperature-dependent global precipitation:

$$\dot{P} = \Upsilon \dot{P}(T). \tag{12}$$

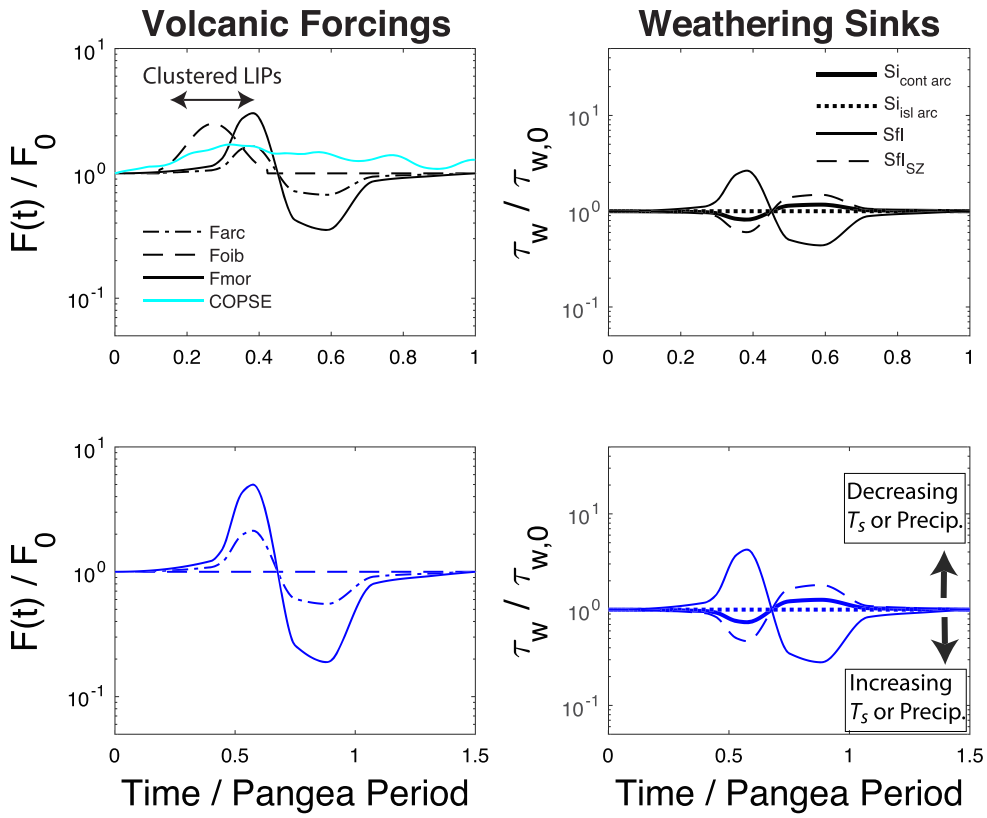

Figure 11. (Left column) Time-varying MOR, arc, and ocean island/LIP volcanic CO_2 forcings drawn from equations (5) and (4) for (black curves) Pangea- and (blue curves) approximate Rodinia-length supercontinental epochs assuming temporal symmetry in the mantle thermal mixing response to assembly and breakup (cf. Figure 9). For the Pangea-length calculation we infer a delayed increase in the ocean island basalt (oib)/large igneous province (LIP) contribution F_{oib} from Figure 4. This volcanic forcing is held constant in all Rodinia calculations. Also shown for comparison is the volcanic forcing inferred from high-resolution sea-level reconstructions and applied in the most recent Carbon, Oxygen, Phosphorous, Sulfur Evolution (COPSE) biogeochemical model (cf. Lenton et al., 2018). (Right column) Surface and seafloor weathering responses to the volcanic forcing are for continental and island arc weathering regimes (CA and IA) (equation (15)) as well as for seafloor weathering (SF) (equation (16)). To isolate the effects of evolving plate spreading and subduction rates alone, these calculations assume a constant surface temperature and precipitation rate. Qualitative consequences of increasing or decreasing Earth's surface temperature or spreading rate are indicated with the heavy black arrows. Changes in the island arc and continental surface weathering sink strengths are indicated by the ratio of the time scale for the weathering response normalized to the pre-supercontinent reference value: Where this ratio is less than 1, the weathering response time is reduced in comparison to a reference response time of 1 million years, and weathering is relatively more intense. Because both the surface temperature and precipitation rates are held fixed, the island arc regime does not change during these model supercontinental cycles. Similarly, we compare the evolving strengths of the seafloor weathering sink that increases with a crustal production rate proportional to V_s as per Sleep and Zahnle (2001) (SZ) with the behavior expected if the sink strength increases as $1/V_s$, in response to increasing fault and fracture permeability as V_s declines. Here the reference "Pangea Period" is 300 million years (see text).

Here, motivated by the global climate modeling results of Donnadieu et al. (2004) who find nearly a factor of 2 reduction in total precipitation with a model Rodinia formation, as well as the analytical models of Roe and Baker (2006) of orographic effects that will evolve with global surface temperature and humidity as the height and aspect ratio of nascent orogens evolve at differing rates (Appendix B), we prescribe an effective rainfall efficiency $0 \leq Y \leq 1$. To explore parametrically the maximal effects of intracontinental drying during formation, we carry out calculations for $\Upsilon = 1$ and $\Upsilon = 0.5$ during Pangea and Rodinia assembly. Although equation (11) with $\dot{P} = \dot{P}(T)$ is justified, on average, over the evolutions of the assemblies and breakups of Pangea and Rodinia, on the basis of recent comparative studies of the Loess Plateau, China, and the Central Range, Taiwan, we recognize that orographic effects may be complex during the very early stages of orogenesis at the margins of spreading continental fragments when topography is potentially far from equilibrium

(Willett et al., 2014). Furthermore, weathering is not confined to the humid tropics where precipitation rates are maximized and weathering and physical erosion can also be decoupled with cooler global temperatures at the start of breakup, as is apparent in proxy data from the South China Sea since 8.5 Ma (Clift et al., 2014). Accordingly, we also carry out climate calculations with a reduced rainfall efficiency over the model period representing the time lag between the start of breakup and the subsequent peak in volcanic forcing corresponding to the arrival of warm subcontinental mantle into the MOR melting region (Figures 9 and 11).

An additional consideration is the value of the power law exponent α. Where long-time averaged landscape-scale evolution is dominated by fluvial erosion (i.e., fluvial erosion rates are much larger than erosion by abiotic and biotic soil creep processes on hill slopes, Culling, 1963; Gabet et al., 2003; Perron, 2017), chemical weathering will be rate limited by mechanical erosion and $\alpha \to 1$ (e.g., Ferrier et al., 2016; Riebe et al., 2004). By contrast, in steep terrains characterized by episodic landslides, the rapid delivery of material outpaces the rate of reaction and $\alpha < 1$ (Gabet, 2007). Where the residence time of water stored in soils trapped within basins adjacent to interior mountains is very large in comparison to the time scale for the flow of groundwater $\alpha \to 0$ (cf. Maher & Chamberlain, 2014), and we recover equation (10). An additional process that probably enters into the global surface weathering sink during the ice sheet retreats that we predict in section 7 to occur during the Cretaceous and in the aftermaths of Neoproterozoic snowball events is glacial erosion. Because the mechanics and chemical weathering efficiency of this mode are complex and influenced by the details of glacier sliding (e.g., Egholm et al., 2012; Herman & Braun, 2008) as well as the meltwater drainage regime (Grau Galofre et al., 2018; Schoof, 2010), we neglect this process here.

Combining mechanical and kinetic considerations, a scaling for the chemical weathering rate of silicate rocks on land is of the form:

$$\dot{W}_{su} \propto \dot{E}(\dot{P}(T), V_s)^{\alpha} \exp(-G_i/RT) \quad , \quad i=_{\mathrm{g,b}}, \tag{13}$$

where the erosion rate, including its explicit dependence on spreading and precipitation rates, enters as a control parameter we must specify. For island arc erosional regimes that do not involve a tectonically driven production of topographic gradients beyond volcanism, we assume weathering to be rate limited by processes acting in soils. On the basis of observational studies (e.g., Dessert et al., 2001, 2003, 2015; Riebe et al., 2004), in this limit $\alpha \approx 1$, and whereas the erosion rate depends on the rate of precipitation, it is independent of the spreading rate V_s.

If over long time scales mechanical bedrock erosion depends mostly on the average turbulent shear stress imparted to rock forming river beds or, alternatively, on the power delivered by turbulent motions to do this work of abrasion, then for a specified erosional efficiency (Whipple & Meade, 2004) the rate at which silicate minerals are weathered at the landscape scale is

$$\dot{W}_{su} \propto \dot{P}^{\phi} V_s^{\gamma} \exp(-G_i/RT) \quad , \quad i=_{\mathrm{g,b}}, \tag{14}$$

where (Roe et al., 2006) $0.2 \leq \phi \leq 0.33$ and $0.33 \leq \gamma \leq 0.6$. Recognizing the range of precipitation and accretion controls, we take $\phi = (1/5)$ and $\gamma = (2\beta/5)$. Here, the subduction rate is related to the accretion rate F_a such that $V_s \propto F_a^{\beta}$. The functional dependence of the accretion rate F_a on the subduction rate V_s will depend on factors affecting the mechanical coupling of the downgoing slab to the overlying continent. The compositions, constitutions, rheologies, and three-dimensional structures of both the continental margin and the subducting slab, as well as the underlying mantle structure (Moresi et al., 2014), ultimately enter into this problem. However, a basic control on accretion is the rate of delivery of new material by subduction, and in the absence of rigorous observational constraints, we take $\beta = 1$.

Assuming that accretion occurs at continental arcs and is negligible at island arcs, we normalize the weathering rates to present-day conditions and write a generalized scaling for global silicate weathering rates in these two tectonic limits (Figure 11):

$$\frac{\dot{W}_{su}}{\dot{W}_{si,0}} \propto \begin{cases} \left(\frac{\dot{P}}{\dot{P}_0}\right)^{\phi_{su}} \exp\left[\frac{-G_{eff}}{RT}\left(1-\frac{T}{T_0}\right)\right] & \text{IA} \\ \left(\frac{\dot{P}}{\dot{P}_0}\right)^{\phi_{su}} \left(\frac{\dot{V}_s}{\dot{V}_{s,0}}\right)^{\gamma_{su}} \exp\left[\frac{-G_{eff}}{RT}\left(1-\frac{T}{T_0}\right)\right] & \text{CA,} \end{cases} \tag{15}$$

where "IA" and "CA" refer to the "island arc" and "continental arc" weathering modes.

Noting the small difference between activation energies for granite and basalt weathering inferred from field-based studies over varied climatic regimes (cf. Dessert et al., 2001; Kump et al., 2000; Riebe et al., 2004), and a growing literature suggesting a weak or complex temperature dependence of weathering kinetics (e.g., Krissansen-Totton & Catling, 2017; Kump et al., 2000; Riebe et al., 2004; White & Brantley, 2019), we take $G_b \approx G_g$ and an average effective activation energy for all rocks $G_{eff} = 40$ KJ/mol K. We also neglect the much higher weathering efficiency of basaltic (or ultramafic) rocks for a given climate regime (Macdonald et al., 2019; Swanson-Hysell & Macdonald, 2017; White & Brantley, 2019) on two practical grounds. The first is that the dependencies of basalt and granite weathering rates on surface runoff differ in studies of individual catchments (Ibarra et al., 2016), which makes parameterizing a global average challenging. Second, compared to the Pangean cycle, the relative surface areas of basaltic and granitic rocks exposed to river systems through the Nuna and Rodinia cylces, including varied and poorly constrained areal extents of LIP volcanism, are challenging to reconstruct (cf. Bluth & Kump, 1991; Gibbs et al., 1999; Goddéris et al., 2014).

In this parameterization the island arc mode is independent of the subduction rate, and weathering occurs implicitly within soil profiles of fixed thickness (e.g., Walker et al., 1981; West, 2012). In form, the island arc scaling is similar to that found by Dessert et al. (2001) in an exhaustive study of the chemical weathering of the Deccan basalts as well as by Ferrier et al. (2016) for kinetically limited weathering in granitic soils. In a pure continental arc regime, by contrast, we assume that denudation rates are sufficiently high for weathering to be governed by bedrock erosion (West, 2012) and there is an additional climate regulation through a power law dependence on V_s. Indeed, the most significant uncertainty in equation (15) is the functional dependence of a global average accretion rate on subduction rate for which there are few constraints. For given rates of subduction, the value for β probably varies with sediment supply and character, as well as the subduction angle, which affects the entrainment and erosion of this material. We neglect strong compositional transients such as rapid emplacements of large igneous provinces (e.g., Cox et al., 2016; Dessert et al., 2001) and the emergence of ophiolite rocks, which are important features of arc-continent collisions (Macdonald et al., 2019). We also ignore differences in the dynamics of the hydrologic storage/flow processes modulating the delivery of alkalinity to the oceans, which will be distinct in the two arc regimes through factors such as the differing proximities of weathering processes to oceans and differences in continental dynamic topography (Maher & Chamberlain, 2014) (Figure 1).

6.2. Seafloor Weathering

Carbonate deposition driven by the low-temperature hydrothermal circulation of seawater through permeable, highly reactive mantle rocks (Kelley et al., 2001; Ludwig et al., 2006), basaltic glasses, and crystalline basalt crust provides an additional important source of alkalinity and a sink for atmospheric CO_2 (Alt & Teagle, 1999; Brady & Gíslason, 1997; Coogan & Gillis, 2018; Gernon et al., 2016; Gillis & Coogan, 2011; Krissansen-Totton & Catling, 2017; Spivack & Staudigel, 1994; Staudigel et al., 1989, 1996) (Figure 7). At present day, the flux of seawater through these hydrothermal systems is comparable to the flux of riverine freshwater into the ocean (Coogan & Dosso, 2015; Elderfield & Schultz, 1996), and the flux of CO_2 into oceanic crust to drive calcite precipitation is also comparable to that which is delivered by MOR degassing (Alt & Teagle, 1999; Saal et al., 2002). More importantly for the drawdown of atmospheric CO_2, the fluxes of alkalinity into the ocean from seafloor and silicate weathering processes are also of the same order of magnitude, although there is considerable uncertainty (potentially $0.5-3\times10^{12}$ mol/year from seafloor weathering, Alt & Teagle, 1999; Coogan & Dosso, 2012; McDuff, 1981; Staudigel et al., 1989, and $3-4\times10^{12}$ mol/year for silicate weathering, e.g., Francois & Walker, 1992).

The intensity of alkalinity production within low-temperature seafloor hydrothermal systems increases with seawater temperature, albeit with a complex dependence on the composition of the material through which water circulates (Brady & Gíslason, 1997), is relatively insensitive to pH for cold ocean bottom water temperatures with pH >6 (Gislason & Oelkers, 2003), and should also increase with the flow rate through permeable host rocks. We extend the seafloor weathering parameterizations of Brady and Gíslason (1997) and Sleep and Zahnle (2001), the former of which introduces and calibrates a linear relationship between the temperature of ocean bottom waters and atmospheric pCO_2 on the basis of GCM calculations by Manabe and Broccoli (1985), which is consistent in form to expectations from constraints arising from a recent exhaustive proxy data analysis (Krissansen-Totton & Catling, 2017). We take the change in the rate of seafloor weathering

relative to present-day conditions to be

$$\frac{W_{sf}}{W_{sfl,0}} \propto \left(\frac{V_s}{V_{s,0}}\right)^{\epsilon_{sf}} \left(\frac{q_c}{q_{c,0}}\right)^{\theta_{sf}} \left(\frac{\mathrm{pCO_2}}{\mathrm{pCO_{2,0}}}\right)^{\alpha_{sf}}. \quad (16)$$

Here, the exponent $\alpha_{sf} \approx 0.3$ (Brady & Gíslason, 1997, equation (1)) captures the temperature dependence of the weathering reactions. We include the dependence on rock composition qc for completeness. However, we set the exponent $\theta_{sf} = 0$ in our calculations: Whether a power law dependence on composition is justified and what is the form of this dependence is unknown.

The dependence on spreading rate enters as a proxy for an increase in deep fault/fracture-controlled permeability and, thus, flow rate, with declining V_s, which we infer from increases in topographic and gravitational roughness (Figure 8). Topographic and gravitational roughness data collapse to a power law with $\epsilon_{sf} \approx -0.95$ and suggest that fracture permeability increases approximately in proportion to $1/V_s$. A significant feature of this parameterization is that the relative extent to which seawater interacts with mantle rocks as opposed to basaltic pillows increases as spreading rates decline. How to constrain a dependence of the spatially and temporally averaged host rock composition on a crustal production rate q_c, which determines the thickness of lava flow and pillow sequences and the overall exposure of mantle rocks to seawater, is challenging. Although a power law dependence is reasonable to expect at large time, the value of θ_{sf} is unclear. In our calculations below, we consequently set $\theta_{sf} = 0$.

Although equation (16) with $\theta_{sf} = 0$ differs in form only by the sign of the exponent ϵ, this parameterization is distinct physically from that proposed by Brady and Gíslason (1997) and Sleep and Zahnle (2001) in two important ways. First, in taking $\epsilon \approx -1$ rather than $\epsilon = 1$, we depart from a conventional assumption that hydrothermal circulation is confined primarily to permeable stacks of pillow basalts, which increase in thickness with V_s and crustal production rate. We propose instead that a tectonically modulated deep regional-scale fracture permeability will exert a greater control over the extent of water-rock interactions and the resulting flux of alkalinity carried by hydrothermal circulation into the ocean. Assuming that Darcy's law holds adequately for regional-scale hydrothermal circulation within connected faults and fractures, this flux will increase in proportion to fracture permeability, which increases as spreading rates decline (Figure 11).

More generally, the value for ϵ_{sf} implies the predominate permeability mode, and the range $-1 \leq \epsilon_{sf} \leq 1$ captures, in principle, the extent to which alkalinity production is governed by flow through stacked pillow basalts or deep faults and fractures that access mantle rocks. By taking ϵ_{sf} to be constant and equal to -1 or 1 over a given epoch provides a way to explore limiting tectonic controls on this sink strength. In reality, both modes will be active except where crustal production rates are negligible or spreading rates are exceedingly large. Furthermore, the permeability regime is likely to be further modulated by the efficiency of mineral precipitation and permeability production from these very reactive flows, which will be enhanced for higher bottom water temperatures and flow rates (Rudge et al., 2010). Last, an additional and newly quantified contribution to alkalinity production on the seafloor may be the reaction of seawater with basaltic glasses to form hyaloclastite (Gernon et al., 2016), which is enhanced at fast spreading ridges. The extent to which this process offsets the control of deep fracture permeability by driving $\epsilon_{sf} \rightarrow 1$ or affect the compositional dependence of equation (16) is unknown. As a final comment here, although speculative, our proposed parameterization is plausible. There is, for example, observational support for greater CO_2 uptake into basalts along the topographically rough Mid-Atlantic Ridge (MAR) than the fast spreading and relatively smooth East Pacific Rise (EPR) over the last 40 million years during periods of relative cold (Figure 4). The apparent similarity in CO_2 uptake at the EPR and MAR during from ~115 to 45 Ma inferred from two drill cores supports the potentially strong sensitivity of the weathering reactions to ocean temperature as discussed in detail by Coogan and Gillis (2013). We test the sensitivity of our climate calculations to the choice of ϵ_{sf} below.

6.3. Supercontinental pCO_2 Modulation in a Mantle Isolation-to-Remixing Regime on a Constant Albedo Earth

The kinetics of surface weathering reactions have a dependence on surface temperature that gives rise to the so-called weathering thermostat (Walker et al., 1981). Consequently, any calculation of the long-term steady-state pCO_2 cycle for an Earth with dynamic ice sheets with equation (8) must couple the weathering sink to a climate model involving a radiation balance affected by a changing ice line latitude and an ice-albedo feedback. We will carry out these numerical calculations in section 7. However, in this section we

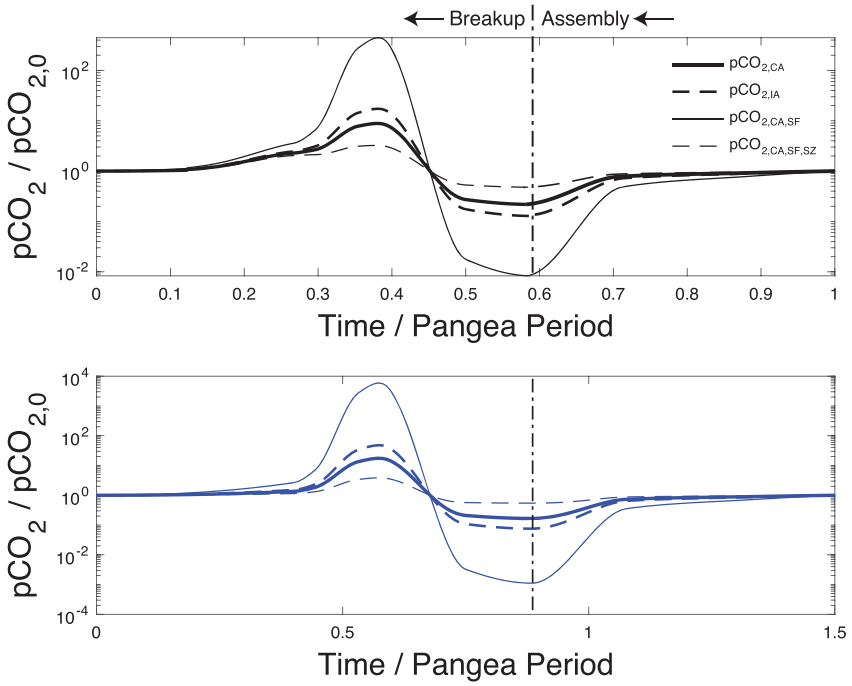

Figure 12. Atmospheric $pCO_2/pCO_{2,0}$ evolutions calculated with equation (18) for the special case $\bar{\alpha} = 0.3$ and a constant precipitation rate. For the temporally symmetric Pangea-length (black curves) and Rodinia-length (blue curves) evolutions, the volcanic forcing shown in Figure 11 is balance by surface weathering operating in the island arc (IA) or continental arc (CA) mode with and without additional seafloor weathering with $\epsilon = -1$ or the more conventional $\epsilon = 1$ (SZ), consistent with Sleep and Zahnle (2001). Through equation (A2) with constant CH_4, the surface weathering rates are each proportional to $pCO_2/pCO_{2,0}{}^{4C/B\ln(2)}$, where the quantity $4/B\ln(2)C \approx 2.9C$ with the climate sensitivity $B = 2$ [W/K m^2]. We take $C = (G/RT_s) \approx 0.1$ over the range of published activation energies (G = 20–100 [KJ/mol], for surface temperatures T_s sufficiently warm that surface weathering contributes significantly to the total chemical weathering sink for atmospheric CO_2, and with the universal gas constant $R = 8.3145 \times 10^{-3}$ [KJ/mol K]. To facilitate an approximate analytical scaling with $\bar{\alpha} = 0.3$, we take $4/B\ln(2)C = 0.3$. These calculations are for $A_{sf} = 0.15$. (See text and Appendix A.)

first consider a constant albedo Earth with a fixed precipitation rate to develop physical intuition for how evolving tectonic controls on the mechanics of surface and seafloor weathering sinks enter into equation (8) to modulate expected time-varying volcanic CO_2 sources (Figure 11). We will show pCO_2 responses for each of the surface and seafloor weathering modes we consider in section 5 in Figure 12. Because we explicitly assume temporal symmetry in the mantle thermal mixing response to supercontinent formation in an isolation-to-remixing regime, the intensity of the variability in the volcanic forcing during a model Rodinia epoch is enhanced in proportion to its greater longevity compared the Pangean epoch. Accordingly, to make clear this control over volcanic forcing, we normalize time to a reference Pangean period of 300 million years in Figures 11 and 12.

For an Earth composed of fixed areas of land, sea, and ice, we can write the temperature dependence of the weathering kinetics in terms of $pCO_2/pCO_{2,0}$ (cf. (A2) with a constant [or specified] $pCH_4/pCH_{4,0}$). For the special case of $\bar{\alpha} = 0.3$ and the power law exponents $\phi = 0.2$, $\theta = 1$ and $\epsilon = 0.1$, for a specified precipitation rate $\dot{P}$ and no dependence of seafloor weathering on rock composition, we combine equations (5), (4), (15), and (16) with

$$\frac{\Sigma W(t)}{\Sigma W_0} = \frac{\Sigma W_{su}(t)}{\Sigma W_0} A_{su} + \frac{\Sigma W_{sf}(t)}{\Sigma W_0} A_{sf}, \tag{17}$$

to obtain approximately, after algebra using (A2):

$$\frac{\mathrm{pCO}_2(t)}{\mathrm{pCO}_{2_0}}(\Delta T_{m,o}, V_s, \dot{P}, t) \propto \left[\left(\frac{\Sigma F_{in}(\Delta T_{m,o}, t)}{F_0} \right) \times \left(\frac{1}{A_{su}\left[\left(\frac{\dot{P}(t)}{P_0} \right)^{\phi} \left(\frac{V_s(t)}{V_{s,0}} \right)^{\gamma} \right]_{su} + A_{sf} \left[\left(\frac{V_s(t)}{V_{s,0}} \right)^{-\epsilon_{sf}-\theta_{sf}} \right]_{sf}} \right) \right]^{1/\bar{\alpha}} . \tag{18}$$

Here, the subscripts $_{su}$ and $_{sf}$ indicate surface and seafloor weathering contributions. We take the areal fraction of the surface weathering sink $A_{su} = 0.85$ and seafloor weathering $A_{sf} = (1-A_{su})$, which is plausible for present-day Earth (Gillis & Coogan, 2011; Krissansen-Totton & Catling, 2017), and potentially a lower bound (Sleep & Zahnle, 2001).

In this heuristic scaling, volcanic forcing depends on the oceanic mantle temperature change, and a tectonic control on surface and seafloor weathering enters through power law dependencies on the spreading/subduction rate V_s and the value of the weathering regime parameter γ. Here, $\gamma = 0$ in a purely island arc tectonic regime, and $\gamma \approx 0.4$ in a purely continental arc regime. In Figure 11 the evolving gain or strength of the weathering sink through model Pangean and Rodinian supercontinental cycles is expressed in terms of a normalized time scale for the weathering response: Where this ratio is less than 1, the time scale of the weathering response is shorter, and weathering rates are consequently enhanced compared to the start of the cycle. For example, during supercontinental formation both volcanic forcing and the time scale for surface weathering response will decline as V_s becomes small compared to present day. As a consequence of the increase in MOR fracture permeability, however, the time scale for the seafloor weathering response becomes shorter. During breakup, as volcanic forcing and spreading rates increase, seafloor weathering becomes negligible, and pCO_2 is modulated by surface weathering alone. If breakup also drives a transition to convergent continental arc tectonics, this sink will also increase with V_s. If we apply instead a more typical seafloor weathering scaling with $\epsilon = 1$, this sink tracks the behavior of the surface weathering sink, with a response time that increases to a maximum at supercontinent formation. In section 7 we will show that this essential difference between the behaviors of these seafloor weathering parameterizations will have significant consequences, for example, for the extent to which plate tectonics modulates Earth's entry into a protracted cold Cryogenian period with global glaciations during Rodinia breakup.

Atmospheric pCO_2 variability predicted for Pangean- and Rodinian-length epochs with equation (18) are shown for a constant precipitation rate in Figure 12 for each weathering mode we consider. The magnitude of the variability is larger for the longer epoch, consistent with the evolving volcanic forcing in Figure 11 to which each weathering mode responds. For an unchanging precipitation rate, when the weathering response to the mantle-controlled volcanic CO_2 forcing is entirely in the island arc mode, $\mathrm{pCO}_2/\mathrm{pCO}_{2,0} \propto \Sigma F_{in}(\Delta T_{m,o}, t)^{1/0.3}$. By contrast, where the volcanic forcing is balanced only by terrestrial surface weathering in the continental mode, the changing rates of subduction and accretion lead to a factor of 2–3 smaller variability: Minimum and maximum $\mathrm{pCO}_2/\mathrm{pCO}_{2,0}$ values at assembly and during breakup are less. If a seafloor weathering sink is included with a response time that grows or shrinks with reduced or enhanced MOR spreading and crustal production rates ($\epsilon_{sf} = 1$) (Brady & Gíslason, 1997; Sleep & Zahnle, 2001), this variability is reduced further. By contrast, if the response time for seafloor weathering declines as spreading and subduction rates grow ($\epsilon_{sf} = -1$), the tectonically driven variability can be 1–3 orders of magnitude larger in amplitude. This very strong climate sensitivity at assembly, in particular, will enter into our discussion of Cryogenian global glaciation in section 7.

7. Supercontinental Climate Control in an Evolving Mantle Thermal Isolation-to-Remixing Regime

To explore more realistic mantle-climate evolution scenarios for Pangea and Rodinia, we now couple the dynamics of chemical weathering in the long-term carbon cycle to a Budyko-style energy balance model (EBM) for Earth's climate (Appendix A). In particular, in carrying out these calculations, we allow global average precipitation rates and the kinetics of weathering reactions to adjust to shifts in surface temperature driven by time-dependent changes in the latitudinal extent of polar ice sheets (the “ice line”), which has a strong effect on the global average albedo and Earth's average surface temperature, in turn (Figure 13). In comparison to the atmospheric pCO_2 predicted with equation (18) (cf. Figure 12), inclusion

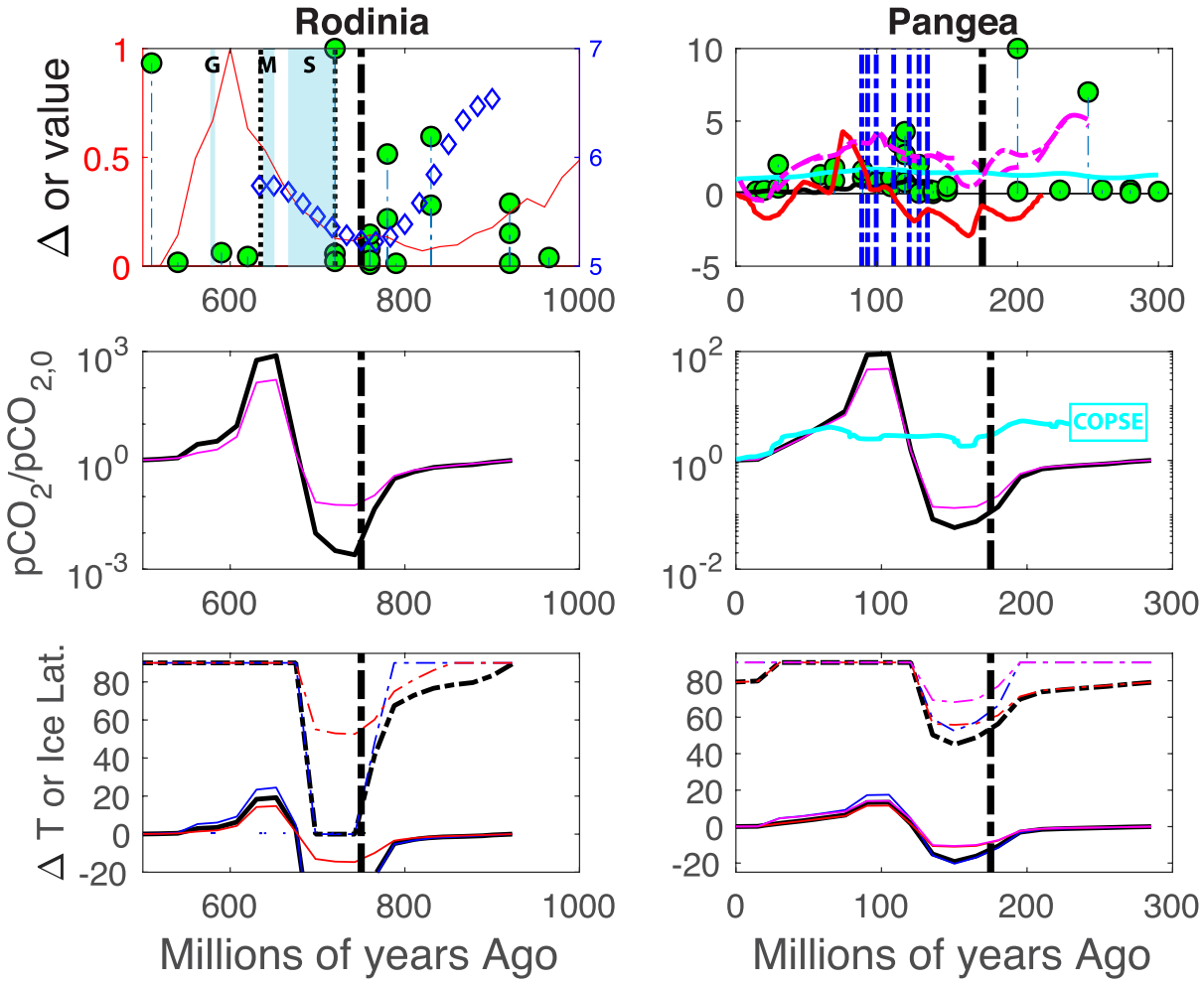

Figure 13. Proxy data from Figures 4 and 3 (top panels) compared with evolutions for Pangean and Rodinian $pCO_2/pCO_{2,0}$ (middle panels), surface temperature change ΔT, and polar ice line latitude (lower panels) predicted by implementing our long-term inorganic carbon cycle model coupled to the EBM outlined in Appendix A (see text). For comparison, we show a $pCO_2/pCO_{2,0}$ evolution during the Pangean epoch calculated using the COPSE biogeochemical model (Lenton et al., 2018). As with Figures 11 and 12, the surface area fractional contribution of the seafloor weathering sink $A_{sf} = 0.15$. Here, $pCH_4 = 5$ ppm. (middle panels) Evolutions of $pCO_2/pCO_{2,0}$ for the Rodinian (left) and Pangean epochs (right) with seafloor weathering sink strength increasing with MOR spreading rate ($\varepsilon_{sf} = 1$, cf. Brady & Gíslason, 1997; Sleep & Zahnle, 2001, and section 6.2) (magenta line) and increasing with declining spreading rate as we propose ($\varepsilon_{sf} = -1$ in equation (16), cf. section 6.2) (heavy black curve). The two limiting values for ε_{sf} are upper and lower bounds expected from our model: Both mechanisms will contribute to seafloor weathering except in the special circumstance of zero MOR crustal production. (bottom panels) Corresponding ice line positions (dash-dot curves) and surface temperature changes (solid lines) for seafloor weathering with $\varepsilon_{sf} = -1$ (black) and $\varepsilon_{sf} = 1$ (red). Also shown are calculations for reduced precipitation rates ($\Upsilon = 0.5$) for seafloor weathering with $\varepsilon_{sf} = -1$ (blue) and $\varepsilon_{sf} = 1$ (magenta) (see text). Calculations incorporating additional modest effects of crustal composition ($0.2 > \theta_{sf} > 0$ in equation (16) for the specified ε_{sf} values) are not shown but give intermediate solutions.

of an EBM-controlled global surface temperature control over global mean precipitation rates and the kinetics of terrestrial surface weathering will produce generally more modest pCO_2 maxima during breakup and similar or greater pCO_2 minima at assembly, depending on the seafloor weathering mode.

Although more complete than the scaling results presented in section 6, the goal of these calculations is not to reproduce the detailed climates of the Mesozoic and Neoproterozoic but to understand basic tectonic controls on the cold-warm climate variability that characterized both periods in greater detail. Indeed, whereas a cooling-warming climate variability is a robust feature of a mantle thermal isolation-to-remixing regime, the precise timing and intensity of this variability depends on the setup of the mantle thermal mixing model, as we discuss above and return to below. Here, we retain the assumption of temporal symmetry between the mantle responses to the Pangea and Rodinia supercontinental epochs (cf. Figure 9) as well as a constant $A_{su} = 0.85$, not inconsistent with recent inferences for the Mesozoic and present day (e.g., Krissansen-Totton & Catling, 2017). We also assume a symmetric northern and southern hemisphere continental distribution,

which simplifies our EBM calculations to be one-dimensional (zonal) and appropriate for capturing the predominant contributions of reconstructed continental areas centered roughly on the equator to the mean albedo. This setup allows for polar ice caps as well as ice-free and panglacial ("snowball") climates that are an intrinsic property of state-of-the-art global climate model calculations (e.g., Abbot et al., 2013; Fiorella & Poulsen, 2013; Pierrehumbert et al., 2011). To limit the model parameter space and not introduce additional degrees of freedom in the absence of similarly rigorous observational constraints for both epochs, we again take arc and MOR lengths to remain unchanged through the Pangean and Rodinian cycles. We neglect, for example, new plate motion modeling constraints suggesting that an increase in MOR length contributed to a factor of 2 increase in the flux of material subducted at continental arcs from 180 to 130 Ma (East et al., 2019). We also ignore contributions of crustal carbonate to magmatism and to topography production and weathering since Pangea breakup (Lee et al., 2013, 2015). For the Pangean epoch, in particular, our approach links the predicted climate change explicitly to the spatially averaged mantle thermal history in Figure 9 using three constraints from the proxy data discussed in section 2 (cf. Figure 4): (a) the inferred lateral continental-oceanic mantle temperature variations, (b) the structure of the time series of LIP volcanism, and (c) the evolution in MOR spreading rate.

For surface weathering sinks, we prescribe a smooth transition from a purely island arc mode to a purely continental arc mode with the supercontinental breakup indicated in Figure 13. In reality, this transition is unlikely to be smooth at the start: Breakup will probably produce topographic disequilibrium the character of which is currently manifest on Taiwan (Willett et al., 2014) that can drive complex orographic as well as erosional responses. The rainfall efficiency Υ introduced in section 6 will, for example, probably evolve with collisional orogen aspect ratio toward our parameterized global mean value that is set by surface temperature. To build intuition of this transient as well as that related to uplift during supercontinent assembly, we carry out crude calculations with reduced total precipitation. In addition, following the breakup of Pangea surface weathering was potentially enhanced in response to temporally clustered large igneous province-related basaltic volcanism (Figure 4) (e.g., Dessert et al., 2001). To explore potential effects of expected abiotic CH_4 production at MORs (cf. section 5), we include 10- to 100-ppm methane during the low-oxygen Rodinian epoch (e.g., Fakhraee et al., 2019; Olson et al., 2016; Pavlov et al., 2003; Roberson et al., 2011). By contrast, we assume that little CH_4 leaves the ocean to enter the atmosphere in the Mesozoic and carry out calculations for 5 ppm CH_4.

To understand the sensitivity of the results to whether seafloor weathering is governed by our proposed tectonically controlled fault/deep fracture permeability (cf. (16) with exponent $\epsilon_{sf} = -1$) or the permeability of MOR lava flows (equation (16) with exponent $\epsilon_{sf} = 1$), we carry out calculations with both weathering parameterizations. As a final remark here, our calculations are intended only to build understanding of general climate trends related to supercontinental cycles occurring in a mantle isolation-to-remixing regime. Although our models are highly simplified, predicted steady-state climates at each stage of the Pangean and Rodinian evolutions would serve as useful starting conditions for full global climate model (GCM) calculations.

7.1. Cooling-Warming Variability Related to Pangea: From Midlatitude Jurassic Ice Sheets to Ocean Anoxia and Cretaceous Warming

The precise timing of a mantle dynamic contribution to the Mesozoic climate change in Figure 4 relative to the well-established start of Pangea breakup depends on the detailed character of the mantle response to Pangea assembly and fragmentation. In particular, whereas we can reliably constrain a 10- to 100-million-year time lag between the start of breakup and the pCO_2 response in the surface Earth system (cf. equation (1)), predicting the exact timing and magnitude of this climate change inevitably depends on the model for thermal isolation and remixing, and, thus, we rely on the proxy data in Figure 4. For a specified magnitude of lateral temperature variation (cf. section 5), the temporal form of the climate variability is, however, a robust feature of the thermal isolation-to-remixing regime (cf. Figures 9 and 11). Consequently, we use our climate calculations to address three questions related to the extent to which a mantle isolation-to-remixing thermal regime driven by the assembly and breakup of Pangea ultimately paced Earth's Jurassic-Cretaceous cooling-warming climate oscillation (Figure 4). The first is simply: Can we understand the qualitative form of the tropical sea-surface temperature evolution in Figure 4? Second, is our predicted climate change consistent with shifts in the latitudinal position of polar glacial ice lines inferred from geological data? Finally, is the predicted terrestrial surface weathering contribution to this climate variability consistent with the occurrence and timing of discrete and global ocean anoxia events (OAE1

and OAE2, Figure 4) which may be partly related to enhanced nutrient delivery governed by land surface processes?

From an initial steady-state model mantle-climate system, the mantle thermal isolation-to-remixing model with a seafloor weathering strength that increases as MOR spreading rates decline predicts that pCO_2 will fall to about 5% of the initial value with Pangea formation and overshoot by a factor of around 100 with breakup of the supercontinent, following a time lag of around 50 million years (Figure 13). By contrast, with a Sleep and Zahnle (2001)-style seafloor weathering mode that increases in strength with MOR crustal production rate, pCO_2 falls to about 13% of the initial value at formation and overshoots by around a factor of 50 during breakup. For both seafloor weathering models, the corresponding global average temperature variation is similar in form to the tropical sea-surface temperature record, although characterized by higher amplitude variability. Peak cooling and warming are reduced and increased for a factor of 2 decrease in the precipitation rate for $\Upsilon = 0.5$. Finally, the maximal increase in terrestrial surface weathering strength required to enforce the steady-state CO_2 mass balance implies an enhanced delivery of nutrients to the oceans that is correlated with temporally clustered global ocean anoxia events (Figure 4, Jenkyns, 2010, 2018).

The model Pangean epoch ice line begins in the high latitudes, advances to around 50° N and S prior to breakup and retreats to the poles as pCO_2 rises to a maximum at 120 Ma, before recovering a 80° N/S latitude by around 30 Ma. The character of the predicted climate change is similar in form to the pattern of variability in reconstructed sea-surface temperatures (Figure 13). The peak ice line advance with the strongest cooling is less with a Sleep and Zahnle (2001)-style seafloor weathering mode and for a reduced precipitation. However, polar ice persists until 120 Ma, nevertheless. These predictions for the occurrence and latitudinal extent of a persistent dynamic ice sheet well into the start of the Cretaceous warm period evident in SST data between 160 and 60 Ma (Figure 4) are consistent qualitatively with global peaks in the frequencies of occurrence of the calcite pseudomorph glendonite as well as glacial deposits such as dropstones (Price, 1999; Price & Nunn, 2010), which indicate deep ocean temperatures ≤ 4 ° C. That polar caps persisted in spite of overall very strong Cretaceous global warming is also consistent with high-latitude ice-rafted debris (Frakes & Francis, 1988; Frakes et al., 1995, 2005). In addition, $\delta^{18}O$ and $\delta^{13}C$ data from glendonites and belemnites from the Euromanga basin, Australia, as well as other basins of comparably high paleolatitude, indicate very cold ocean bottom temperatures at latitudes of around 70° S (De Lurio & Frakes, 1999) during the warm period between 140 and 100 Ma.

An additional implication of a persistent ice sheet during the Cretaceous warm period is that the well-known intermittent cold excursions (e.g., Lee et al., 2013), which are evident in paleosea-level reconstructions (Haq et al., 1988; Miller et al., 2005), in proxy data for Cretaceous Arctic deep ocean temperatures (Price & Nunn, 2010), and varied proxy data from a broad range of paleolatitudes (e.g., Amiot et al., 2011; Stoll & Schrag, 1996) are not unexpected. The presence of polar ice indicates that Earth's climate is sufficiently cool that small changes in the global radiation balance related to, say, orbital forcings or protracted volcanic aerosol forcing (e.g., "Climate change 2007: The physical science basis. Contribution of Working Group I to the Fourth Assessment Report of the Intergovernmental Panel on Climate Change," 2007; Ridley et al., 2014; Schmidt et al., 2012, 2016) will drive ice line advances or retreats, affecting Earth system characteristics such as sea level, in turn. Although tractable within this modeling framework, these additional effects are beyond the scope of this paper.

That our predicted Pangean climate variability is enhanced particularly in the magnitude of projected warming is partly an expected consequence of our conservative parameterizations for the surface weathering sink for CO_2 during and after breakup. In particular, we neglect a number of potentially significant, albeit complex, contributions to the total flux of alkalinity to the oceans that will affect the magnitude of the variation but not the overall climatic trend. We ignore the notable addition of highly weatherable LIP basalt between 120 and about 80 Ma (Figure 4) and the uplift of basaltic seafloor (Macdonald et al., 2019) during breakup along with a possible increase in the total length of continental arcs during breakup (Lee et al., 2013). We also neglect the expected changing conditions for hydrologic storage and flow to the oceans related to changes in dynamic topography (Maher & Chamberlain, 2014), as well as effects on the efficiency of surface weathering sinks for CO_2 related to the greater surface area of fragmented continental margins. Indeed, whereas our expectation of a persistent dynamic ice sheet through the Cretaceous warm period is qualitatively consistent with geological data, our conservative treatment of the surface weathering sink for CO_2 contributed to an overly warm model Pangean Earth. The failure of the model to explain the tropical SST proxy data

over the last 40 to 50 million years is unclear but possibly related partly to the $\delta^{18}O$-based SST proxies being affected by the appearance of extensive Antarctic and Greenland ice sheets (e.g., Zachos et al., 2008, and references therein) and their attendant effects on the global freshwater mass balance. Furthermore, that peak surface temperatures occur approximately order 10 million years earlier than observed is a consequence of the form of the mantle transient in our models and is not critical to the comparison of the predicted and inferred climate trends.

As a final comment here, although our simplified treatment of the dynamics modulating particularly surface weathering effects on pCO_2 will certainly affect the magnitude of the climate change, a climate cooling/warming trend is inevitable through the Pangean epoch nevertheless. This climate change is driven by expected large-amplitude variations in volcanic CO_2 forcing that are in marked contrast to the more conventional factor of ~2 variation inferred predominantly from sea-level reconstructions (Figures 4 and 11). Indeed, our model places a much greater emphasis on the mantle convective and tectonic control of the Pangean climate variability than is conventionally applied (see Lenton et al., 2018, and references therein).

7.2. Cooling-Warming Variability Related to Rodinia: Global Glaciations and a Tropical Aftermath to the Cryogenian

The extent to which the mantle thermal isolation-to-remixing response to the formation and breakup of Rodinia modulated volcanic outgassing and weathering processes to ultimately pace Earth's enigmatic Neoproterozoic climate is a critical issue. In addition to being among the most enigmatic epochs in Earth history, this remarkable period was terminated by the abrupt rise of complex animals (Knoll, 2011) following the Gaskiers glacial advance at around 580 Ma. Whether a supercontinental modulation of this climate provided a critical driving environmental stress is unclear and certainly beyond the scope of this paper. However, a major aim of this paper is to identify and understand the specific expression of the very rich mantle dynamics of this period in the surface Earth system. Accordingly, we address two questions. First, can predicted volcanic and weathering regimes that lead to an cooling-warming oscillation analogous with the Pangean epoch explain Earth's entry into, and exit from, a Cryogenian period characterized by a proclivity for intermittent global glaciations or "snowball solutions"? Second, are the same transient dynamics of breakup also responsible for the abrupt termination of the short-lived Marinoan global glaciation (640–635 Ma) compared with the long-lived Sturtian event (717–662 Ma) (Macdonald et al., 2010; Rooney et al., 2015), and consistent with the comparatively brief (340 thousand-year-long) Gaskiers glaciation at 580 Ma?

Although the climate of the Neoproterozoic is now well characterized (Hoffman et al., 2017), compared with the Pangean cycle, there are objectively fewer observational or proxy constraints on the tectonic, mantle dynamic, volcanic, and weathering regimes during the formation and breakup of Rodinia. Although our assumed temporal and mechanical symmetry with Pangea is a reasonable starting point, to the extent that the timing of LIP volcanism relative to the formation and breakup of Rodinia reflects partly the spatial character of mantle convective stirring and thermal mixing, this assumption must be viewed cautiously. For example, in contrast to a Pangean epoch marked by extensive LIP volcanism only after breakup, extensive LIP activity occurred continuously over much of the Rodinia episode, potentially indicating a difference in the structure of mantle overturning motions (Figure 3).

Key to applying a Pangea-style mantle thermal mixing picture to Rodinia is to resolve the timings of both the breakup of the supercontinent and the expected syn- and post-breakup increases in volcanism and CO_2 outgassing we discussed briefly in section 2. On the basis of careful paleomagnetic plate reconstructions, stratigraphic studies, and high-resolution geochronology, the supercontinent Rodinia was formed by about 1–1.1 Ga (Li et al., 2008), in a low-latitude/equatorial position by about 780 Ma, and began breaking up in earnest between 720 and 650 Ma (Li et al., 2013) and was fragmented by about 600 Ma. In addition, recent exhaustive statistical analyses of the U-Pb age distributions from detrital zircons provide a clue for the relationship between the formation and breakup of Rodinia and the evolving dynamics of continental arc magmatism (Gehrels, 2014; McKenzie et al., 2014, 2016) (Figure 13). To the extent that the sedimentary record of zircon accumulation accurately reflects magmatic zircon production at active and actively eroded continental arcs (cf. section 2), whereas silicic magmatism was apparently minimized between 900 and about 750 Ma, it increases to a peak at about 600 Ma and declines to a minimum value by 520 Ma (McKenzie et al., 2016). Such steadily increasing rates of delivery of eroded material as well as continental magmatism are potentially consistent with a synchronous monotonic increase in Neoproterozoic seawater $^{87}Sr/^{86}Sr$ from 0.7055 to a value of 0.7067 at 665 Ma, followed by stepwise increases to approximately steady

values of 0.7075 by 621 Ma and a peak of 0.7085 by 565 Ma (Halverson et al., 2007) (Figure 13). This behavior is also apparent in recent time series of $\delta^{18}O$ on zircons the variability of which is proposed to correlate with surface weathering rate (Hartmann et al., 2017) (Figure 3). The maximum rate of increase is between about 640 and 560 Ma that is broadly consistent with the peak in zircon ages. Bearing in mind that an accurate resolution of the timing of peak magmatism and/or surface weathering rates is a critical gap, we use these loose sedimentary zircon, seawater Sr isotopic and $\delta^{18}O_{zircon}$ constraints only to position approximately where in the geological record our model peak in volcanism might be expressed following breakup. We do not use these data to influence the shape of the coupled mantle-climate evolution (Figure 13), which we assume to be proportional to the Pangean epoch (Figure 9). We return to challenges emerging from applying this assumption in detail at the end of this discussion.

In marked contrast to the calculation for Pangea, compared to the initial steady-state mantle-climate system, the mantle thermal isolation-to-remixing model with a seafloor weathering strength that increases as MOR spreading rates decline predicts that pCO_2 will fall by an additional order of magnitude with Rodinia formation. With breakup, compared to the Pangea calculation, pCO_2 overshoots the initial value by an additional factor of 6 (Figure 13). By contrast, implementation of the Sleep and Zahnle (2001)-style seafloor weathering model leads to more moderate variability where pCO_2 falls to about 1% of the initial value at formation and overshoots by around a factor of 170 during breakup. Consistent with expectations from equation (1), the predicted peak cooling persists well into Rodinia fragmentation as mantle thermal remixing occurs. However, the model cold period emerges prior to the Sturtian glaciation and that the Marinoan event occurs close to where some of the highest pCO_2 values occur during the remixing phase of the mantle response. This feature of the calculation is a consequence of our assumed temporal symmetry in the mantle thermal mixing responses to Pangea and Rodinia formation and breakup, and we will return to this timing issue below. Compared to the Pangean calculation, the more intense climate variability arises because the greater longevity of this supercontinent leads to proportionally larger relative oceanic mantle cooling (Figure 9), to reduced mantle melting and volcanic CO_2 outgassing (Figure 11), and to a lower spreading rate minimum prior to breakup, in turn.

The enhanced climate change is also related to the large sensitivity of the weathering response to the mode of seafloor weathering (Figures 11 and 12). Depending on the parameters applied to the seafloor weathering model, during model Rodinia formation, the ice line advances from 65–75° N or S to 50–0° N or S, respectively. If our proposed tectonically modulated seafloor weathering sink is appropriate ($\epsilon_{sf} = -1$), Cryogenian global glaciation is an inevitable consequence of our mantle dynamic model. This result is largely insensitive to reasonable changes in parameterizations for the mean albedo of Earth, the mean albedo for the atmosphere, and the strength of imposed meridional heat transfer. In comparison to the Pangea calculation, a reduced rate of precipitation with formation has a negligible effect on the climate largely because the low temperatures preclude significant terrestrial surface weathering (the response time for surface weathering approaches infinity). One caveat is that the minimum pCO_2 assumes that the atmosphere and ocean remain coupled physically to allow for air-sea exchange of CO_2. This picture is incorrect or at least misleading if the oceans are covered in a crack-free ice shell over million-year time scales. Our picture is, however, justified if this ice shell is either fractured or has small areas or oases of open ocean that enable air-sea gas exchange (Goodman & Strom, 2013; Higgins & Schrag, 2003; Le Hir, Goddéris, et al., 2008; Le Hir, Ramstein, et al., 2008). Nevertheless, our predicted pCO_2 minima for the Cryogenian are potentially low.

By contrast, if seafloor weathering increases with spreading and crustal production rates ($\epsilon_{sf} = 1$) (cf., Brady & Gíslason, 1997; Sleep & Zahnle, 2001), this sink, along with surface weathering, will approach zero strength as spreading rates become negligible and the maximum decrease in pCO_2 is limited to be about a factor of 100. Global glaciation does not occur in this scenario in our models because the steady-state atmospheric pCO_2 remains too high. This prediction should be viewed, however, as an upper bound. If the total seafloor weathering response involves even a very small contribution ($\lesssim$5% by area, say) from a region where our proposed tectonic control enters the mechanics of this sink and $\epsilon_{sf} = -1$, global glaciation is possible. Furthermore, even if seafloor weathering acts entirely in a mode where $\epsilon_{sf} = 1$, the predicted decline in pCO_2 is significant, and the latitudinal extent of Earth's glacial mean-state climate will be particularly sensitive to the effects of external triggers such as the recently proposed volcanic aerosol forcing related to the eruption of the Franklin large igneous province (Macdonald & Wordsworth, 2017). However, enhanced warming through a hypothetical factor of 2 decline in precipitation during formation and at the

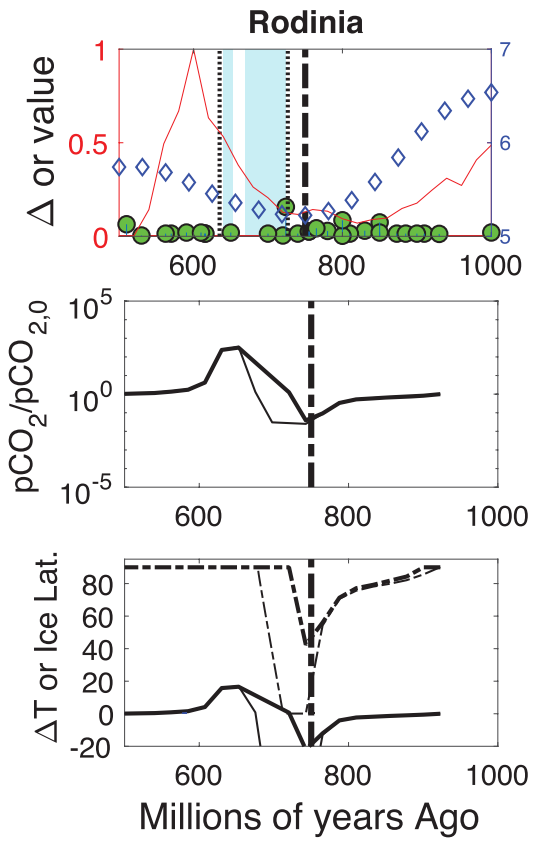

Figure 14. Evolutions for Pangean and Rodinian $pCO_2/pCO_{2,0}$, surface temperature change ΔT, and polar ice line latitude predicted with $pCH_4 = 200$ ppm and a reduced $A_{sf} = 0.075$ (thin black line) and with $pCH_4 = 300$ ppm and $A_{sf} = 0.075$ (heavy black lines). Compared with Figure 13, the calculation with $pCH_4 = 200$ ppm produces a shorter period of global glaciation and a reduced $pCO_2/pCO_{2,0}$ variability. Global glaciation does not occur for $pCH_4 = 300$ ppm (see text).

start of breakup causes the ice line to retreat by 10–15° N/S, reducing the climate sensitivity to external triggers. Although this magnitude of precipitation decline may be unrealistically large at the start of breakup, an implication is that the likelihood of global glaciation in response to powerful external triggers may be small until $\Upsilon \rightarrow 1$.

With our proposed seafloor weathering parameterization global glaciation solutions similar in form to the relatively low methane calculations in Figure 13 are generally unavoidable for abiotic methane concentrations up to 100 ppm. Calculations for ≥200–300 ppm, by contrast, can produce both partial ice and panglacial solutions of varying resilience and longevity, depending with greater sensitivity on the aerial fraction of the seafloor weathering sink A_{sf} and our treatment of the mean surface and sky albedos. Reducing A_{sf} by a factor of 2 for $pCH_4 = 300$ ppm, for example, with all other parameters unchanged, gives a partial ice solution with an ice line at around 40° N/S (Figure 14). Overall, our calculations require $pCH_4 < 200$–300 ppm for Cryogenian global glaciations to be possible. This limit is comparable with upper bounds from recent Proterozoic seawater sulfate modeling constraints (Fakhraee et al., 2019) and similar to inferences from earlier studies (Pavlov et al., 2003). More generally, our results suggest that if expected MOR abiotic methane production maintained atmospheric pCH_4 at order 100-ppm levels, an enhanced climate sensitivity driven by this tectonically controlled greenhouse forcing may have enabled intermittent global glaciations. That is, the likelihood for periodic rather than continuous global glaciations or stochastic panglacial climates of varying longevity and intensity akin to the Sturtian and order of magnitude-shorter Marinoan events may have been increased.

Possibly more remarkable even than the occurrence of intermittent global glaciations in the Neoproterozoic is that the Marinoan event was nearly an order of magnitude shorter in duration than the Sturtian. Following a ~60- to 70-million-year time lag after Rodinia breakup, over the model interval of 685–665 Ma, enhanced volcanic CO_2 outgassing causes pCO_2 to rebound from the very low values that permitted global glaciation to values that are a factor of 10^3 greater than the preformation basic state. In a way qualitatively similar to the Pangea calculation, this behavior reflects enhanced volcanic outgassing and a transition away from a pCO_2 sink governed globally by seafloor weathering processes to one controlled by intense surface weathering operating at the margins of spreading continental fragments in a continental arc regime. As with Pangea, by neglecting compositional controls including the likely emergence of ophiolite rocks in forearc-continent sutures during breakup (Macdonald et al., 2019) and by fixing MOR and arc lengths, we almost certainly underestimate the strength of this surface weathering sink and overestimate the peak pCO_2.

As a final remark in this discussion, the character of the mantle thermal evolution imposed through our assumed temporal symmetry with the thermal mixing regime of the Pangea epoch (cf. Figure 9) is potentially inconsistent with an Edicaran Gaskiers-like glacial advance to midlatitudes at 580 Ma. If this comparatively brief period of climate cooling is a feature of the mean-state climate of this period, on the basis of the Rodinia calculations in Figure 13, a return to a thermally well-mixed mantle leaves at least 10–100 times too much CO_2 in the atmosphere to be consistent with an ice line at 60°–<40° S (Trindade & Macouin, 2007). The predicted high-latitude ice line shown in Figure 13 is, in detail, not appropriate until near the start of the ice-free Cambrian period at 541 Ma. A failure of the model to produce a mean-state climate consistent with the Gaskiers event may, thus, reflect that our assumed temporal symmetry with the Pangean mantle thermal mixing behavior breaks down in detail during the waning stages of Rodinia fragmentation. Although this reality would be unsurprising given the simplicity of our problem design, this interpretation is, however, frought. Because the longevity of this glaciation is an order of magnitude shorter than the Marinoan event and comparable in duration to a surface weathering response time that is predicted to be reduced compared

to the 1-million-year reference we apply (Figure 11), it is difficult to argue that it is a feature of a mean-state climate. More likely is that this glaciation was a climate excursion reflecting the response of the surface Earth system to transient or impulsive triggers we do not consider such as periods of intense stratospheric volcanism, anomalously intense chemical weathering, or both. Viewed this way, our predicted average climate enters primarily through establishing the time scale for the recovery of a plausible background mean-state climate.

7.3. Extensive Mantle Thermal Mixing, the Irrepressibly Clement Climate, and the Potential Challenge of Extensive Magmatism During the Nuna Epoch

In contrast to the cooling-warming climate variabilities that define the Rodinian and Pangean supercontinental cycles, the longer Nuna epoch is remarkable for an absence of recognizable climate change. If the extent of mantle thermal mixing ultimately governs Earth's climate response to supercontinental cycles, one interpretation of the previously enigmatic resilience of the Nuna climate is that it simply reflects a period of extensive mantle thermal mixing. As we discuss in section 3 and summarize schematically on the basis of published studies reviewed in Lenardic et al. (2011) in Figures 2 and 1, supercontinent formation can modulate mantle convective motions to produce the thermal isolation regime we infer for Pangea and Rodinia, but it can also drive very efficient mixing (cf. Lenardic et al., 2011). The key control on the extent of thermal mixing is the spatial arrangement of subducting slabs. Where a slab curtain around a nascent supercontinent emerges, the extent of thermal isolation depends on its continuity and permeability. For partial or nonexistent slab curtains, thermal mixing can remain extensive through the assembly and breakup of a supercontinent. An unchanged (or even enhanced) rate of volcanic CO_2 source in this regime, balanced by a weakened surface weathering sink that concentrated in the dry interior of Nuna, a long distance from the oceans, is likely to lead to both little climate variability and an overall warmer climate, on average. Indeed, our climate calculations for the Nuna epoch with a constant volcanic flux, a background $pCH_4 = 5$ ppm, and a prescribed 40% decline in total precipitation at peak supercontinent formation (cf. Donnadieu et al., 2004) predict an approximately factor of 10 increase in pCO_2, a nearly 7° increase in the global surface temperature and the retreat of initial high-latitude ice sheets to the poles. Such a picture is consistent with the dearth of evidence for significant polar ice sheets during this period in spite of an extensive sedimentary record.

As an additional remark, that Nuna assembly is correlated approximately with the end of a well-known peak in the global expression of banded iron formation (Isley & Abbott, 1999) is potentially unsurprising within the framework of our model. We expect that the continental surface weathering-related flux of Fe^{2+} from particularly subaerial large igneous provinces and exposed ophiolite rocks, as well as the delivery of limiting nutrients that drive biological productivity, to decline as Nuna forms (cf. section 4.1). Although provocative, the extent to which this modulation of the requisite anoxic and ferruginous ocean conditions is related to the decreasing strength of the surface weathering sink for CO_2 expected with Nuna assembly and not simply related to the timing of large igneous province magmatism (Isley & Abbott, 1999) is, however, unclear.

Finally, although the absence of significant ice sheets is an explicit prediction for the Nuna epoch if the mantle remained thermally well mixed, the well-established correlation with unusually extensive anorogenic intraplate silicic magmatism is a potential challenge to our picture. For example, vigorous crustal magmatism between 1.7 and 1.2 Ga is expressed through the production, rise, and emplacement of the vast majority of crustally derived anorthosite massifs in the geologic record as well as related silicic magmatism (e.g., Ashwal, 2013; Emslie, 1985; Longhi, 2005; Morse, 1982). Much of this activity occurs between 1.5 and 1.3 Ga and is associated directly with the breakup of Nuna (e.g., Condie, 2002; Ernst et al., 2008; Fan et al., 2013; Hoffman, 1989; Hoffman et al., 1989; Zhang et al., 2012). Whether this extensive magmatism reflects an increased mantle heatflow related to effects of the Nuna supercontinent on the structure and planform of upwelling motions in a thermally well-stirred mantle (Hoffman, 1989) or requires enhanced subcontinental mantle temperatures and melting more characteristic of mantle thermal isolation is unclear on petrologic grounds (e.g., Longhi, 2005; Morse, 1982; Taylor et al., 1984)Enhanced mantle temperatures are, for example, not required by statistical reconstructions of the MgO contents of mafic melts and of the extent of mantle melting during this period (Keller & Schoene, 2012). However, a marked feature of simulations with extensive (or assumed extensive) mantle thermal mixing is that mantle upwelling flows can become reorganized and focused beneath a growing or well-established supercontinent (e.g., Coltice et al., 2009; Grigné et al., 2007; Holmes, 1931; Lenardic et al., 2011; Li & Zhong, 2009; O'Neill et al., 2009; Pekeris, 1935; Rolf et al., 2012). Thus, an absence of significant ice sheets and the extensive occurrence of anorthosite massifs and

related granitic and granodioritic plutonic bodies are not unexpected. More detailed mantle dynamic models of thermal mixing that incorporate the production, distribution, rise, and differentiation of melts in the continental lithosphere are required to test the reality that the mantle-controlled global volcanic input of CO_2 remained approximately unchanged over this period.

8. Concluding Remarks

The inherent spatiotemporal variability in the style and heat transfer properties of Earth's current plate tectonic mode of mantle convection can have a strong expression in long-term climate change. The intermittent assembly and breakup of supercontinents that locally insulate the underlying mantle is one class of tectonically driven transient that can modulate significantly global average rates of mantle melt production and CO_2 outgassing, as well as the predominant mechanisms for the drawing down of atmospheric CO_2 through chemical weathering. Depending on the character and intensity of these effects on the long-term carbon cycle, supercontinental cycles can drive strong order 100-million-year climate variability or stabilize the surface Earth system against significant long-term climate change. Bearing in mind the assumptions and limitations of our models, our work supports a hypothesis that the clement and unchanging climate during the Nuna supercontinental cycle and the cooling-warming climate variabilities of the Rodinia and Pangea supercontinental cycles reflect consequences of differing extents of oceanic-continental mantle thermal mixing for both volcanic sources and weathering sinks for CO_2. Indeed, our work suggests that the protracted cooling-warming variability that characterizes particularly the Cryogenian-Ediacaran climates is probably not possible if the mantle remains thermally well mixed during these epochs. More broadly, that the major qualitative features of the climates of the Nuna, Rodinia, and Pangea epochs can be understood to some degree as consequences of Earth's supercontinentally modulated mantle thermal mixing regime is provocative. In addition to highlighting an inherently mantle convective control, an important general implication is that qualitative trends in Earth's record of long-term climate variability may ultimately provide novel and largely unexplored constraints on the character and thermal mixing properties of whatever mode of mantle convection is active during a given geological epoch.

Our results for the Rodinia and Pangea epochs also highlight key requirements as well as knowledge gaps related to using order 100-million-year climate variability to infer the mantle dynamics quantitatively: Additional proxy constraints on the magnitude as well as the spatial distribution and timing of oceanic-continental upper mantle temperature variations, along with a thorough characterization of the kinematics of plate motions since 1 Ga, are critical for improving parameterizations for both volcanic sources and weathering sinks for CO_2. Our assumption of temporal symmetry between the Pangean and Rodinian epochs, for example, relies on extensive proxy data consistent with the two epochs sharing a similar overall cooling-warming climate pattern. This assumption may break down with the failure of the model to predict climate conditions consistent with the Ediacaran Gaskiers glaciation, unless this event is triggered by transient volcanic or weathering processes that are not included in our model. With more reliable petrologic, geological, and geochronological constraints on the extent, type, timing, and location in latitude of continental magmatism and better-resolved Neoproterozoic plate reconstructions constraining the locations, extent, and geometry of bounding arcs and/or the rate of component plate assembly or fragmentation, such an assumption may not be necessary. Crucial to this discussion are also more detailed reconstructions of the evolving locations, lengths, planforms, and longevities of island and continental arcs through these epochs, as well as the lengths of mid-ocean ridge systems. Given the very strong sensitivity of the Rodinia climate calculations to seafloor weathering mode, observational as well as modeling constraints on the control of fault and fracture permeability on seafloor weathering will be key for fully exploring the mantle thermal mixing control over climate we propose. Furthermore, additional constraints on the mechanics of compositional effects on the global surface weathering sink arising as a result of LIP volcanism and the emergence of ophiolite rocks in sutures related to forearc-continent collisions will also be important for developing more robust parameterizations for terrestrial surface weathering in both the island arc and continental arc modes we discuss.

In this initial and highly simplified thought experiment, the extent to which embryonic supercontinents are encircled by impermeable subducting slabs governs the lateral advective exchange and thermal mixing of subcontinental mantle into relatively cold suboceanic mantle. These thermal mixing properties can introduce lateral mantle interior temperature variations that far exceed secular mean internal temperature changes related to slow cooling of the Earth and will modulate volcanic sources as well as the regime,

mechanics, and strength of surface and seafloor weathering sinks for atmospheric CO_2. Where the process of supercontinent assembly maintains or enhances thorough lateral mantle thermal mixing and an approximately isothermal internal temperature, volcanic sources potentially remain close to a pre-supercontinent mantle regime. A migration of the majority of surface weathering into the relatively dry continental interior, however, can reduce this sink for atmospheric CO_2, leading to a warmer world with little long-term climate change. The absence of evidence for significant ice sheets and of indicators for significant climate variability suggest that the the Nuna cycle operated in a thorough mantle thermal mixing regime. To the extent that anoxic and ferruginous conditions are related partly to nutrient delivery that is modulated by the strength of the surface weathering sink, such a picture is potentially supported by the notable disappearance of banded iron formations by the time of Nuna assembly.

In marked contrast, where supercontinent formation and breakup inhibits the lateral thermal exchange of upper mantle material to drive first thermal isolation followed by remixing, the distinct responses of volcanic sources and surface and seafloor weathering sinks will cause an order 10^2-million-year long cooling-warming climate variability. This essential prediction is a robust feature of the thermal isolation-to-remixing mantle regime. To the extent that the magnitude of this climate change reflects an intensity of isolation proportional to the longevity of the supercontinent in a thermal isolation-to-remixing mantle convective regime (i.e., temporal symmetry) explains the similar overall climate trends surrounding the Pangean and longer Rodinian cycles, as well as related proxy data including Mesozoic episodes of ocean anoxia during breakup. Through this assumption of temporal symmetry, our work can also explain significant differences, including the latitudinal extent of polar glaciation and, potentially, the conditions leading to the occurrence and intermittency of Neoproterozoic global glaciations and the short longevity of the Marinoan event compared to the Sturtian glaciation. However, our assumed temporal symmetry makes capturing the precise timing of these events relative to Rodinia breakup challenging.

In more detail, our conclusions for the Pangea-driven Mesozoic cooling-warming climate variability are largely insensitive to our parameterizations for surface and seafloor weathering and, thus, robust. For the Neoproterozoic, the occurrence of order 10- to 10^2-million-year global glaciations consistent with the Sturtian and Marinoan events is particularly sensitive to the seafloor weathering parameterization applied and influenced by the intensity of abiotic methane production through an extensive serpentinization of oceanic mantle rocks that is predicted to occur with model Rodinia assembly. Panglacial solutions are, for example, an inevitable consequence of the mantle thermal isolation-to-remixing regime if the strength of the seafloor weathering strength increases with a MOR fault- and fracture-controlled permeability that is maximized at the very low spreading rates predicted prior to and during Rodinia breakup. Such solutions are, however, challenging if the strength of the seafloor weathering sink increases with mid-ocean ridge spreading and crustal production rate (Brady & Gíslason, 1997; Sleep & Zahnle, 2001) because too much CO_2 remains in the atmosphere. More generally, very strong global climate cooling at Rodinia assembly is a robust consequence of the reduced mantle-controlled volcanic CO_2 outgassing in this mantle thermal regime. An implication of our work is that under these conditions there will be an inherently greater potential for myriad potential external triggers of climate cooling not considered in this paper to drive Earth into global glaciation. A challenge, however, is to sustain such panglacial climates over order 10–100 million years. Finally, intermittent global glaciations in the Cryogenian require snowball solutions to be close to marginal stability. In our climate calculations, this condition can occur under a range of conditions with 100- to 300-ppm abiotic CH_4. Intermittent global glaciations are also consequently possible at assembly and during breakup if the seafloor weathering sink, acting predominantly in a conventional regime governed by MOR crustal production (Brady & Gíslason, 1997), involves even very modest contributions from low-temperature hydrothermal circulations through fault and fractured rocks at very slow spreading MORs, as proposed here.

Appendix A: One-Dimensional Budyko-Style Energy Balance Model

The weathering sinks for CO_2 in equations (16) and (15) depend on Earth's global mean temperature $\bar{T}$. To implement a one-dimensional (zonal) Budyko energy balance model to find this temperature as a function of the extent of polar glaciation (ice line position), we use a meridional coordinate $y = \sin\phi$, where ϕ is latitude. This coordinate system automatically accounts for the area weighting when computing integral properties for the radiation balance.

Following Budyko (1969), the energy balance equation solved at each y is

$$0 = (1 - \alpha(y, y_{ice}))\frac{1}{4}L(t)_{\odot} - OLR(T, CO_2, CH_4) - k \cdot (T(y) - \bar{T}), \tag{A1}$$

where k is a meridional heat transfer coefficient, $L(t)_{\odot}$ is the time-varying incoming solar short-wave radiation (cf. Feulner, 2012), the global mean temperature $\bar{T} = \int_{-1}^{1} T dy$, and $\alpha(y, y_{ice})$ is the area-weighted albedo determined on the basis of an albedo of the sky including clouds $\alpha_{sky} = 0.125$ and initial fractional contributions of land (27%, $\alpha_l = 0.4$) and sea (73%, $\alpha_s = 0.1$) that are symmetric about the equator. These contributions to the albedo are modified by a temperature-dependent ice coverage for which we solve (Pierrehumbert, 2010; Pierrehumbert et al., 2011). We choose values for k and α_{sky} such that we recover a present-day Earth ice line of ~75–80° N/S and global mean temperature of around 288 K.

Through equation (8), any shift in the globally averaged volcanic sources for CO_2 relative to the pre-supercontinent value is balanced by a weathering response that depends on $\bar{T}$ through the kinetic contributions to the seafloor and surface weathering modes. To find the steady-state pCO_2, equation (A1) is, consequently, solved numerically by iterating on the ice line y_{ice} until the ice line temperature satisfies a freeze criterion . We assume that the Outgoing Long-wave Radiation OLR is a linear function of temperature T, making it possible to solve for the global mean temperature $\bar{T}$ given a guess at y_{ice}:

$$0 = (1 - \overline{\alpha(y, y_{ice})})\frac{1}{4}L_{\odot} - (A + B \cdot (\bar{T} - T_{ref})). \tag{A2}$$

Here, $T_{ref} = 285$ K, $A = A_0 - 4\log_2(CO_2/CO_{2,0}) - .036 * (CH_4/CH_{4,0})^{1/2}$ [W/m^2] with $A_0 = 240$ [W/m^2], $CO_{2,0} = 300$ [ppm], and $CH_{4,0} = 1$ [ppm] and the climate sensitivity $B = 2$ [W/K m^2]. Once $\bar{T}$ is known, $T(y)$ is found analytically.

Appendix B: Scaling Theory for the Growth of a Wedge-Shaped Orogen

Arc-continent collision during supercontinent breakup and continent-continent collisions during assembly drive orogenesis. This appendix is consistent in spirit with Dahlen (1984) and develops scalings for the time evolution of the height $h(t)$, width $w(t)$, and aspect ratio $\Lambda(t)$ of a symmetric, wedge-shaped orogen with a yielding rheology in response to the one-sided accretion of crust at a continental arc. The same time-varying functional forms are expected for the construction of a two-sided intracontinental plateau during supercontinental formation. The aspect ratio sets the mean topographic profile that enters into the mechanics governing the establishing of long-time averaged river profiles that govern the fluvial erosion rate $\dot{E}$ (cf. section 6).

This development refers to the problem defined in Figure 10. A quasi-two-dimensional wedge-shaped orogen with height H_o, root depth H_r, and width W grows through the combined effects of oceanic crustal accretion and continental crustal shortening driven as a result of the mass flow $\bar{\rho}V_s H_c$ delivered over a specified time t.

Assuming Airy compensation in mantle lithosphere with a density $\bar{\rho} + \Delta\rho$, where $\Delta\rho > 0$

$$H_r = (\bar{\rho}/\Delta\rho)H_o. \tag{B1}$$

With (B1), conservation of volume requires that

$$CW(H_o + H_r) \sim CRWH_o \sim V_s H_c t, \tag{B2}$$

where the density ratio $R = ((\bar{\rho}/\Delta\rho) + 1)$ and the geometric constant $C = 1/2$ for a triangular-shaped wedge. This density ratio can readily be adjusted for compositional effects including complex mixtures of obducted oceanic crust, shortened continental crust, and magmatism. From Newton's second law, the steady-state aspect ratio of the growing wedge (the taper angle, cf. Dahlen, 1984) at any time is governed by a buoyancy stress arising as a result of lateral variations in hydrostatic pressure that balances the average yield stress τ_y of the orogen (e.g., England & Houseman, 1986; Jellinek et al., 2006). Consequently,

$$\tau_{y,i} \sim 2\bar{\rho}_i g H_i^2 / W_{mtn}, \tag{B3}$$

where i is for either the orogen or the underlying root. We reasonably assume that $\tau_{y,o} < \tau_{y,r}$ and restrict this analysis to the special case where the orogen strength governs its evolution. Combining (B2) and (B3) gives

$$H_o \sim \left[(V_s H_c \tau_{y,o}/2CR\bar{\rho}g)t\right]^{1/3}. \tag{B4}$$

Similarly,

$$W_o \sim (\bar{\rho}g/C\tau_{y,o})^{1/3}(2V_s H_c t/R)^{2/3}. \tag{B5}$$

The ratio of (B5) to (B4) is the aspect ratio of a critically tapered wedge (cf. Dahlen, 1984)

$$\Lambda \sim 1/C\left[(VsH_c t/R)^{1/3}(\bar{\rho}g/\tau_{y,o})^{2/3}\right]. \tag{B6}$$

Differentiating (B6) with respect to time indicates that $d\Lambda/dt \propto t^{-2/3}$ and, thus, that the aspect ratio reaches a constant value relatively quickly, which helps to justify our steady-state erosion assumption that underlies our treatment of surface weathering. Climate transients during the fragmentations of Rodinia and Pangea are 1–10 million years (Figures 3 and 4). A concern raised in the text is the extent to which a nascent orogen will reach the condition where equation (11) is appropriate.

One issue during breakup is, for example, the extent to which rainfall is distributed over the majority of windward flanks of growing orogens at fragmenting continental margins such that alkalinity is delivered to the oceans efficiently by resulting surface runoff. This condition helps to justify the assumption that precipition rates are a reasonable proxy for global surface runoff during these tectonic transients. Recognizing that orographic precipitation is inherently a regional phenomenon that must be considered cautiously in this global context, we nevertheless follow Roe and Baker (2006) to build understanding. Assuming that orogen heights are comparable to or lower than a 2- to 4-km altitude at which droplet condensation occurs, for order 10 m/s of wind speeds, flank lengths must be at least a few tens of kilometers for droplets to form and fall as hydrometeors to the ground to produce spatially extensive surface water flows (order 10–100 km, say). For an order of magnitude calculation, over a plausible time scale for weathering and erosion to be in balance at the landscape scale for a given precipitation rate (e.g., Whipple, 2001) $t = 10^5 - 10^6$ years, a global mean subduction/spreading rate $V_s = 1$ cm/year, $R = 1$, $\bar{\rho} = 3{,}000$ kg/m^3, $g = 10$ m/s^2, $H_c = 5$ km and a typical $\tau_{y,mtn} = 10^7$ Pa predicts an orogen that is around 1–3 km high and 100–140 km wide. We note that this choice for V_s is potentially very low during Pangea and particularly Rodinia breakup and thus that windward flank lengths may be larger (and orogen crest heights lower compared to the droplet condensation height) over a $t = 10^5 - 10^6$ years of landscape response time. Thus, equation (11) is reasonable. Equation (11) is likely violated only for unrealistically high yield stresses ($\tau_{y,mtn} > 10^8$ Pa with $V_s < 1$ cm/s).

Acknowledgments
This project grew partly out of colorful discussions during ski trips with AL and RTP. This work evolved through many engaging and often intense discussions with members of the Canadian Institute for Advanced Research Earth Systems Evolution Program over an extended period. Discussions with, as well as careful, thorough, and highly engaging reviews from, P. F. Hoffman were instrumental to building this manuscript. AMJ is particularly indebted to PFH for his thoughtful and patient mentoring over many years. Thorough, thoughtful, and challenging reviews from N. Planavsky and B. Foley also improved this paper significantly. F. Macdonald and A. Turchyn provided comments on early drafts that were important in framing as well as building this story. Stimulating discussions with N. Sleep, S. Crowe, J. Braun, L. Derry, L. Kump, D. Schrag, N. Swanson-Hysell, and K. Whipple were also helpful. Additional discussions with K. Ferrier, C.-T. Lee, L. Moresi, C. Schoof, and A. Grau-Galofre informed our thinking. AMJ was supported by NSERC during this project. The authors report no financial conflicts of interest in completing this work or preparing this manuscript.

References

Abbot, D. S., Cowan, N. B., & Ciesla, F. J. (2012). Indication of insensitivity of planetary weathering behavior and habitable zone to surface land fraction. *The Astrophysical Journal*, *756*(2), 178.

Abbot, D. S., Voigt, A., Li, D., Le Hir, G., Pierrehumbert, R. T., Branson, M., et al. (2013). Robust elements of snowball earth atmospheric circulation and oases for life. *Journal of Geophysical Research: Atmospheres*, *118*, 6017–6027. https://doi.org/10.1002/jgrd.50540

Ahm, A.-S. C., Bjerrum, C. J., Blättler, C. L., Swart, P. K., & Higgins, J. A. (2018). Quantifying early marine diagenesis in shallow-water carbonate sediments. *Geochimica et Cosmochimica Acta*, *236*, 140–159.

Ahm, A.-S. C., Maloof, A. C., Macdonald, F. A., Hoffman, P. F., Bjerrum, C. J., Bold, U., et al. (2019). An early diagenetic deglacial origin for basal Ediacaran "cap dolostones". *Earth and Planetary Science Letters*, *506*, 292–307.

Ahnert, F. (1970). Functional relationships between denudation, relief, and uplift in large, mid-latitude drainage basins. *American Journal of Science*, *268*(3), 243–263.

Alt, J. C., & Teagle, D. A. (1999). The uptake of carbon during alteration of ocean crust. *Geochimica et Cosmochimica Acta*, *63*(10), 1527–1535.

Amiot, R., Wang, X., Zhou, Z., Wang, X., Buffetaut, E., Lécuyer, C., et al. (2011). Oxygen isotopes of east asian dinosaurs reveal exceptionally cold early cretaceous climates. *Proceedings of the National Academy of Sciences*, *108*(13), 5179–5183.

Anbar, A. D., & Knoll, A. H. (2002). Proterozoic ocean chemistry and evolution: A bioinorganic bridge? *Science*, *297*(5584), 1137–1142.

Ashwal, L. D. (2013). *Anorthosites* (Vol. 21). Verlag Berlin Heidelberg: Springer Science & Business Media.

Bao, H., Lyons, J., & Zhou, C. (2008). Triple oxygen isotope evidence for elevated CO_2 levels after a Neoproterozoic glaciation. *Nature*, *453*(7194), 504.

Becker, T. W., Conrad, C. P., Buffett, B., & Müller, R. D. (2009). Past and present seafloor age distributions and the temporal evolution of plate tectonic heat transport. *Earth and Planetary Science Letters*, *278*, 233–242.

Beerling, D. J., & Royer, D. L. (2011). Convergent Cenozoic CO_2 history. *Nature Geoscience*, *4*(7), 418.

Bergman, N. M., Lenton, T. M., & Watson, A. J. (2004). COPSE: A new model of biogeochemical cycling over Phanerozoic time. *American Journal of Science*, *304*(5), 397–437.

Berndt, M. E., Allen, D. E., & Seyfried Jr, W. E. (1996). Reduction of CO_2 during serpentinization of olivine at 300 ° C and 500 bar. *Geology*, *24*(4), 351–354.
Berner, R. A. (1998). The carbon cycle and carbon dioxide over Phanerozoic time: The role of land plants. *Philosophical Transactions of the Royal Society B: Biological Sciences*, *353*(1365), 75–82.
Berner, R. A. (2004). *The Phanerozoic carbon cycle*. Oxford: Oxford University Press.
Bjerrum, C. J., Bendtsen, J., & Legarth, J. J. F. (2006). Modeling organic carbon burial during sea level rise with reference to the Cretaceous. *Geochemistry, Geophysics, Geosystems*, *7*, Q05008. https://doi.org/10.1029/2005GC001032
Bjerrum, C. J., & Canfield, D. E. (2011). Towards a quantitative understanding of the late Neoproterozoic carbon cycle. *Proceedings of the National Academy of Sciences*, *108*(14), 5542–5547. https://doi.org/10.1073/pnas.1101755108
Blättler, C. L., Henderson, G. M., & Jenkyns, H. C. (2012). Explaining the Phanerozoic Ca isotope history of seawater. *Geology*, *40*(9), 843–846.
Blättler, C. L., & Higgins, J. A. (2014). Calcium isotopes in evaporites record variations in Phanerozoic seawater SO_4 and Ca. *Geology*, *42*(8), 711–714.
Blättler, C. L., Jenkyns, H. C., Reynard, L. M., & Henderson, G. M. (2011). Significant increases in global weathering during Oceanic Anoxic Events 1a and 2 indicated by calcium isotopes. *Earth and Planetary Science Letters*, *309*(1), 77–88. https://doi.org/10.1016/j.epsl.2011.06.029
Bleeker, W. (2003). The late Archean record: A puzzle in ca. 35 pieces. *Lithos*, *71*(2-4), 99–134.
Bluth, G. J. S., & Kump, L. R. (1991). Phanerozoic paleogeology. *American Journal of Science*, *291*(3), 284–308.
Bougault, H., Charlou, J.-L., Fouquet, Y., Needham, H. D., Vaslet, N., Appriou, P., et al. (1993). Fast and slow spreading ridges: Structure and hydrothermal activity, ultramafic topographic highs, and CH4 output. *Journal of Geophysical Research*, *98*(B6), 9643–9651.
Bradley, A. S., & Summons, R. E. (2010). Multiple origins of methane at the lost city hydrothermal field. *Earth and Planetary Science Letters*, *297*(1-2), 34–41.
Brady, P. V., & Gíslason, S. R. (1997). Seafloor weathering controls on atmospheric CO2 and global climate. *Geochimica et Cosmochimica Acta*, *61*(5), 965–973.
Brandl, P. A., Regelous, M., Beier, C., & Haase, K. M. (2013). High mantle temperatures following rifting caused by continental insulation. *Nature Geoscience*, *6*(5), 391.
Braun, J., Guillocheau, F., Robin, C., Baby, G., & Jelsma, H. (2014). Rapid erosion of the Southern African Plateau as it climbs over a mantle superswell. *Journal of Geophysical Research: Solid Earth*, *119*, 6093–6112. https://doi.org/10.1002/2014JB010998
Brune, S., Williams, S. E., & Müller, R. D. (2017). Potential links between continental rifting, CO2 degassing and climate change through time. *Nature Geoscience*, *10*(12), 941.
Buck, W. R., Lavier, L. L., & Poliakov, A. N. (2005). Modes of faulting at mid-ocean ridges. *Nature*, *434*(7034), 719.
Budyko, M. I. (1969). The effect of solar radiation variations on the climate of the Earth. *Tellus*, *21*(5), 611–619.
Buffett, B. A., & Rowley, D. B. (2006). Plate bending at subduction zones: Consequences for the direction of plate motions. *Earth and Planetary Science Letters*, *245*(1-2), 359–364.
Cao, X., & Bao, H. (2013). Dynamic model constraints on oxygen-17 depletion in atmospheric O2 after a snowball Earth. *Proceedings of the National Academy of Sciences*, *110*(36), 14,546–14,550.
Carazzo, G., Jellinek, A. M., & Turchyn, A. V. (2013). The remarkable longevity of submarine plumes: Implications for the hydrothermal input of iron to the deep-ocean. *Earth and Planetary Science Letters*, *382*, 66–76. https://doi.org/10.1016/j.epsl.2013.09.008
Cawood, P. A., Hawkesworth, C., & Dhuime, B. (2012). Detrital zircon record and tectonic setting. *Geology*, *40*(10), 875–878.
Charlou, J. L., Fouquet, Y., Bougault, H., Donval, J. P., Etoubleau, J., Jean-Baptiste, P., et al. (1998). Intense CH_4 plumes generated by serpentinization of ultramafic rocks at the intersection of the 15° 20′ N fracture zone and the Mid-Atlantic Ridge. *Geochimica et Cosmochimica Acta*, *62*(13), 2323–2333.
Christensen, U. R. (1984). Heat transport by variable-viscosity convection and implications for the Earth's thermal evolution. *Physics of the Earth and Planetary Interiors*, *35*, 264–282.
Clift, P. D., Wan, S., & Blusztajn, J. (2014). Reconstructing chemical weathering, physical erosion and monsoon intensity since 25 Ma in the northern South China Sea: A review of competing proxies. *Earth-Science Reviews*, *130*, 86–102.
Climate change (2007): The physical science basis. Contribution of Working Group I to the Fourth Assessment Report of the Intergovernmental Panel on Climate Change (2007). Paleoclimate.
Coltice, N., Bertrand, H., Rey, P., Jourdan, F., Phillips, B. R., & Ricard, Y. (2009). Global warming of the mantle beneath continents back to the Archaean. *Gondwana Research*, *15*(3-4), 254–266.
Condie, K. C. (2002). Breakup of a paleoproterozoic supercontinent. *Gondwana Research*, *5*(1), 41–43. https://doi.org/10.1016/S1342-937X(05)70886-8
Condie, K. C., & Aster, R. C. (2010). Episodic zircon age spectra of orogenic granitoids: The supercontinent connection and continental growth. *Precambrian Research*, *180*(3-4), 227–236.
Condie, K. C., Belousova, E., Griffin, W., & Sircombe, K. N. (2009). Granitoid events in space and time: Constraints from igneous and detrital zircon age spectra. *Gondwana Research*, *15*(3-4), 228–242.
Conrad, C. P., & Hager, B. H. (2001). Mantle convection with strong subduction zones. *Geophysical Journal International*, *144*, 271–288.
Coogan, L. A., & Dosso, S. (2012). An internally consistent, probabilistic, determination of ridge-axis hydrothermal fluxes from basalt-hosted systems. *Earth and Planetary Science Letters*, *323*, 92–101.
Coogan, L. A., & Dosso, S. E. (2015). Alteration of ocean crust provides a strong temperature dependent feedback on the geological carbon cycle and is a primary driver of the Sr-isotopic composition of seawater. *Earth and Planetary Science Letters*, *415*, 38–46.
Coogan, L. A., & Gillis, K. M. (2013). Evidence that low-temperature oceanic hydrothermal systems play an important role in the silicate-carbonate weathering cycle and long-term climate regulation. *Geochemistry, Geophysics, Geosystems*, *14*, 1771–1786. https://doi.org/10.1002/ggge.20113
Coogan, L. A., & Gillis, K. M. (2018). Low-temperature alteration of the seafloor: Impacts on ocean chemistry. *Annual Review of Earth and Planetary Sciences*, *46*, 21–45.
Cooper, C., Lenardic, A., & Moresi, L. (2006). Effects of continental insulation and the partitioning of heat producing elements on the Earth's heat loss. *Geophysical Research Letters*, *33*, L13313. https://doi.org/10.1029/2006GL026291
Cox, G. M., Halverson, G. P., Minarik, W. G., Le Heron, D. P., Macdonald, F. A., Bellefroid, E. J., & Strauss, J. V. (2013). Neoproterozoic iron formation: An evaluation of its temporal, environmental and tectonic significance. *Chemical Geology*, *362*, 232–249.
Cox, G. M., Halverson, G. P., Stevenson, R. K., Vokaty, M., Poirier, A., Kunzmann, M., et al. (2016). Continental flood basalt weathering as a trigger for Neoproterozoic Snowball Earth. *Earth and Planetary Science Letters*, *446*, 89–99.

Cox, S., Thomson, S., Reiners, P. W., Hemming, S., & Van De Flierdt, T. (2010). Extremely low long-term erosion rates around the Gamburtsev Mountains in interior East Antarctica. *Geophysical Research Letters*, *37*, L22307. https://doi.org/10.1029/2010GL045106
Crockford, P. W., Cowie, B. R., Johnston, D. T., Hoffman, P. F., Sugiyama, I., Pellerin, A., et al. (2016). Triple oxygen and multiple sulfur isotope constraints on the evolution of the post-Marinoan sulfur cycle. *Earth and Planetary Science Letters*, *435*, 74–83.
Culling, W. (1963). Soil creep and the development of hillside slopes. *The Journal of Geology*, *71*(2), 127–161.
Dahlen, F. (1984). Noncohesive critical Coulomb wedges: An exact solution. *Journal of Geophysical Research*, *89*(B12), 10,125–10,133.
Dahlen, F. (1990). Critical taper model of fold-and-thrust belts and accretionary wedges. *Annual Review of Earth and Planetary Sciences*, *18*(1), 55–99.
Dasgupta, R. (2013). Ingassing, storage, and outgassing of terrestrial carbon through geologic time. *Reviews in Mineralogy and Geochemistry*, *75*(1), 183–229.
Davies, G. F. (1980). Thermal histories of convective Earth models and constraints on radiogenic heat production in the Earth. *Journal of Geophysical Research*, *85*, 2517–2530.
Davies, G. F., & Richards, M. A. (1992). Mantle convection. *The Journal of Geology*, *100*, 151–206.
De Lurio, J. L., & Frakes, L. (1999). Glendonites as a paleoenvironmental tool: Implications for early Cretaceous high latitude climates in Australia. *Geochimica et Cosmochimica Acta*, *63*(7-8), 1039–1048.
Derry, L. A., Kaufman, A. J., & Jacobsen, S. B. (1992). Sedimentary cycling and environmental change in the Late Proterozoic: Evidence from stable and radiogenic isotopes. *Geochimica et Cosmochimica Acta*, *56*(3), 1317–1329.
Dessert, C., Dupré, B., François, L. M., Schott, J., Gaillardet, J., Chakrapani, G., & Bajpai, S. (2001). Erosion of Deccan Traps determined by river geochemistry: Impact on the global climate and the 87Sr/86Sr ratio of seawater. *Earth and Planetary Science Letters*, *188*(3-4), 459–474.
Dessert, C., Dupré, B., Gaillardet, J., François, L. M., & Allegre, C. J. (2003). Basalt weathering laws and the impact of basalt weathering on the global carbon cycle. *Chemical Geology*, *202*(3-4), 257–273.
Dessert, C., Lajeunesse, E., Lloret, E., Clergue, C., Crispi, O., Gorge, C., & Quidelleur, X. (2015). Controls on chemical weathering on a mountainous volcanic tropical island: Guadeloupe (French West Indies). *Geochimica et Cosmochimica Acta*, *171*, 216–237. https://doi.org/10.1016/j.gca.2015.09.009
DiBiase, R. A., & Whipple, K. X. (2011). The influence of erosion thresholds and runoff variability on the relationships among topography, climate, and erosion rate. *Journal of Geophysical Research*, *116*, F04036. https://doi.org/10.1029/2011JF002095
Dickinson, W. R., Lawton, T. F., & Gehrels, G. E. (2009). Recycling detrital zircons: A case study from the Cretaceous Bisbee Group of southern Arizona. *Geology*, *37*(6), 503–506.
Dixon, J. L., Hartshorn, A. S., Heimsath, A. M., DiBiase, R. A., & Whipple, K. X. (2012). Chemical weathering response to tectonic forcing: A soils perspective from the San Gabriel Mountains, California. *Earth and Planetary Science Letters*, *323*, 40–49.
Donnadieu, Y., Goddéris, Y, Pierrehumbert, R., Dromart, G., Fluteau, F., & Jacob, R. (2006). A GEOCLIM simulation of climatic and biogeochemical consequences of Pangea breakup. *Geochemistry, Geophysics, Geosystems*, *7*, Q11019. https://doi.org/10.1029/2006GC001278
Donnadieu, Y., Goddéris, Y., Ramstein, G., Nédélec, A., & Meert, J. (2004). A 'snowball Earth' climate triggered by continental break-up through changes in runoff. *Nature*, *428*(6980), 303.
East, M., Müller, D., Williams, S., Zahirovic, S., & Heine, C. (2019). Subduction history reveals cretaceous slab superflux as a possible cause for the mid-cretaceous plume pulse and superswell events. *Gondwana Research*, *79*, 125–139. https://doi.org/10.31223/osf.io/t28zx
Edmond, J. M., & Huh, Y. (2003). Non-steady state carbonate recycling and implications for the evolution of atmospheric pCO2. *Earth and Planetary Science Letters*, *216*(1-2), 125–139.
Egholm, D., Pedersen, V. K., Knudsen, M. F., & Larsen, N. K. (2012). Coupling the flow of ice, water, and sediment in a glacial landscape evolution model. *Geomorphology*, *141*, 47–66.
Elderfield, H., & Schultz, A. (1996). Mid-ocean ridge hydrothermal fluxes and the chemical composition of the ocean. *Annual Review of Earth and Planetary Sciences*, *24*(1), 191–224.
Emslie, R. (1985). Proterozoic anorthosite massifs, *The deep proterozoic crust in the north atlantic provinces* (pp. 39–60). Dordrecht: Springer.
England, P., & Houseman, G. (1986). Finite strain calculations of continental deformation: 2. Comparison with the India-Asia collision zone. *Journal of Geophysical Research*, *91*(B3), 3664–3676.
Ernst, R., Wingate, M., Buchan, K., & Li, Z.-X. (2008). Global record of 1600–700 Ma large igneous provinces (LIPs): Implications for the reconstruction of the proposed Nuna (Columbia) and Rodinia supercontinents. *Precambrian Research*, *160*(1-2), 159–178.
Evans, D. A. D. (2009). The palaeomagnetically viable, long-lived and all-inclusive Rodinia supercontinent reconstruction. *Geological Society, London, Special Publications*, *327*, 371–404. https://doi.org/10.1144/SP327.16
Fakhraee, M., Hancisse, O., Canfield, D. E., Crowe, S. A., & Katsev, S. (2019). Proterozoic seawater sulfate scarcity and the evolution of ocean–atmosphere chemistry. *Nature Geoscience*, *12*(5), 375.
Fan, H.-P., Zhu, W.-G., Li, Z.-X., Zhong, H., Bai, Z.-J., He, D.-F., et al. (2013). Ca. 1.5 Ga mafic magmatism in South China during the break-up of the supercontinent Nuna/Columbia: The Zhuqing Fe-Ti-V oxide ore-bearing mafic intrusions in western Yangtze Block. *Lithos*, *168*, 85–98.
Ferrier, K. L., & Kirchner, J. W. (2008). Effects of physical erosion on chemical denudation rates: A numerical modeling study of soil-mantled hillslopes. *Earth and Planetary Science Letters*, *272*(3-4), 591–599.
Ferrier, K. L., Kirchner, J. W., Riebe, C. S., & Finkel, R. C. (2010). Mineral-specific chemical weathering rates over millennial timescales: Measurements at Rio Icacos, Puerto Rico. *Chemical Geology*, *277*(1-2), 101–114.
Ferrier, K. L., Riebe, C. S., & Jesse Hahm, W. (2016). Testing for supply-limited and kinetic-limited chemical erosion in field measurements of regolith production and chemical depletion. *Geochemistry, Geophysics, Geosystems*, *17*, 2270–2285. https://doi.org/10.1002/2016GC006273
Feulner, G. (2012). The faint young Sun problem. *Reviews of Geophysics*, *50*, RG2006. https://doi.org/10.1029/2011RG000375
Feulner, G. (2017). Formation of most of our coal brought Earth close to global glaciation. *Proceedings of the National Academy of Sciences*, *114*(43), 11,333–11,337.
Fiorella, R. P., & Poulsen, C. J. (2013). Dehumidification over tropical continents reduces climate sensitivity and inhibits snowball Earth initiation. *Journal of Climate*, *26*(23), 9677–9695.
Frakes, L., Alley, N., & Deynoux, M. (1995). Early Cretaceous ice rafting and climate zonation in Australia. *International Geology Review*, *37*(7), 567–583.
Frakes, L., & Francis, J. (1988). A guide to Phanerozoic cold polar climates from high-latitude ice-rafting in the Cretaceous. *Nature*, *333*(6173), 547.
Frakes, L. A., Francis, J. E., & Syktus, J. I. (2005). *Climate modes of the Phanerozoic*. Cambridge: Cambridge University Press.
France-Lanord, C., & Derry, L. A. (1997). Organic carbon burial forcing of the carbon cycle from Himalayan erosion. *Nature*, *390*(6655), 65.

Francois, L. M., & Walker, J. C. (1992). Modelling the Phanerozoic carbon cycle and climate: Constraints from the 87Sr/86Sr isotopic ratio of seawater. *American Journal of Science*, *292*(2), 81–135.
Gabet, E. J. (2007). A theoretical model coupling chemical weathering and physical erosion in landslide-dominated landscapes. *Earth and Planetary Science Letters*, *264*(1-2), 259–265.
Gabet, E. J., Reichman, O., & Seabloom, E. W. (2003). The effects of bioturbation on soil processes and sediment transport. *Annual Review of Earth and Planetary Sciences*, *31*(1), 249–273.
Gaillardet, J., Dupré, B, Louvat, P., & Allegre, C. (1999). Global silicate weathering and CO2 consumption rates deduced from the chemistry of large rivers. *Chemical Geology*, *159*(1-4), 3–30.
Gehrels, G. (2014). Detrital zircon U-Pb geochronology applied to tectonics. *Annual Review of Earth and Planetary Sciences*, *42*, 127–149.
German, C., Thurnherr, A., Knoery, J., Charlou, J.-L., Jean-Baptiste, P., & Edmonds, H. (2010). Heat, volume and chemical fluxes from submarine venting: A synthesis of results from the Rainbow hydrothermal field, 36 N MAR. *Deep Sea Research Part I: Oceanographic Research Papers*, *57*(4), 518–527.
German, C., & Von Damm, K. (2006). Hydrothermal processes. *Treatise on Geochemistry*, *6*, 181–222.
Gernon, T., Hincks, T., Tyrrell, T., Rohling, E., & Palmer, M. (2016). Snowball Earth ocean chemistry driven by extensive ridge volcanism during Rodinia breakup. *Nature Geoscience*, *9*(3), 242.
Gibbs, M. T., Bluth, G. J., Fawcett, P. J., & Kump, L. R. (1999). Global chemical erosion over the last 250 my; variations due to changes in paleogeography, paleoclimate, and paleogeology. *American Journal of Science*, *299*(7-9), 611–651.
Gillis, K., & Coogan, L. (2011). Secular variation in carbon uptake into the ocean crust. *Earth and Planetary Science Letters*, *302*(3), 385–392.
Gislason, S. R., & Oelkers, E. H. (2003). Mechanism, rates, and consequences of basaltic glass dissolution: II. An experimental study of the dissolution rates of basaltic glass as a function of pH and temperature. *Geochimica et Cosmochimica Acta*, *67*(20), 3817–3832.
Goddéris, Y., Donnadieu, Y., Carretier, S., Aretz, M., Dera, G., Macouin, M., & Regard, V. (2017). Onset and ending of the late Palaeozoic ice age triggered by tectonically paced rock weathering. *Nature Geoscience*, *10*(5), 382.
Goddéris, Y., Donnadieu, Y., Le Hir, G., Lefebvre, V., & Nardin, E. (2014). The role of palaeogeography in the Phanerozoic history of atmospheric CO2 and climate. *Earth-Science Reviews*, *128*, 122–138.
Goddéris, Y., Donnadieu, Y., Lefebvre, V., Le Hir, G., & Nardin, E. (2012). Tectonic control of continental weathering, atmospheric CO2, and climate over Phanerozoic times. *Comptes Rendus Geoscience*, *344*(11-12), 652–662.
Goddéris, Y., Donnadieu, Y., Nédélec, A., Dupré, B., Dessert, C., Grard, A., et al. (2003). The Sturtian 'snowball' glaciation: Fire and ice. *Earth and Planetary Science Letters*, *211*(1-2), 1–12.
Goddéris, Y., Donnadieu, Y., Tombozafy, M., & Dessert, C. (2008). Shield effect on continental weathering: Implication for climatic evolution of the Earth at the geological timescale. *Geoderma*, *145*(3-4), 439–448.
Goodman, J. C., & Strom, D. C. (2013). Feedbacks in a coupled ice-atmosphere-dust model of the glacial Neoproterozoic "Mudball Earth". *Journal of Geophysical Research: Atmospheres*, *118*, 11,546–11,557. https://doi.org/10.1002/jgrd.50849
Goudie, A. S., & Viles, H. A. (2012). Weathering and the global carbon cycle: Geomorphological perspectives. *Earth-Science Reviews*, *113*(1-2), 59–71.
Grau Galofre, A., Jellinek, M., Osinski, G., Zanetti, M., & Kukko, A. (2018). Subglacial drainage patterns of Devon Island, Canada: Detailed comparison of rivers and subglacial meltwater channels. *The Cryosphere*, *12*, 1461–1478.
Griffiths, R., & Campbell, I. (1991). Interaction of mantle plume heads with the Earth's surface and onset of small-scale convection. *Journal of Geophysical Research*, *96*(B11), 18,295–18,310.
Grigné, C., Labrosse, S., & Tackley, P. (2007). Convection under a lid of finite conductivity: Heat flux scaling and application to continents. *Journal of Geophysical Research*, *112*, B08402. https://doi.org/10.1029/2005JB004192
Hallam, A. (1987). Alfred Wegener and the hypothesis of continental drift, *Scientific genius and creativity: Readings from 'Scientific American'* (pp. 77–85), (reprinted from Scientific American, February, 1975.)America: W.H. Freeman & Co.
Halverson, G. P., Dudás, F. Ö, Maloof, A. C., & Bowring, S. A. (2007). Evolution of the 87Sr/86Sr composition of Neoproterozoic seawater. *Palaeogeography, Palaeoclimatology, Palaeoecology*, *256*(3-4), 103–129.
Haq, B. U., Hardenbol, J., & Vail, P. R. (1988). Mesozoic and Cenozoic chronostratigraphy and cycles of sea-level change, *Sea level changes: An integrated approach* (pp. 71–108). Houston: SEPM Special Publication.
Haqq-Misra, J. D., Domagal-Goldman, S. D., Kasting, P. J., & Kasting, J. F. (2008). A revised, hazy methane greenhouse for the Archean Earth. *Astrobiology*, *8*(6), 1127–1137.
Hartmann, J., Li, G., & West, A. J. (2017). Running out of gas: Zircon 18O-Hf-U/Pb evidence for Snowball Earth preconditioned by low degassing. *Geochemical Perspective Letters*, *4*, 41–46.
Hayes, J. M., Strauss, H., & Kaufman, A. J. (1999). The abundance of 13C in marine organic matter and isotopic fractionation in the global biogeochemical cycle of carbon during the past 800 Ma. *Chemical Geology*, *161*(1-3), 103–125.
Hayes, J. M., & Waldbauer, J. R. (2006). The carbon cycle and associated redox processes through time. *Philosophical Transactions of the Royal Society B: Biological Sciences*, *361*(1470), 931–950.
Herman, F., & Braun, J. (2008). Evolution of the glacial landscape of the Southern Alps of New Zealand: Insights from a glacial erosion model. *Journal of Geophysical Research*, *113*, F02009. https://doi.org/10.1029/2007JF000807
Higgins, J. A., & Schrag, D. P. (2003). Aftermath of a snowball Earth. *Geochemistry, Geophysics, Geosystems*, *4*(3), 1028. https://doi.org/10.1029/2002GC000403
Hilley, G. E., & Porder, S. (2008). A framework for predicting global silicate weathering and CO2 drawdown rates over geologic time-scales. *Proceedings of the National Academy of Sciences*, *105*(44), 16,855–16,859.
Hilley, G., & Strecker, M. R. (2004). Steady state erosion of critical Coulomb wedges with applications to Taiwan and the Himalaya. *Journal of Geophysical Research*, *109*, B01411. https://doi.org/10.1029/2002JB002284
Hoffman, P. F. (1989). Speculations on Laurentia's first gigayear (2.0 to 1.0 Ga). *Geology*, *17*(2), 135–138.
Hoffman, P. F. (2009). Pan-glacial—A third state in the climate system. *Geology Today*, *25*(3), 100–107.
Hoffman, P. F., Abbot, D. S., Ashkenazy, Y., Benn, D. I., Brocks, J. J., Cohen, P. A., et al. (2017). Snowball Earth climate dynamics and Cryogenian geology-geobiology. *Science Advances*, *3*(11), e1600983.
Hoffman, P. F., Bally, A., & Palmer, A. (1989). Precambrian geology and tectonic history of North America, *The geology of North American overview* (pp. 447–512). America: The Geology of North America.
Hoffman, P. F., & Li, Z.-X. (2009). A palaeogeographic context for Neoproterozoic glaciation. *Palaeogeography, Palaeoclimatology, Palaeoecology*, *277*(3-4), 158–172.
Höink, T., Lenardic, A., & Richards, M. (2012). Depth-dependent viscosity and mantle stress amplification: Implications for the role of the asthenosphere in maintaining plate tectonics. *Geophysical Journal International*, *191*(1), 30–41.
Holmes, A. (1931). Radioactivity and Earth movements. *Transactions of the Geological Society of Glasgow*, *18*, 559–606.

Horita, J., & Berndt, M. E. (1999). Abiogenic methane formation and isotopic fractionation under hydrothermal conditions. *Science*, *285*(5430), 1055–1057.
Hörst, S. M., He, C., Ugelow, M. S., Jellinek, A. M., Pierrehumbert, R. T., & Tolbert, M. A. (2018). Exploring the atmosphere of Neoproterozoic Earth: The effect of O2 on haze formation and composition. *The Astrophysical Journal*, *858*(2), 119.
Ibarra, D. E., Caves, J. K., Moon, S., Thomas, D. L., Hartmann, J., Chamberlain, CPage, & Maher, K. (2016). Differential weathering of basaltic and granitic catchments from concentration–discharge relationships. *Geochimica et Cosmochimica Acta*, *190*, 265–293.
Isley, A. E., & Abbott, D. H. (1999). Plume-related mafic volcanism and the deposition of banded iron formation. *Journal of Geophysical Research*, *104*(B7), 15,461–15,477.
Ivanov, A. V., Mazukabzov, A. M., Stanevich, A. M., Palesskiy, S. V., & Kozmenko, O. A. (2013). Testing the snowball Earth hypothesis for the Ediacaran. *Geology*, *41*(7), 787–790.
Jacoby, W. R. (1981). Modern concepts of Earth dynamics anticipated by Alfred Wegener in 1912. *Geology*, *9*(1), 25–27.
Jagoutz, O., Macdonald, F. A., & Royden, L. (2016). Low-latitude arc–continent collision as a driver for global cooling. *Proceedings of the National Academy of Sciences*, *113*(18), 4935–4940.
Jaupart, C., & Mareschal, J.-C. (2010). *Heat generation and transport in the Earth*. Cambridge: Cambridge university press.
Jellinek, A. M., Gordon, R. G., & Zatman, S. (2006). Experimental tests of simple models for the dynamics of diffuse oceanic plate boundaries. *Geophysical Journal International*, *164*(3), 624–632.
Jellinek, A., & Jackson, M. (2015). Connections between the bulk composition, geodynamics and habitability of Earth. *Nature Geoscience*, *8*(8), 587.
Jellinek, A., & Lenardic, A. (2009). Effects of spatially varying roof cooling on thermal convection at high Rayleigh number in a fluid with a strongly temperature-dependent viscosity. *Journal of Fluid Mechanics*, *629*, 109.
Jellinek, A., & Lenardic, A. (2009). Effects of spatially varying roof cooling on Rayleigh-Bénard convection in a fluid with a strongly temperature-dependent viscosity. *Journal of Fluid Mechanics*, *692*, 109–137.
Jellinek, A. M., & Manga, M. (2004). Links between long-lived hot spots, mantle plumes, d", and plate tectonics. *Reviews of Geophysics*, *42*, RG3002. https://doi.org/10.1029/2003RG000144
Jenkyns, H. C. (2010). Geochemistry of oceanic anoxic events. *Geochemistry, Geophysics, Geosystems*, *11*, Q03004. https://doi.org/10.1029/2009GC002788
Jenkyns, H. C. (2018). Transient cooling episodes during Cretaceous Oceanic Anoxic Events with special reference to OAE 1a (Early Aptian). *Philosophical Transactions of the Royal Society of London A: Mathematical, Physical and Engineering Sciences*, *376*(2130). https://doi.org/10.1098/rsta.2017.0073
Johnston, D. T., Macdonald, F. A., Gill, B., Hoffman, P., & Schrag, D. P. (2012). Uncovering the Neoproterozoic carbon cycle. *Nature*, *483*(7389), 320.
Jones, C. E., & Jenkyns, H. C. (2001). Seawater strontium isotopes, oceanic anoxic events, and seafloor hydrothermal activity in the Jurassic and Cretaceous. *American Journal of Science*, *301*(2), 112–149.
Kaufman, A. J., & Xiao, S. (2003). High CO2 levels in the Proterozoic atmosphere estimated from analyses of individual microfossils. *Nature*, *425*(6955), 279.
Kelemen, P. B., & Holbrook, W. S. (1995). Origin of thick, high-velocity igneous crust along the US East Coast Margin. *Journal of Geophysical Research*, *100*(B6), 10,077–10,094.
Keller, C. B., & Schoene, B. (2012). Statistical geochemistry reveals disruption in secular lithospheric evolution about 2.5 Gyr ago. *Nature*, *485*(7399), 490.
Kelley, D. S., Karson, J. A., Blackman, D. K., FruÈh-Green, G. L., Butterfield, D. A., Lilley, M. D., et al. AT3-60 Shipboard Party (2001). An off-axis hydrothermal vent field near the Mid-Atlantic Ridge at 30° N. *Nature*, *412*(6843), 145.
Kelley, D. S., Karson, J. A., Früh-Green, G. L., Yoerger, D. R., Shank, T. M., Butterfield, D. A., et al. (2005). A serpentinite-hosted ecosystem: The Lost City hydrothermal field. *Science*, *307*(5714), 1428–1434.
Knoll, A. H. (2011). The multiple origins of complex multicellularity. *Annual Review of Earth and Planetary Sciences*, *39*, 217–239.
Konn, C., Charlou, J.-L., Donval, J.-P., Holm, N., Dehairs, F., & Bouillon, S. (2009). Hydrocarbons and oxidized organic compounds in hydrothermal fluids from Rainbow and Lost City ultramafic-hosted vents. *Chemical Geology*, *258*(3-4), 299–314.
Korenaga, J. (2007). Eustasy, supercontinental insulation, and the temporal variability of terrestrial heat flux. *Earth and Planetary Science Letters*, *257*(1-2), 350–358.
Krissansen-Totton, J., & Catling, D. C. (2017). Constraining climate sensitivity and continental versus seafloor weathering using an inverse geological carbon cycle model. *Nature Communications*, *8*, 15423.
Kump, L. R. (2018). Prolonged Late Permian–Early Triassic hyperthermal: Failure of climate regulation? *Philosophical Transactions of the Royal Society A: Mathematical, Physical and Engineering Sciences*, *376*(2130), 20170078.
Kump, L. R., Brantley, S. L., & Arthur, M. A. (2000). Chemical weathering, atmospheric CO2, and climate. *Annual Review of Earth and Planetary Sciences*, *28*(1), 611–667.
Kump, L. R., Pavlov, A., & Arthur, M. A. (2005). Massive release of hydrogen sulfide to the surface ocean and atmosphere during intervals of oceanic anoxia. *Geology*, *33*(5), 397–400.
Kump, L. R., & Seyfried, W. E. Jr. (2005). Hydrothermal Fe fluxes during the Precambrian: Effect of low oceanic sulfate concentrations and low hydrostatic pressure on the composition of black smokers. *Earth and Planetary Science Letters*, *235*(3-4), 654–662.
Le Hir, G., Donnadieu, Y., Goddéris, Y., Pierrehumbert, R. T., Halverson, G. P., Macouin, M., et al. (2009). The snowball Earth aftermath: Exploring the limits of continental weathering processes. *Earth and Planetary Science Letters*, *277*(3-4), 453–463.
Le Hir, G., Goddéris, Y, Donnadieu, Y., & Ramstein, G. (2008). A geochemical modelling study of the evolution of the chemical composition of seawater linked to a "snowball" glaciation. *Biogeosciences*, *5*(1), 253–267.
Le Hir, G., Ramstein, G., Donnadieu, Y., & Goddéris, Y. (2008). Scenario for the evolution of atmospheric pCO2 during a snowball Earth. *Geology*, *36*(1), 47–50.
Le Pichon, X., Şengör, A. C., & Imren, C. (2019). Pangea and the lower mantle. *Tectonics*, *38*, 3479–3504.
Lee, C.-T. A., & Lackey, J. S. (2015). Global continental arc flare-ups and their relation to long-term greenhouse conditions. *Elements*, *11*(2), 125–130.
Lee, C.-T. A., Shen, B., Slotnick, B. S., Liao, K., Dickens, G. R., Yokoyama, Y., et al. (2013). Continental arc–island arc fluctuations, growth of crustal carbonates, and long-term climate change. *Geosphere*, *9*(1), 21–36.
Lee, Cin-TyA, Thurner, S., Paterson, S., & Cao, W. (2015). The rise and fall of continental arcs: Interplays between magmatism, uplift, weathering, and climate. *Earth and Planetary Science Letters*, *425*, 105–119.
Lenardic, A., Jellinek, A., Foley, B., O'Neill, C., & Moore, W. (2016). Climate-tectonic coupling: Variations in the mean, variations about the mean, and variations in mode. *Journal of Geophysical Research: Planets*, *121*, 1831–1864. https://doi.org/10.1002/2016JE005089

Lenardic, A., Moresi, L.-N., Jellinek, A., & Manga, M. (2005). Continental insulation, mantle cooling, and the surface area of oceans and continents. *Earth and Planetary Science Letters*, *234*(3-4), 317–333.
Lenardic, A., Moresi, L., Jellinek, A., O'neill, C., Cooper, C., & Lee, C. (2011). Continents, supercontinents, mantle thermal mixing, and mantle thermal isolation: Theory, numerical simulations, and laboratory experiments. *Geochemistry, Geophysics, Geosystems*, *12*, Q10016. https://doi.org/10.1029/2011GC003663
Lenton, T. M., Daines, S. J., & Mills, B. J. (2018). COPSE reloaded: An improved model of biogeochemical cycling over Phanerozoic time. *Earth-Science Reviews*, *178*, 1–28.
Li, Z.-X., Bogdanova, S., Collins, A., Davidson, A., De Waele, B., Ernst, R., et al. (2008). Assembly, configuration, and break-up history of Rodinia: A synthesis. *Precambrian Research*, *160*(1-2), 179–210.
Li, Z.-X., Evans, D. A., & Halverson, G. P. (2013). Neoproterozoic glaciations in a revised global palaeogeography from the breakup of Rodinia to the assembly of Gondwanaland. *Sedimentary Geology*, *294*, 219–232.
Li, G., Hartmann, J., Derry, L. A., West, A. J., You, C.-F., Long, X., et al. (2016). Temperature dependence of basalt weathering. *Earth and Planetary Science Letters*, *443*, 59–69.
Li, Z.-X., & Zhong, S. (2009). Supercontinent–superplume coupling, true polar wander and plume mobility: Plate dominance in whole-mantle tectonics. *Physics of the Earth and Planetary Interiors*, *176*(3), 143–156.
Longhi, J. (2005). A mantle or mafic crustal source for Proterozoic anorthosites? *Lithos*, *83*(3-4), 183–198.
Ludwig, K. A., Kelley, D. S., Butterfield, D. A., Nelson, B. K., & Früh-Green, G. (2006). Formation and evolution of carbonate chimneys at the Lost City Hydrothermal Field. *Geochimica et Cosmochimica Acta*, *70*(14), 3625–3645.
Macdonald, F. A., Schmitz, M. D., Crowley, J. L., Roots, C. F., Jones, D. S., Maloof, A. C., et al. (2010). Calibrating the cryogenian. *Science*, *327*(5970), 1241–1243.
Macdonald, F. A., Swanson-Hysell, N. L., Park, Y., Lisiecki, L., & Jagoutz, O. (2019). Arc-continent collisions in the tropics set Earth's climate state. *Science*, *364*, 181–184.
Macdonald, F. A., & Wordsworth, R. (2017). Initiation of Snowball Earth with volcanic sulfur aerosol emissions. *Geophysical Research Letters*, *44*, 1938–1946. https://doi.org/10.1002/2016GL072335
Maher, K., & Chamberlain, C. (2014). Hydrologic regulation of chemical weathering and the geologic carbon cycle. *Science*, *343*(6178), 1502–1504.
Manabe, S., & Broccoli, A. (1985). A comparison of climate model sensitivity with data from the last glacial maximum. *Journal of the Atmospheric Sciences*, *42*(23), 2643–2651.
Marty, B., & Tolstikhin, I. N. (1998). CO2 fluxes from mid-ocean ridges, arcs and plumes. *Chemical Geology*, *145*(3-4), 233–248.
McDuff, R. E. (1981). Major cation gradients in DSDP interstitial waters: The role of diffusive exchange between seawater and upper oceanic crust. *Geochimica et Cosmochimica Acta*, *45*(10), 1705–1713.
McKay, C. P., Pollack, J. B., & Courtin, R. (1991). The greenhouse and antigreenhouse effects on Titan. *Science*, *253*(5024), 1118–1121.
McKenzie, N. R., Horton, B. K., Loomis, S. E., Stockli, D. F., Planavsky, N. J., & Lee, C.-T. A. (2016). Continental arc volcanism as the principal driver of icehouse-greenhouse variability. *Science*, *352*(6284), 444–447.
McKenzie, N. R., Hughes, N. C., Gill, B. C., & Myrow, P. M. (2014). Plate tectonic influences on Neoproterozoic and early Paleozoic climate and animal evolution. *Geology*, *42*(2), 127. https://doi.org/10.1130/G34962.1
Meert, J. G. (2012). What's in a name? The Columbia (Paleopangaea/Nuna) supercontinent. *Gondwana Research*, *21*(4), 987–993.
Merdith, A. S., Williams, S. E., Brune, S., Collins, A. S., & Müller, R. D. (2019). Rift and plate boundary evolution across two supercontinent cycles. *Global and Planetary Change*, *173*, 1–14.
Miller, K. G., Kominz, M. A., Browning, J. V., Wright, J. D., Mountain, G. S., Katz, M. E., et al. (2005). The Phanerozoic record of global sea-level change. *Science*, *310*(5752), 1293–1298.
Mills, B., Daines, S. J., & Lenton, T. M. (2014). Changing tectonic controls on the long term carbon cycle from Mesozoic to present. *Geochemistry, Geophysics, Geosystems*, *15*(12), 4866–4884.
Mills, B., Lenton, T. M., & Watson, A. J. (2014). Proterozoic oxygen rise linked to shifting balance between seafloor and terrestrial weathering. *Proceedings of the National Academy of Sciences*, *111*(25), 9073–9078.
Mills, B., Watson, A. J., Goldblatt, C., Boyle, R., & Lenton, T. M. (2011). Timing of Neoproterozoic glaciations linked to transport-limited global weathering. *Nature Geoscience*, *4*(12), 861.
Moecher, D. P., & Samson, S. D. (2006). Differential zircon fertility of source terranes and natural bias in the detrital zircon record: Implications for sedimentary provenance analysis. *Earth and Planetary Science Letters*, *247*(3-4), 252–266.
Montgomery, D. R., & Brandon, M. T. (2002). Topographic controls on erosion rates in tectonically active mountain ranges. *Earth and Planetary Science Letters*, *201*(3-4), 481–489.
Moresi, L., Betts, P. G., Miller, M. S., & Cayley, R. A. (2014). Dynamics of continental accretion. *Nature*, *508*(7495), 245.
Morse, S. (1982). A partisan review of Proterozoic anorthosites. *American Mineralogist*, *67*(11-12), 1087–1100.
Müller, R. D., Seton, M., Zahirovic, S., Williams, S. E., Matthews, K. J., Wright, N. M., et al. (2016). Ocean basin evolution and global-scale plate reorganization events since Pangea breakup. *Annual Review of Earth and Planetary Sciences*, *44*, 107–138.
O'Neill, C., Lenardic, A., Jellinek, A., & Moresi, L. (2009). Influence of supercontinents on deep mantle flow. *Gondwana Research*, *15*(3-4), 276–287.
Olson, S. L., Reinhard, C. T., & Lyons, T. W. (2016). Limited role for methane in the mid-Proterozoic greenhouse. *Proceedings of the National Academy of Sciences*, *113*(41), 11,447–11,452.
Otto-Bliesner, B. L. (1995). Continental drift, runoff, and weathering feedbacks: Implications from climate model experiments. *Journal of Geophysical Research*, *100*(D6), 11,537–11,548.
Ouimet, W. B., Whipple, K. X., & Granger, D. E. (2009). Beyond threshold hillslopes: Channel adjustment to base-level fall in tectonically active mountain ranges. *Geology*, *37*(7), 579–582.
Pavlov, A. A., Hurtgen, M. T., Kasting, J. F., & Arthur, M. A. (2003). Methane-rich Proterozoic atmosphere? *Geology*, *31*(1), 87–90.
Pekeris, C. L. (1935). Thermal convection in the interior of the Earth. *Geophysical Journal International*, *3*, 343–367.
Perron, J. T. (2017). Climate and the pace of erosional landscape evolution. *Annual Review of Earth and Planetary Sciences*, *45*, 561–591.
Pesonen, L. J., Mertanen, S., & Veikkolainen, T. (2012). Paleo-Mesoproterozoic supercontinents—A paleomagnetic view. *Geophysica*, *48*(1-2), 5–47.
Peuble, S., Andreani, M., Gouze, P., Pollet-Villard, M., Reynard, B., & Van de Moortele, B. (2018). Multi-scale characterization of the incipient carbonation of peridotite. *Chemical Geology*, *476*, 150–160.
Phillips, B. R., & Coltice, N. (2010). Temperature beneath continents as a function of continental cover and convective wavelength. *Journal of Geophysical Research*, *115*, B04408. https://doi.org/10.1029/2009JB006600
Pierrehumbert, R. T. (2010). *Principles of planetary climate*. Cambridge: Cambridge University Press.

Pierrehumbert, R. T., Abbot, D. S., Voigt, A., & Koll, D. (2011). Climate of the Neoproterozoic. *Annual Review of Earth and Planetary Sciences*, *39*, 417–460. https://doi.org/10.1146/annurev-earth-040809-152447

Planavsky, N. J., Tarhan, L. G., Bellefroid, E. J., Evans, D. A., Reinhard, C. T., Love, G. D., & Lyons, T. W. (2015). Late Proterozoic transitions in climate, oxygen, and tectonics, and the rise of complex life. *Earth-Life Transitions: Paleobiology in the Context of Earth System Evolution*, *21*, 1–36.

Plank, T., & Manning, C. E. (2019). Subducting carbon. *Nature*, *574*(7778), 343–352.

Price, G. D. (1999). The evidence and implications of polar ice during the Mesozoic. *Earth-Science Reviews*, *48*(3), 183–210.

Price, G. D., & Nunn, E. V. (2010). Valanginian isotope variation in glendonites and belemnites from Arctic Svalbard: Transient glacial temperatures during the Cretaceous greenhouse. *Geology*, *38*(3), 251–254.

Pu, J. P., Bowring, S. A., Ramezani, J., Myrow, P., Raub, T. D., Landing, E., et al. (2016). Dodging snowballs: Geochronology of the Gaskiers glaciation and the first appearance of the Ediacaran biota. *Geology*, *44*(11), 955–958.

Rainbird, R., Cawood, P., & Gehrels, G. (2011). The great Grenvillian sedimentation episode: Record of supercontinent Rodinia's assembly, *Tectonics of Sedimentary Basins: Recent Advances* (pp. 583–601). Chichester: Wiley.

Ridgwell, A., & Zeebe, R. E. (2005). The role of the global carbonate cycle in the regulation and evolution of the Earth system. *Earth and Planetary Science Letters*, *234*(3-4), 299–315.

Ridley, D. A., Solomon, S., Barnes, J. E., Burlakov, V. D., Deshler, T., Dolgii, S. I., et al. (2014). Total volcanic stratospheric aerosol optical depths and implications for global climate change. *Geophysical Research Letters*, *41*, 7763–7769. https://doi.org/10.1002/2014GL061541

Riebe, C. S., Kirchner, J. W., & Finkel, R. C. (2004). Erosional and climatic effects on long-term chemical weathering rates in granitic landscapes spanning diverse climate regimes. *Earth and Planetary Science Letters*, *224*(3-4), 547–562.

Roberson, A. L., Roadt, J., Halevy, I., & Kasting, J. (2011). Greenhouse warming by nitrous oxide and methane in the Proterozoic Eon. *Geobiology*, *9*(4), 313–320.

Robin, C. M., Jellinek, A. M., Thayalan, V., & Lenardic, A. (2007). Transient mantle convection on Venus: The paradoxical coexistence of highlands and coronae in the BAT region. *Earth and Planetary Science Letters*, *256*(1-2), 100–119.

Roe, G. H. (2005). Orographic precipitation. *Annual Review of Earth and Planetary Sciences*, *33*, 645–671.

Roe, G. H., & Baker, M. B. (2006). Microphysical and geometrical controls on the pattern of orographic precipitation. *Journal of the Atmospheric Sciences*, *63*(3), 861–880.

Roe, G. H., & Brandon, M. T. (2011). Critical form and feedbacks in mountain-belt dynamics: Role of rheology as a tectonic governor. *Journal of Geophysical Research*, *116*, B02101. https://doi.org/10.1029/2009JB006571

Roe, G. H., Stolar, D. B., & Willett, S. D. (2006). Response of a steady-state critical wedge orogen to changes in climate and tectonic forcing. *Special Papers-Geological Society of America*, *398*, 227.

Roe, G. H., Whipple, K. X., & Fletcher, J. K. (2008). Feedbacks among climate, erosion, and tectonics in a critical wedge orogen. *American Journal of Science*, *308*(7), 815–842.

Rogers, J. J., & Santosh, M. (2004). *Continents and supercontinents*. Oxford: Oxford University Press.

Rolf, T., Coltice, N., & Tackley, P. (2012). Linking continental drift, plate tectonics and the thermal state of the Earth's mantle. *Earth and Planetary Science Letters*, *351*, 134–146.

Rolf, T., Coltice, N., & Tackley, P. (2014). Statistical cyclicity of the supercontinent cycle. *Geophysical Research Letters*, *41*, 2351–2358. https://doi.org/10.1002/2014GL059595

Rona, P., Bougault, H., Charlou, J., Appriou, P., Nelsen, T., Trefry, J., et al. (1992). Hydrothermal circulation, serpentinization, and degassing at a rift valley-fracture zone intersection: Mid-Atlantic Ridge near 15° N, 45° W. *Geology*, *20*(9), 783–786.

Rooney, A. D., Strauss, J. V., Brandon, A. D., & Macdonald, F. A. (2015). A Cryogenian chronology: Two long-lasting synchronous Neoproterozoic glaciations. *Geology*, *43*(5), 459–462.

Rothman, D. (2015). Earth's carbon cycle: A mathematical perspective. *Bulletin of the American Mathematical Society*, *52*(1), 47–64.

Rothman, D. H., & Forney, D. C. (2007). Physical model for the decay and preservation of marine organic carbon. *Science*, *316*(5829), 1325–1328.

Rothman, D. H., Hayes, J. M., & Summons, R. E. (2003). Dynamics of the Neoproterozoic carbon cycle. *Proceedings of the National Academy of Sciences*, *100*(14), 8124–8129.

Royer, D. L., Berner, R. A., Montañez, I. P., Tabor, N. J., & Beerling, D. J. (2004). CO_2 as a primary driver of Phanerozoic climate. *GSA Today*, *14*(3), 4–10.

Royer, D. L., Berner, R. A., & Park, J. (2007). Climate sensitivity constrained by CO2 concentrations over the past 420 million years. *Nature*, *446*(7135), 530.

Rudge, J. F., Kelemen, P. B., & Spiegelman, M. (2010). A simple model of reaction-induced cracking applied to serpentinization and carbonation of peridotite. *Earth and Planetary Science Letters*, *291*(1-4), 215–227.

Saal, A. E., Hauri, E. H., Langmuir, C. H., & Perfit, M. R. (2002). Vapour undersaturation in primitive mid-ocean-ridge basalt and the volatile content of Earth's upper mantle. *Nature*, *419*(6906), 451.

Schmidt, A., Carslaw, K. S., Mann, G. W., Rap, A., Pringle, K. J., Spracklen, D. V., et al. (2012). Importance of tropospheric volcanic aerosol for indirect radiative forcing of climate. *Atmospheric Chemistry and Physics*, *12*(16), 7321–7339. https://doi.org/10.5194/acp-12-7321-2012

Schmidt, A., Skeffington, R. A., Thordarson, T., Self, S., Forster, P. M., Rap, A., et al. (2016). Selective environmental stress from sulphur emitted by continental flood basalt eruptions. *Nature Geoscience*, *9*, 77–82. https://doi.org/10.1038/ngeo2588

Schoof, C. (2010). Ice-sheet acceleration driven by melt supply variability. *Nature*, *468*(7325), 803.

Schrag, D. P., Berner, R. A., Hoffman, P. F., & Halverson, G. P. (2002). On the initiation of a snowball Earth. *Geochemistry, Geophysics, Geosystems*, *3*(6), 1–21. https://doi.org/10.1029/2001GC000219

Schrag, D. P., Higgins, J. A., Macdonald, F. A., & Johnston, D. T. (2013). Authigenic carbonate and the history of the global carbon cycle. *Science*, *339*(6119), 540–543.

Shields-Zhou, G. A., Porter, S., & Halverson, G. P. (2016). A new rock-based definition for the Cryogenian Period (circa 720-635 Ma). *Episodes*, *39*(1), 3–8.

Sleep, N. H., & Zahnle, K. (2001). Carbon dioxide cycling and implications for climate on ancient Earth. *Journal of Geophysical Research*, *106*, 1373–1399.

Small, C. (1998). Global systematics of mid-ocean ridge morphology, *Faulting and magmatism at mid-ocean ridges* (pp. 1–25). Washington, DC: AGU.

Small, C., & Sandwell, D. T. (1989). An abrupt change in ridge axis gravity with spreading rate. *Journal of Geophysical Research*, *94*(B12), 17,383–17,392.

Small, C., & Sandwell, D. T. (1994). Imaging mid-ocean ridge transitions with satellite gravity. *Geology*, *22*(2), 123–126.

Solomatov, V. S., & Moresi, L.-N. (2000). Scaling of time-dependent stagnant lid convection: Application to small-scale convection on Earth and other terrestrial planets. *Journal of Geophysical Research*, *105*(B9), 21,795–21,817.

Spencer, C., Murphy, J., Hoiland, C., Johnston, S., Mitchell, R., & Collins, W. (2019). Evidence for whole mantle convection driving Cordilleran tectonics. *Geophysical Research Letters*, *46*, 4239–4248. https://doi.org/10.1029/2019GL082313

Spivack, A. J., & Staudigel, H. (1994). Low-temperature alteration of the upper oceanic crust and the alkalinity budget of seawater. *Chemical Geology*, *115*(3-4), 239–247.

Squire, R. J., Campbell, I. H., Allen, C. M., & Wilson, C. J. (2006). Did the Transgondwanan Supermountain trigger the explosive radiation of animals on Earth? *Earth and Planetary Science Letters*, *250*(1-2), 116–133.

Staudigel, H., Hart, S. R., Schmincke, H.-U., & Smith, B. M. (1989). Cretaceous ocean crust at DSDP Sites 417 and 418: Carbon uptake from weathering versus loss by magmatic outgassing. *Geochimica et Cosmochimica Acta*, *53*(11), 3091–3094.

Staudigel, H., Plank, T., White, B., & Schmincke, H.-U. (1996). Geochemical fluxes during seafloor alteration of the basaltic upper oceanic crust: DSDP Sites 417 and 418. *Subduction: Top to Bottom*, *96*, 19–38.

Stoll, H. M., & Schrag, D. P. (1996). Evidence for glacial control of rapid sea level changes in the Early Cretaceous. *Science*, *272*(5269), 1771–1774.

Summerfield, M., & Hulton, N. (1994). Natural controls of fluvial denudation rates in major world drainage basins. *Journal of Geophysical Research*, *99*(B7), 13871–13883.

Swanson-Hysell, N. L., & Macdonald, F. A. (2017). Tropical weathering of the Taconic orogeny as a driver for Ordovician cooling. *Geology*, *45*(8), 719–722.

Taylor, S., Campbell, I., McCulloch, M., & McLennan, S. (1984). A lower crustal origin for massif-type anorthosites. *Nature*, *311*(5984), 372.

Tennenbaum, S., Berezovskaya, F., & Schwartzman, D. (2013). Potential multiple steady states in the long-term carbon cycle. arXiv preprint arXiv:1310.0427.

Thayalan, V., Jellinek, A. M., & Lenardic, A. (2006). Recycling the lid: Effects of subduction and stirring on boundary layer dynamics in bottom-heated planetary mantle convection. *Geophysical research letters*, *33*, L20318. https://doi.org/10.1029/2006GL027668

Torres, M. A., Limaye, A. B., Ganti, V., Lamb, M. P., West, A. J., & Fischer, W. W. (2017). Model predictions of long-lived storage of organic carbon in river deposits. *Earth Surface Dynamics*, *5*(4), 711–730.

Tozer, D. C. (1972). The present thermal state of the terrestrial planets. *Physics of the Earth and Planetary Interiors*, *6*, 182–197.

Trindade, R. I., & Macouin, M. (2007). Palaeolatitude of glacial deposits and palaeogeography of Neoproterozoic ice ages. *Comptes Rendus Geoscience*, *339*(3-4), 200–211.

Tziperman, E., Halevy, I., Johnston, D. T., Knoll, A. H., & Schrag, D. P. (2011). Biologically induced initiation of Neoproterozoic snowball-Earth events. *Proceedings of the National academy of Sciences*, *108*(37), 15091–15096.

Van Avendonk, H. J., Davis, J. K., Harding, J. L., & Lawver, L. A. (2017). Decrease in oceanic crustal thickness since the breakup of Pangaea. *Nature Geoscience*, *10*(1), 58–61.

Veevers, J. J., & Powell, C. M. (1994). *Permian-triassic Pangean basins and foldbelts along the Panthalassan margin of Gondwanaland* (Vol. 184). America: Geological Society of America.

Veizer, J., Godderis, Y., & François, L. M. (2000). Evidence for decoupling of atmospheric CO2 and global climate during the Phanerozoic eon. *Nature*, *408*(6813), 698.

Walker, J., Hayes, P., & Kasting, J. (1981). A negative feedback mechanism for the long-term stabilization of Earth's surface temperature. *Journal of Geophysical Research*, *86*, 9776–9782.

Wegener, A. (1924). *The origin of continents and oceans*. London: Methuen and Co., Ltd.

West, A. J. (2012). Thickness of the chemical weathering zone and implications for erosional and climatic drivers of weathering and for carbon-cycle feedbacks. *Geology*, *40*(9), 811–814.

West, A. J., Galy, A., & Bickle, M. (2005). Tectonic and climatic controls on silicate weathering. *Earth and Planetary Science Letters*, *235*(1-2), 211–228.

Whipple, K. X. (2001). Fluvial landscape response time: How plausible is steady-state denudation? *American Journal of Science*, *301*(4-5), 313–325.

Whipple, K. X. (2004). Bedrock rivers and the geomorphology of active orogens. *Annual Review of Earth and Planetary Sciences*, *32*, 151–185.

Whipple, K., & Meade, B. (2004). Controls on the strength of coupling among climate, erosion, and deformation in two-sided, frictional orogenic wedges at steady state. *Journal of Geophysical Research*, *109*, F01011. https://doi.org/10.1029/2003JF000019

Whipple, K. X., & Meade, B. J. (2006). Orogen response to changes in climatic and tectonic forcing. *Earth and Planetary Science Letters*, *243*(1-2), 218–228.

Whipple, K. X., & Tucker, G. E. (1999). Dynamics of the stream-power river incision model: Implications for height limits of mountain ranges, landscape response timescales, and research needs. *Journal of Geophysical Research*, *104*(B8), 17,661–17,674.

White, A. F., & Brantley, S. L. (2019). *Chemical weathering rates of silicate minerals* (Vol. 31). Washington DC: Walter de Gruyter GmbH & Co KG.

Whittaker, J. M., Müller, R. D., Roest, W. R., Wessel, P., & Smith, W. H. (2008). How supercontinents and superoceans affect seafloor roughness. *Nature*, *456*(7224), 938.

Willett, S. D., McCoy, S. W., Perron, J. T., Goren, L., & Chen, C.-Y. (2014). Dynamic reorganization of river basins. *Science*, *343*(6175), 1248765.

Williams, R. G., & Follows, M. J. (2011). *Ocean dynamics and the carbon cycle: Principles and mechanisms*. Cambridge: Cambridge University Press.

Zachos, J. C., Dickens, G. R., & Zeebe, R. E. (2008). An early Cenozoic perspective on greenhouse warming and carbon-cycle dynamics. *Nature*, *451*(7176), 279.

Zahirovic, S., Müller, R. D., Seton, M., & Flament, N. (2015). Tectonic speed limits from plate kinematic reconstructions. *Earth and Planetary Science Letters*, *418*, 40–52.

Zhang, S., Li, Z.-X., Evans, D. A., Wu, H., Li, H., & Dong, J. (2012). Pre-Rodinia supercontinent Nuna shaping up: A global synthesis with new paleomagnetic results from North China. *Earth and Planetary Science Letters*, *353*, 145–155.

Zhang, S., & Planavsky, N. J. (2019). The silicate weathering feedback in the context of ophiolite emplacement: Insights from an inverse model of global weathering proxies. *American Journal of Science*, *319*(2), 75–104.